Acoustic Emission Testing of
Repaired Prestressed Concrete Bridge Girders

by

Thomas James Hadzor

A thesis submitted to the Graduate Faculty of
Auburn University
in partial fulfillment of the
requirements for the Degree of
Master of Science

Auburn, Alabama
August 6, 2011

Keywords: acoustic emission, bridge girders, cracking, damage, fiber-reinforced
polymer, nondestructive testing, prestressed concrete

Copyright 2011 by Thomas James Hadzor

Approved by

Robert W. Barnes, Chair, Associate Professor of Civil Engineering
Anton K. Schindler, Associate Professor of Civil Engineering
Justin D. Marshall, Assistant Professor of Civil Engineering

Abstract

Acoustic emission (AE) monitoring has proven to be a useful nondestructive testing tool in ordinary reinforced concrete beams. Over the past decade, however, the technique has been used to test other concrete structures to provide information on its usefulness. It has been seen that acoustic emission monitoring can be used on in-service bridges to obtain knowledge regarding the structural integrity of individual components of the structure. In this thesis, acoustic emission testing was used to examine the structural integrity of four prestressed girders in an elevated portion of the I-565 highway in Huntsville, Alabama. The testing was performed to assess the evaluation criteria used for in-situ testing and to determine the effectiveness of a fiber-reinforced-polymer (FRP) repair that was applied after substantial cracking occurred in the girder ends near the continuity diaphragms. The evaluation methods that were implemented were the NDIS-2421 evaluation criterion, the Signal Strength Moment (SSM) Ratio evaluation, and the Peak Cumulative Signal Strength (CSS) Ratio analysis. It was concluded that although the testing procedure provided results efficiently, the evaluation criteria need to be adjusted for the testing of in-service prestressed concrete bridge girders. It was also determined that the FRP repair did have an effect on the AE data, but a direct correlation between the two was not established due to the complexity of the testing.

Table of Contents

List of Tables

List of Figures

List of Abbreviations and Symbols

A   Amplitude (expressed in decibels)

AASHTO   American Association of State Highway and Transportation Officials

ACI   American Concrete Institute

AE   Acoustic emission

ALDOT   Alabama Department of Transportation

ASNT   American Society for Nondestructive Testing

ASTM   American Society for Testing and Materials

CARP   Committee on Acoustic Emission for Reinforced Plastics

CFRP   Carbon fiber-reinforced polymer

CLT   Cyclic load test

CMOD   Crack-mouth opening displacements

COD   Crack-opening device

CSS   Cumulative signal strength

dB   Decibel

ERSG   Electrical-resistance strain gauge

f'_c Specified 28-day compressive strength of concrete

f_+ Positive signal envelope function

f_- Negative signal envelope function

FHWA   Federal Highway Administration

FRP	Fiber-reinforced polymer
Hz	Hertz
H(t)	Historic Index at time, t
in.	Inch
m	Meter
J	Joule
K	Empirically derived factor
LC	Load configuration
N	Number of hits
NDIS	Japanese Society for Non-Destructive Inspection Standard
NDT	Nondestructive testing
NMAB	National Materials Advisory Board
Pa	Pascal
PAC	Physical Acoustics Corporation
PCI	Peripheral component interconnect
s, sec	Second
$S_{0,i}$	Signal strength value of ith hit
SAMOS	Sensor-based Acoustic Multi-channel Operation Systems
ST-6400	Standard Truck 6400
ST-6538	Standard Truck 6538
ST-6902	Standard Truck 6902
t_1	Time at first threshold crossing
t_2	Time at last threshold crossing

UCM	Ultimate capacity margin
V	Volt
V_{ref}	Reference voltage
W	Watt
Ω	Ohm

Chapter 1: Introduction

1.1 Introduction

Throughout the 1900s, the art of testing without destroying the test object

developed from a laboratory-based experiment to an indispensable tool of fabrication,

construction, manufacturing, and maintenance processes. Nondestructive testing (NDT)

is defined as comprising of those methods used to test a part, material, or system without

impairing its future usefulness (ASNT 1996). Visual testing has been replaced by NDT

as the primary means of testing the quality of a product. Nondestructive tests of all sorts

are in use worldwide to detect variations in structure, small changes in surface finish, the

presence of cracks or other physical discontinuities, and to measure the thickness of

materials.

Since 1992, the Federal Highway Administration (FHWA) has made available a

database of information on about 600,000 bridges on federal, state, and county roads.

The National Bridge Inventory summarizes the total number of bridges reported by each

state. More than a third of the bridges in the United States were reported as structurally

deficient or functionally obsolete in 1992 (FHWA 1996). As of 2004, roughly one in

four bridges were considered deficient, with two out of three not meeting safety standards

and nearly one in four recommended for replacement (FHWA 2004).

The state of the civil infrastructure is a major problem in the United States. Some

problems faced by bridge owners are the detection of deficiencies and the cost of repair,

rehabilitation, and maintenance. Although there exists funding from local, state, and federal agencies, spending restrictions often keep owners from resolving these issues. Bridge owners are now using nondestructive testing to assess the condition of bridges. Although visual inspection has been the main nondestructive tool used in the assessment of these bridges, this method is inadequate for identification of smaller discontinuities or those hidden or located in areas that are not easily accessible (ASNT 2005).

Acoustic emission testing is an important method within the broad field of nondestructive testing. Acoustic emission (AE) is defined by the American Society of Testing Materials (ASTM) in its *Standard Terminology for Nondestructive Evaluations* (ASTM E 1316) as "the class of phenomena whereby transient elastic waves are generated by the rapid release of energy from localized sources within a material, or the transient elastic waves so generated." Acoustic emission testing differs from most other NDT methods in two key aspects: (1) the signal originates in the material itself as opposed to an external source; (2) AE monitoring detects movements or condition changes as they occur, while other methods simply detect existing geometrical discontinuities (ASNT 2005).

Acoustic emission testing has been increasingly used to help ensure the integrity and performance of bridges subjected to concrete cracking. It has been proven that materials used in bridge structures, such as steel, concrete, and composites, will produce a rapid release of energy, in the form of transient elastic stress waves, during certain load levels or from initial degradation of the material. This degradation can be a result of cracking initiation or growth, crack-opening or closing, dislocation movement, as well as fiber breakage or delamination in composite materials. The ability to detect the acoustic

emission sources helps provide information about the type and severity of the damage. The knowledge provided by acoustic emission monitoring also allows for the identification of critical areas of the structure for prioritizing repair, maintenance, and rehabilitation (ASNT 2005).

1.2 Objective and Scope

The main objective of this research was to investigate the feasibility of using acoustic emission testing to assess the performance of prestressed concrete bridge girders. Specifically, acoustic emission monitoring was performed on an elevated portion of the I-565 interstate highway in Huntsville, Alabama, which can be seen in Figure 1-1.

Figure 1-1: Elevated spans of I-565 bridge in Huntsville, Alabama

The AE testing gave insight into the overall method and its usefulness as it applies to prestressed concrete girders. The specific objectives of this research are summarized as follows:

3

1. Utilize AE parameter-based analysis methods to determine a correlation between AE parameters and the structural integrity of prestressed concrete beams.

2. Assess the practicability of AE evaluation criteria as they apply to prestressed concrete beams.

3. Use AE monitoring to evaluate the structural integrity of four girders in the I-565 bridge structure in Huntsville, Alabama.

4. Assess the evaluation criteria used to process the AE data and determine how these criteria can be adapted for in-situ testing.

5. Evaluate the effectiveness of the fiber-reinforced polymer repair used on damaged portions of the I-565 bridge girders by comparing AE monitoring results from before and after the fiber-reinforced polymer repair.

To satisfy these objectives, the AE monitoring technique was applied in the field on an actual damaged prestressed concrete bridge. The damage occurred quickly after the construction of the bridge. At the end of the girders near the continuity diaphragms, cracks began to occur. To remediate the problem, a fiber-reinforced polymer (FRP) repair was used on the cracked end girder sections. The results of this research were compared to the previous work done by Xu (2008), which was prior to the installation of the FRP repair. The comparison shows the difference in the behavior of the bridge before and after the repair.

1.3 Organization of Thesis

In Chapter 2 of this thesis, an introduction to acoustic emission testing is presented. The selection process for acoustic emission testing is covered, as well as a brief introduction to other nondestructive testing methods. The advantages and

disadvantages of acoustic emission monitoring are also presented, along with testing specifications and standards. Also covered in Chapter 2 is a discussion of the fundamentals of acoustic emission, including source mechanisms, applications, and testing equipment. Finally, a brief overview of acoustic emission terminology and parameters is discussed.

Chapter 3 is a discussion of the history of acoustic emission as it applies to the research being conducted for this project. Early observations of acoustic emission are described, as well as current research being done in both the reinforced and prestressed concrete fields.

Chapter 4 is focused on the experimental procedure used for the in-field testing of the I-565 bridge girders in Huntsville, Alabama. This chapter includes a brief introduction to the history of the bridge as well as the research significance for the AE testing procedure. The specific testing equipment and instrumentation are described as well as the procedure used for the pre-repair testing in 2005 (Xu 2008) and the post-repair testing in 2010. The findings of both experiments are discussed in Chapter 5 of this thesis.

A comparison of the results from the pre- and post-repair testing was conducted to assess the effectiveness of the fiber-reinforced polymer repair placed on the bridge. This comparison is presented in Chapter 5 of this thesis. The results within this chapter include a crack-opening displacement analysis as well as other AE evaluation criteria. The predicted position of cracks using AE 2D-LOC analysis is also covered in this chapter.

Finally, Chapter 6 includes a summary of the research as well as all conclusions from field testing. Recommendations for further research are also presented in this chapter.

Chapter 2: Introduction to Acoustic Emission Testing

2.1 Introduction to Nondestructive Testing

Acoustic emission testing is an important method within the broad field of nondestructive testing. Modern nondestructive tests are used by manufacturers for many purposes. These include ensuring product integrity, avoiding failures, guaranteeing customer satisfaction, aiding in better product design, lowering costs, maintaining quality levels, and controlling manufacturing processes. As technology has improved over the years, machines and structures are subjected to greater variations and to wider extremes of all kinds of stress. These increased demands on machines and structures have allowed nondestructive testing to become more prevalent in industry to ensure that adequate materials are being used in the design. Another justification for the use of nondestructive tests is the designer's demand for sounder materials (ASNT 2005). As size and weight decrease and the factor of safety is lowered, more emphasis is placed on better raw material control and higher quality of materials. There has also been a growing demand by the public for greater safety, which has also contributed to the development of nondestructive testing. Finally, the rising costs of failure have led to new ways of testing materials and structures. Nondestructive testing continues to grow as a new way to test materials and limit the costs associated with full-scale testing (ASNT 2005).

The National Materials Advisory Board (NMAB) Ad Hoc Committee on

Nondestructive Evaluation adopted a system that classified nondestructive techniques into six major method categories: visual, penetrating radiation, magnetic-electrical, mechanical vibration, thermal, and chemical/electrochemical. Acoustic emission is classified in the mechanical vibration category. The limitations of a method include conditions to be met for its application and requirements to adapt the probe or probe medium to the object examined (ASNT 2005). No single nondestructive testing method is all revealing, and, in most cases, it takes a series of test methods to get a complete view of the test object. Nondestructive testing should be used in conjunction with other testing techniques to get a more comprehensive study of the test specimen.

2.2 Introduction to Acoustic Emission Testing

2.2.1 Selection of Testing Technique

Acoustic emission test methods usually fall into one of the following categories: pressure testing, diagnostics, condition monitoring, and leak detection (ASNT 2005). Acoustic emission instrumentation is designed to detect the structure- or liquid-borne sound generated by some material that is either yielding or failing. The American Society for Testing and Materials (ASTM) defines acoustic emission in its *Standard Terminology for Nondestructive Examinations* (ASTM E 1316) as "the class of phenomena whereby transient elastic waves are generated by the rapid release of energy from localized sources within a material, or the transient elastic waves so generated." Acoustic emission is a type of microseismic wave generated from dislocations, microcracking, or other irreversible changes in a stressed material (Xu 2008). These waves are detected using transducers which convert the mechanical waves into electric signals that can be monitored and assessed to determine characteristics of the test object.

8

2.2.2 Advantages and Limitations

Modern acoustic emission testing techniques offer an economical means for high-speed, large-scale testing of materials and structures found in almost every industry. In the typical test, a controlled mechanical load is used to cause acoustic emission in the test object. Nearly every kind of material generates acoustic emission under load (ASNT 2005). When correctly instrumented, an entire structure can be tested by applying loads equal to or slightly greater than those experienced during normal operation. Since the test has minimal effect on operations, acoustic emission testing is often used to test structures in service. Multiple sensors can be used to determine different sources of emission and triangulation can be used to determine the location of certain discontinuities.

Even though acoustic emission is a nondestructive test, it is an irreversible process. Once a material or discontinuity generates acoustic emission under load, the discontinuity must either grow or be subjected to a higher load to generate more acoustic emission. This irreversibility, known as the *Kaiser effect*, can be a limitation because most nondestructive testing requires retesting to verify a discontinuity (ASNT 2005). Background noise can have a large effect on acoustic emission testing and can prevent a test from providing useable data. This noise can usually be isolated to mechanical sources, electrical sources, and environmental sources (ASNT 2005). If these sources of noise cannot be removed or controlled by filtering or adjustment of the measurement threshold, then a test cannot be effective.

Another disadvantage, as it relates to the application of acoustic emission to concrete structures, is that the propagation of acoustic emission through concrete is

affected by both the constituents of concrete and the cracks formed within concrete (Uomoto 1987). Concrete is a composite material made with cement, water, aggregate, air, and admixtures. Each of these components is different in shape, size, and mechanical properties. During the placing and curing process, segregation may cause non-uniformities in the concrete. These non-uniformities and the cracks caused by curing and in-service loading affect AE wave propagation through concrete. These considerations must be taken into account when looking at the application of AE monitoring to structural concrete applications (Uomoto 1987).

2.2.3 Testing Specifications

The test specifications for acoustic emission deal with certain issues that arise during testing and the steps taken once the data are collected. The acoustic emission techniques use either operational or applied loads to stimulate emissions from a variety of sources. These applied loads must be accounted for in the specifications. Specifications for acoustic emission testing also account for the test frequency. A single acoustic emission test system can be used for many different measurements through the selection of test frequencies. The frequencies are usually those that match the resonant frequency of the acoustic emission transducer designed for a specific application. Frequency is measured in hertz (Hz), where 1 Hz = 1 cycle per second. In terms of acoustic emission, the standard usable range is 30-300 kHz (ASNT 2005). The interpretation of the acoustic emission data can be a complex procedure. The data interpreter must have good knowledge of the testing procedure as well as the principles of wave propagation through objects. Once the test results are evaluated, the results must be verified using conventional measurements and other testing methods. Accurate results can lead to

10

conclusions about the integrity of the material or structure.

2.2.4 Testing Standards

The purpose of testing standards is to define the requirements that goods or

services must meet. The standards dealing with acoustic emission come in three areas:

equipment, processes, and personnel. Standards for acoustic emission equipment include

criteria that address transducers and other parts of a system. ASTM International and

other organizations publish standards for test techniques, such as ASTM E 569, ASTM E

750, and ASTM E 2374 (ASNT 2005). One of the most important factors of the acoustic

emission test process is the qualification of testing personnel. Nondestructive testing is

referred to as a special process, meaning that it is very difficult to determine the adequacy

of a test by merely observing the process. The quality of the test is very dependent on the

skills and knowledge of the inspector. The American Society of Nondestructive Testing

(ASNT) has worked with the personnel qualification process for 50 years, and many

standards have been adopted that address this process (ASNT 2005).

2.2.5 Measurement Units for Acoustic Emission Testing

Acoustic emission is basically a shock wave inside a stressed material, where a

displacement (distance) ripples through the material and moves its surface. This

displacement induces a pressure in a transducer on the surface. This pressure is measured

as force per unit area in pascal (Pa), equivalent to newton per square meter (N/m^2).

Properties of piezoelectric transducers are related to electric charge in that the pressure on

the element creates a charge (measured in coulomb) on the electrodes. A rapidly

changing pressure alters the charge fast enough to allow the use of either voltage or

charge amplifiers. After this, signal processing can be performed to analyze and obtain

data in terms of distance in meter (m), velocity in meters per second (m/s), acceleration in

meters per second per second (m/s^2), signal strength in volt-second (V•s), energy in joule

(J), signal in volt (V), or power in watt (W) (ASNT 2005).

Frequencies usually correspond to bandwidths for specific applications. The term

loudness refers to amplitude in audible frequencies. Some acoustic waves are audible,

but others are not. The customary unit for measuring amplitude of an acoustic signal is

the decibel (dB), one tenth of a bel (B). The decibel is not a fixed unit of measurement

but rather expresses a logarithmic ratio between two conditions of the same dimension

(ASNT 2005).

2.3 Fundamentals of Acoustic Emission Testing

2.3.1 Source Mechanisms

Acoustic emission is the elastic wave that is released by materials when they

undergo deformation. In the 1960s, a new nondestructive test technology was born when

it was recognized that growing cracks and discontinuities in pressure vessels could be

detected by monitoring their acoustic emission signals (ASNT 2005). Sources of

acoustic emission include many different mechanisms of deformation and fracture. In

metals, sources identified include crack growth, moving dislocations, slip, twinning,

grain boundary sliding, and fracture (ASNT 2005). There are also other AE-producing

mechanisms that are not caused by mechanical deformation of stressed materials. These

are known as secondary sources, to differentiate them from the classic sources of acoustic

emission.

2.3.2 Comparison with Other NDT Methods

Acoustic emission testing is different from other nondestructive testing methods in two major areas. First, the energy that is detected is released from within the test object rather than being supplied by the test method, as in radiographic or ultrasonic testing. Second, the acoustic emission method can detect the dynamic processes associated with the degradation of structural integrity (ASNT 2005). Acoustic emission testing is non-directional. Most AE sources appear to function as point sources that radiate energy on spherical wave fronts. If the transducer is located anywhere in the vicinity of the source, it can detect the resulting acoustic emission. This ability is in contrast to other NDT methods which depend on prior knowledge of the location and orientation of the discontinuity to direct a beam of energy on a path that will properly intersect the area of interest (ASNT 2005).

The acoustic emission method offers many advantages over other nondestructive testing methods. It is a dynamic test method in that it provides a response to discontinuity growth under an imposed structural stress. Also, acoustic emission testing has the ability to detect and evaluate the significance of discontinuities throughout an entire structure during a single test. Since only limited access is required for the testing procedure, discontinuities may be detected that are inaccessible to other methods. Another advantage is that vessels and other pressure systems can often be re-qualified during an in-service test that requires little or no downtime. Finally, the AE method may be used to prevent catastrophic failure of systems with unknown discontinuities and to limit the maximum pressure during containment system tests (ASNT 2005).

2.3.3 Applications of Acoustic Emission Testing

A wide variety of structures and materials can be monitored using acoustic emission techniques during the application of an external load. The primary acoustic emission mechanism should be characterized when dealing with varying materials. Many applications of acoustic emission testing have been proven to succeed in assessing the integrity of a structure or material. Pressure vessels and other pressure containment vessels have been tested to locate active discontinuities. Aerospace and other engineering structures have been assessed for fatigue failures using acoustic emission techniques. Acoustic emission testing has also been used to monitor material behavior to characterize different failure mechanisms (ASNT 2005).

Examples of AE applications in the field of concrete engineering include the estimation of prior load applied to existing concrete structures and the monitoring of cracks and their locations in concrete beams. It has also been used in the prediction of fatigue failure of reinforced concrete beams and some prestressed concrete applications (Uomoto 1987). In the recent past, acoustic emission has been used in conjunction with other nondestructive tests to determine the structural integrity of concrete structures. The growing weight of carried goods, natural aging processes, and delays in making immediate repairs has resulted in the quick decline of bridges and roads (Swit 2009). There have been considerable strides made in the development of AE technology because of its potential applications for evaluating the weakening infrastructure of roads and bridges.

2.3.4 Acoustic Emission Testing Equipment

Acoustic emission processing equipment is available in a variety of forms ranging

from small and portable instruments to large multichannel systems. All systems, however, have common components, including transducers (sensors), preamplifiers, filters, and amplifiers. The equipment used for measurement, display, and storage varies widely depending on the demands of the application. Figure 2-1 shows a block diagram of a generic four-channel acoustic emission system.
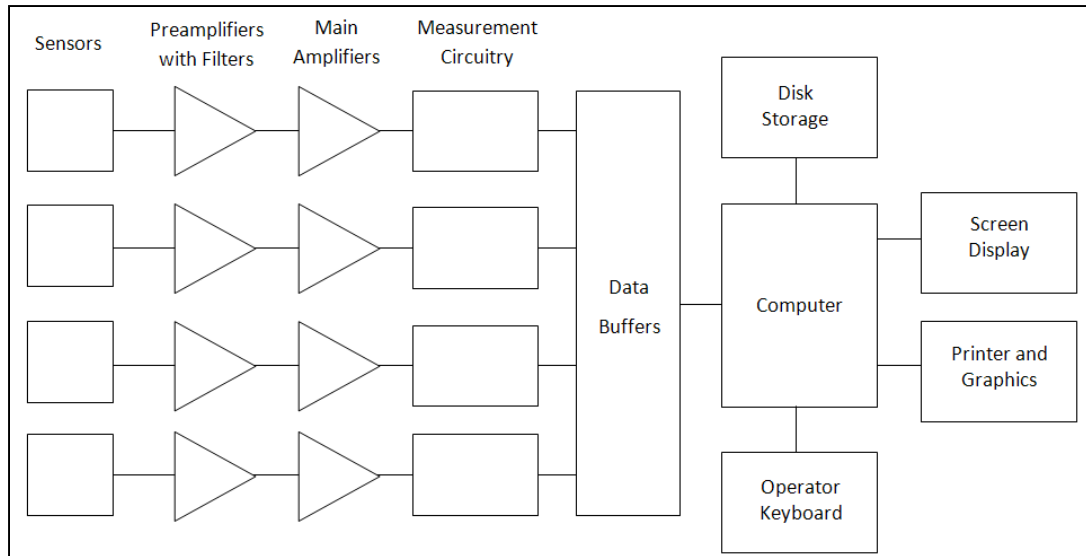
Figure 2-1: Basic four-channel acoustic emission test system (adapted from ASNT 2005)

When an acoustic emission wave reaches the surface of the test object, extremely small movements of the surface molecules occur. The transducer is used to detect these movements and convert them into electrical signals. The transducers used for AE testing often use a piezoelectric sensor as the electromechanical conversion device. The main considerations during transducer selection are operating frequency, sensitivity, and environmental and physical characteristics.

The preamplifiers must be located near the transducers, and, in most cases, are incorporated into the housing of the transducer. The purpose of the preamplifier is to

provide filtering, gain, and cable drive capacity. Filtering in the preamplifier is the primary means of defining the monitoring frequency for the acoustic emission test (ASNT 2005). The frequency spectrum of acoustic emission signals is significantly influenced by the resonance and transmission characteristics of both the test object and the transducer. The most common frequency range for acoustic emission testing is 100 to 300 kHz (ASNT 2005).

The system computer allows the data being gathered to be displayed and stored. The computer also houses the main amplifiers and threshold settings, which can be adjusted to control the sensitivity of the test. Each acoustic emission signal is measured by hardware circuits and the measured parameters are passed through the central computer to a disk file of signal descriptions. These descriptions include hits, hit rate, amplitude, duration, rise time, and the energy of the signal, which will all be defined later in this chapter. Once the data has been gathered, the computer can be used to assess the data and create plots of the data for future interpretation (ASNT 2005).

2.4 Data Interpretation

Proper interpretation of the acoustic emission response obtained during monitoring of structures requires considerable technical knowledge and experience with the acoustic emission method. Background noise from vibrations in the structure and other environmental conditions need to be accounted for in most tests. Special precautions may need to be used to limit the background noise to tolerable levels. Some of these precautions include mechanical or acoustic isolation, electronic filtering within the acoustic emission system, and modifications to the mechanical or hydraulic loading process.

Josef Kaiser is credited as the founder of modern acoustic emission technology and was the first to truly understand the inner workings of acoustic emission data interpretation. His work during the 1950s had two major breakthroughs. The first of these discoveries was the near universality of the acoustic emission phenomenon. He observed emission in all of the materials he tested. The second of these discoveries was the *Kaiser effect*. The effect can be defined as the "absence of detectable acoustic emission until the previous maximum applied stress level has been exceeded" (ASNT 1987). This discovery lent a special significance to acoustic emission investigations, because "by the measurement of emission during loading a clear conclusion can be drawn about the magnitude of the maximum loading experienced before the test by the material under investigation" (Kaiser 1953). A more appropriate term for the Kaiser effect is irreversibility. An important feature affecting acoustic emission applications is the generally irreversible response from most metals. In practice, it is found that once a given load has been applied and the acoustic emission from that stress has ceased, additional acoustic emission will not occur until that stress level is exceeded (ASNT 2005). However, the degree to which the Kaiser effect is present varies between materials and may disappear after several hours or days due to recovery characteristics. Ultimately, the Kaiser effect must be taken into account during data interpretation, and the effect may yield important data regarding the maximum load a structure has experienced.

A major application of the Kaiser effect arose from the study of when it *does not* occur. Emission is often observed at load levels lower than the previous maximum in fiber-reinforced plastic components. The term *Felicity effect* was introduced to describe

the breakdown of the Kaiser effect (the observance of the *Felicity effect* and its implications are generally attributed to Dr. Timothy J. Fowler). The *Felicity effect* is defined as "the presence of detectable acoustic emission at a fixed, predetermined sensitivity level at stress levels below those previously applied" (ASTM E 1316). In essence, the Felicity effect is the breakdown of the Kaiser effect, in that the test object generates emission during reloading before the previous maximum stress is achieved. The *Felicity ratio* has been used as an indication of the amount of damage. It is defined (Fowler et al. 1989) as:

$$\text{Felicity ratio} = \frac{\text{load at which emissions occur}}{\text{previous maximum load}} \qquad \text{(Eq. 2-1)}$$

According to this equation, smaller Felicity ratio values indicate increased levels of damage (Fowler et al. 1989).

The Kaiser effect and Felicity effect are illustrated in Figure 2-2. Cumulative acoustic emission is plotted directly against applied load. As can be seen in the figure, emission is generated during the first load rise (A-B), but as the load is reduced (B-C) and increased again (C-B), there is no further emission until the previous maximum load (B) is exceeded. Emission continues as the load is increased further (B-D), and stops as the load is reduced the second time (D-E). On increasing the load for the last time, a different emission pattern is observed. The emission begins (F) before the previous maximum load (D) is achieved. Emission continues as the load is increased further (F-G) (Pollock 1995).
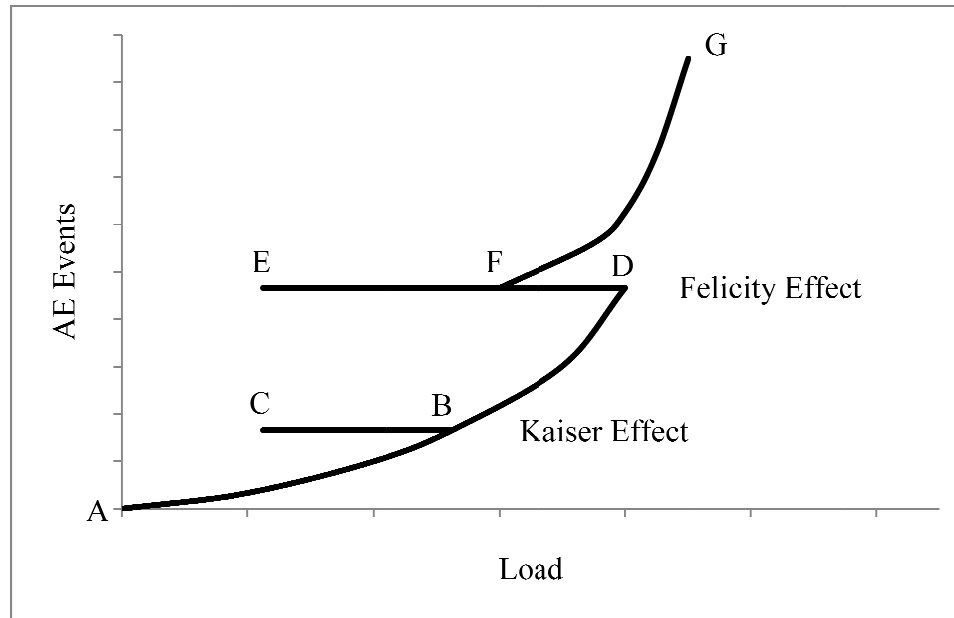
Figure 2-2: Illustration of Kaiser effect and Felicity effect (Adapted from Pollock 1995)

The behavior observed at B (no emission until previous maximum load is exceeded) is known as the Kaiser effect. Likewise, the behavior at F (emission at load levels less than the previous maximum) is known as the Felicity effect. According to Pollock (1995), insignificant flaws tend to exhibit the Kaiser effect, while structurally significant flaws tend to exhibit the Felicity effect.

According to research, the Kaiser effect fails to occur most noticeably in situations where time-dependent mechanisms control the deformation (ASNT 2005). Once again, the structure must be assessed to determine whether the Kaiser effect should be considered for the particular material and loading process. The Felicity effect can be used in data interpretation depending on the validity of the Kaiser effect for a certain test.

Another important consideration when dealing with the Kaiser effect is the fact that friction between free surfaces in damaged regions is a prominent emission

mechanism in composite materials. Such source mechanisms contravene the Kaiser effect by emitting waves at low load levels, but they can still be important for detection of damage and discontinuities (ASNT 2005).

One major complication with interpretation of the Felicity effect is that the "onset of emission" is not sufficient to establish the effect. Rather, the "onset of *significant* emission" is required. The definition of "significant" emission is to some degree subjective and much of the work related to the Felicity ratio and damage qualifications has been related to quantification of the term "significant." This has been addressed by some authors through the use of *Historic Index* (Ziehl and Fowler 2003), and this approach has been adopted for an ASTM standard test method related to the design of FRP components (ASTM 2006).

Data interpretation begins with observing the signal waveform. The signal waveform is affected by the characteristics of the source, the path taken from the source to the transducer, the transducer's characteristics, and the measuring system (ASNT 2005). For the most part, information is extracted by simple waveform parameter measurements. In addition to the characteristics of the individual waveforms, there is also information available from the cumulative characteristics of the signals and from rate statistics.

2.5 Waveform Parameters

Acoustic emission can be described by relatively simple parameters. A simple signal waveform with typical AE features can be seen in Figure 2-3. The signal amplitude is of short duration, usually a few microseconds to a few milliseconds.
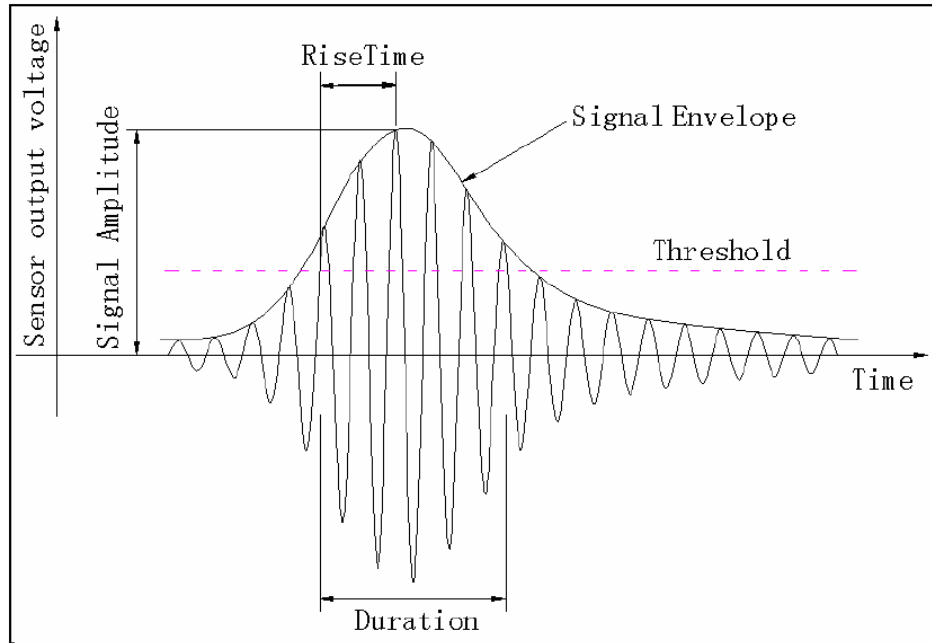
Figure 2-3: Features of a typical AE signal (adapted from Huang et al. 1998)

Acoustic emission monitoring is usually carried out in the presence of background noise. A threshold detection level is set slightly above this background level and serves as a reference for several of the simple waveform properties. AE parameters are used to characterize the source mechanisms such as crack growth. As stated before, it may be more advantageous to combine parameters to establish correlations. Some parameters that are commonly used for signal processing are described below.

1. **Hit**—A *hit* is defined as the detection and measurement of an individual AE signal on an individual sensor channel (ASTM E 1316).

2. **Event**—An *event* is defined as a local material change giving rise to acoustic emission (ASTM E 1316). A single event may result in multiple hits (at one or more sensors).

3. **Threshold level**—The *threshold level* is defined as the voltage level on an electronic comparator such that signals with amplitudes larger than this level

21

will be recognized. The threshold level may be user-adjustable, fixed, or automatically floating (ASTM E 1316). It is used to selectively reject signals with smaller amplitudes, which may not provide useful information because they often correspond to ambient, electronic, or electromagnetic noise (Xu 2008).

4. **Signal Amplitude**—The *signal amplitude* is defined as the magnitude of the peak voltage of the largest excursion attained by the signal waveform from a single emission event (ASTM E 1316). It is taken as the absolute value of the peak value. Signal amplitude is usually measured in decibels (dB), to which voltage is converted using the following equation:

$$A = 20 \log\left(\frac{V}{V_{ref}}\right)$$
(Eq. 2-2)

where

A = Amplitude in decibels (dB),

V = Voltage of peak excursion, and

V_{ref} = Reference voltage.

The amplitude of an acoustic emission signal is an indication of the source intensity (Pollock 1995).

5. **Signal Duration**—The *signal duration* is defined as the time between AE signal start and AE signal end (ASTM E 1316). It is the length of time from the first threshold crossing to the last threshold crossing and is usually reported in milliseconds. Therefore, the duration of the signal will be affected by the choice of threshold level. The relationship between the signal amplitude and the signal duration is an indication of the signal's shape.

22

6. **Signal Rise Time**—The *signal rise time* is defined as the time between AE signal start and the peak amplitude of that AE signal (ASTM E 1316). It is measured in milliseconds and also yields information about the signal's shape when used in conjunction with the signal duration and amplitude.

7. **Signal Strength**—The *signal strength* is defined as the measured area of the rectified AE signal, with units proportional to volt-seconds (ASTM E 1316). The signal strength is often referred to as relative energy which is a measure of the amount of energy released by the specimen. Signal strength is a function of the amplitude and duration of the signal. The signal strength is expressed by Fowler et al. (1989) as:

$$S_0 = \frac{1}{2}\int_{t_1}^{t_2} f_+(t)dt + \frac{1}{2}\left|\int_{t_1}^{t_2} f_-(t)dt\right| \qquad \text{(Eq. 2-3)}$$

where

S_0 = signal strength,

f_+ = positive signal envelope function,

f_- = negative signal envelope function,

t_1 = time at first threshold crossing, and

t_2 = time at last threshold crossing.

8. **Signal energy**—The *signal energy* is defined as the energy contained in a detected acoustic emission burst signal, with units usually reported in joules or values that can be expressed in logarithmic form (dB, decibels) (ASTM E 1316). The AE signal energy is expressed by Fowler et al. (1989) as:

$$E_t = \frac{1}{2}\int_{t_1}^{t_2} f_+^2(t)dt - \frac{1}{2}\int_{t_1}^{t_2} f_-^2(t)dt \qquad \text{(Eq. 2-4)}$$

9. **Count**—The *count* is defined as the number of times the acoustic emission signal exceeds a preset threshold during any selected portion of a test (ASTM E 1316). The total number of counts, as well as the count rate (number of counts during a fixed period of time), are common parameters used for acoustic emission data interpretation. Counts are useful in giving information about the signal shape when used in conjunction with the signal amplitude and duration (ASNT 2005).

10. **Frequency**—The *frequency* is the number of cycles per second of the pressure variation in a wave, measured in hertz. An acoustic emission waveform usually consists of several frequency components.

2.6 General Acoustic Emission Monitoring Procedure

The acoustic emission monitoring process is relatively easy and can yield valuable insight into the integrity of the test object. A general overview of the acoustic emission monitoring procedure for a structure begins with a preliminary survey.

A preliminary visual survey of the existing structure should be conducted prior to any testing. Structural drawings should be viewed and the testing areas should be chosen based on access and damage assessment. Once all preliminary steps are taken care of, the acoustic emission testing equipment should be chosen. Calibration tests should be conducted to ensure that the testing equipment is fully functional. Testing times should be chosen so there is minimal effect on the operation of the structure. These times should also be confirmed by any agencies that will help in the testing.

The equipment used for the AE testing must have adequate capacity to handle large quantities of information at high data acquisition rates (Xu 2008). The computer

system being used should have a large storage capacity and sufficient processing

capacity. According to Pollock (1995), the most important technical choice for AE

monitoring is the operating frequency. The transducers being used in the testing can be

resonant or broadband and can cover a variety of frequency ranges. Resonant transducers

give the advantage of operating in a known and well-established frequency band.

Resonant transducers are generally more sensitive and less expensive than broadband

transducers. Broadband transducers deliver more information but can overload the

system computer (PCI-8 2002). In most applications, resonant sensors are preferred over

broadband sensors (Pollock 1995).

      Once the testing equipment is chosen, the equipment must be set up at the testing

site. Sensor mounting is an integral part to the success of the AE monitoring procedure.

The surface where the sensors will be placed must be cleaned and smoothed. Dirty

surfaces are undesirable because the particles between the sensor pad and the surface will

decrease the acoustic contact, causing variations in the emission signals (Pollock 1995).

Once the surface is cleaned, the sensor must be mounted to the concrete surface. If a

sensor is simply placed on the surface of the test object, the signal tends to be very weak.

However, if a thin layer of a viscous medium is placed in between the surface and the

sensor, a much stronger signal is attained. This can be explained by looking at the

acoustic wave as a pressure wave being transmitted across two surfaces in contact with

one another (Pollock 1995). Without the medium, only a few contact points exist

between the sensor pad and the surface, causing the pressure to only be transmitted

through these points. With the medium (couplant) employed, the pressure is able to

consistently transfer from one surface to the other. High-silicone vacuum grease has

been successfully used to obtain good contact between the test surface and the sensors

(Yepez 1999). To finish the mounting of the sensors, the cables that connect the data

acquisition system and the sensors must be secured. This is done to prevent slippage of

the sensor and possible interference from the sensor cable. Some sort of hold-down

device should be used to keep the sensor in place during the testing procedure. The hold-

down device can also protect the sensor from environmental hazards and act as an

insulator for the sensor (Pollock 1995).

Once the testing equipment is in place, a calibration test should take place to

ensure that all the equipment is in proper working order. A calibration test can also be

used to identify sensors that have higher or lower sensitivities. The preferred technique

for conducting calibration tests is the pencil-lead break test. A standard calibration

procedure for the sensors is specified in ASTM E 2374, where a 2H, 0.5 mm diameter,

mechanical-pencil lead is broken as shown in Figure 2-4.
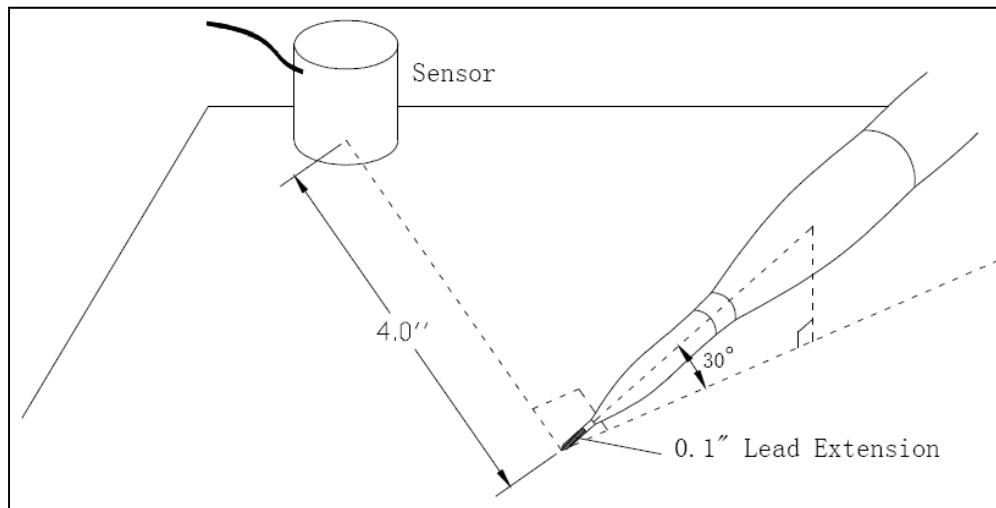
Figure 2-4: Calibration of AE sensor (Pollock 1995)

As the lead is pressed against the surface, a small deformation occurs, which is relieved

once the lead is broken. The breaking of the lead produces a short-duration, localized

impulse that is quite similar to a natural acoustic emission source (ASNT 2005). The amplitude of the lead break source is also well within the range of typical crack sources (CARP 1999).

Once the system is calibrated, the environmental conditions must be considered. Any ambient noise that may affect the AE data should be noted and threshold limits should be used to limit the effect of such noise. Any change in background noise should be noted by the AE testing operator. Any other changes in testing, such as traffic patterns, weather, or procedural modifications should also be noted. If possible, the changes should be time stamped so that the corresponding data can be reviewed during the post-test analysis (Pollock 1995).

Acoustic emission is a measure of damage growth. Because of this fact, it is a load-history dependent test procedure (Ohtsu 1989). Therefore, the method of load application must be designed so that proper data are recorded. The testing procedure should have a detailed schedule of load application including magnitude of load and location.

Before any load testing is conducted, a background check should be conducted for a predetermined amount of time (Ridge and Ziehl 2006). The specimen should remain undisturbed during this period. Normal ambient noise should be measured and noted for post-test analysis purposes. After load testing, there should also be a similar period during which the structure remains undisturbed. Analysis of any emissions measured during this period may indicate if significant changes have been made to the structure during testing.

During load testing, the data should be displayed so that real-time analysis can take place. This is used to make sure that the testing proceeds as planned and to ensure that data are being obtained correctly. The display may also alert the operator in the event of an imminent failure. This is crucial for the safety of the testing crew. Because the data are also stored by the acquisition system, any complex analysis can be performed later.

Sensors should be removed once testing is complete. To prevent sensor damage, sensors should be removed prior to sudden or catastrophic specimen failure if the AE test is performed in conjunction with destructive testing.

The acoustic emission testing setup can be used in a variety of different ways depending on the needs of the experiment. The procedure described in this chapter is a general procedure that has been used in the testing of structural concrete members. However, this procedure and setup can be modified to test a number of different materials in a number of different ways. Ultimately, this procedure is one of many different options for acoustic emission testing.

Chapter 3: History of Acoustic Emission Testing and Applications to Structural Concrete

3.1 Early Observations

This chapter contains a brief overview of acoustic emission testing, beginning with early observations of acoustic emission and concluding with modern day techniques. It also includes a discussion on how acoustic emission testing/monitoring has been applied to engineering materials, as well as a focused review of how acoustic emission has been applied to assess structural concrete behavior.

3.1.1 Recording Acoustic Emission

Acoustic emission and microseismic activity occur naturally. It is not known exactly when the first acoustic emissions were heard, but the snapping of twigs, cracking of rocks, and breaking of bones were probably among the earliest observations (ASNT 2005). The first observations of acoustic emission in metals were the audible emissions produced by mechanical twinning of pure tin during plastic deformation. This phenomenon is known as "tin cry." The transition from the incidental observation of tin cry to the deliberate study of the acoustic emission phenomenon consisted of a few separate and unrelated experiments in which instrumentation was used to detect, amplify, and record acoustic emission events occurring in test objects (ASNT 2005).

The first of these experiments was conducted in 1933 by a seismologist by the

name of Fuyuhiko Kishinouye. His experiment, performed in Japan, was a study on the

fracture of the earth's crust due to earthquakes. His experiment was designed to amplify

and record the acoustic emission from the fracture of wood (Kishinouye 1932). The

oscillograms made by Kishinouye showing the "inaudible vibrations and cracking sounds

from fracture of wooden board" were recordings of acoustic emission waveforms

(Kishinouye 1937).

Around the same time as Kishinouye's testing, another series of experiments was

conducted in Germany. Friedrich Förster and Erich Scheil designed experiments dealing

with the measurement of extremely small voltage changes and resistance variations

produced by sudden, jerky strain movements caused by transformations in a wire-shaped,

nickel-steel test specimen (Förster and Scheil 1936). For the testing, Förster designed an

electrodynamic transmitter and receiver system to convert mechanical vibrations and

acoustic emission into electrical voltages that could be amplified and recorded (ASNT

2005).

In the United States, Warren P. Mason, Herbert J. McSkimin, and William

Shockley performed and published a series of acoustic emission tests in 1948. The

experiment consisted of pressing a specimen of pure tin directly against a quartz crystal

transducer and then applying stress to deform the specimen and cause dislocation, which

produced acoustic emission (Mason et al. 1948).

Another instrumented experiment was performed in the United Kingdom. D.J.

Millard conducted twinning experiments on single crystal wires of cadmium. For this

experiment, the twinning was detected using a Rochelle salt transducer (Millard 1950).

Microseismic activity, which is identical to the AE phenomenon, was also being

studied around the same time. Leonard A. Obert reported the discovery of microseismic emissions in rocks (Obert 1977). In 1938, he was conducting seismic velocity tests in mines in northern Oklahoma. Throughout the tests, signals kept causing interference with the equipment. He eventually deduced that the interference was caused by self-generated signals in the rock. Obert clarified that microseismic activity could be detected in controlled environments (Obert and Duvall 1945).

3.1.2 Founders and Terminology

Although the work was a necessary step in understanding the phenomenon of acoustic emission, the early observations of audible sounds and the instrumented experiments were not primarily directed at a study of acoustic emission itself. Even after the tests, the researchers did not carry on any further studies into the field of acoustic emission. Instead, the beginning of today's technology of acoustic emission testing was the work of Josef Kaiser in Germany (Henning 1988).

In 1955, Kaiser published his dissertation in which he reported the first comprehensive investigation into the phenomenon of acoustic emission. Kaiser used tensile tests of different materials to determine the acoustic processes involved and the noises generated within each material. He also explored the frequency levels involved in each test and the relationship between those frequencies and the stress-strain curve for each material (Kaiser 1950). His most significant discovery, however, was the irreversibility phenomenon that is now known as the *Kaiser effect*. Kaiser's conclusions included a distinction between continuous and burst emission as well as some of the causes of acoustic emission.

The first extensive research conducted after Kaiser's work was completed in the

United States during the 1950s. In 1954, Schofield initiated a research program that focused on acoustic emission in materials engineering. His main purpose was to verify the findings of Kaiser's work and to determine the source of acoustic emission (Schofield et al. 1958). In addition to verifying Kaiser's work, Schofield's most important conclusion was that acoustic emission was mainly a volume effect and not a surface effect. Schofield published his pioneering work in 1961 and used the term "acoustic emission" in the title, marking the first use of the terminology in history (Schofield 1961).

3.2 Acoustic Emission in Concrete Engineering

Three papers, dating back to the 1960s, are well known in concrete technology dealing with acoustic emission. H. Rüsch's work focused on the noise emitted during the application of compressive load in concrete. This was one of the first studies on the Kaiser effect in engineering materials (Grosse and Ohtsu 2008). Rüsch determined that the Kaiser effect was observed up to around 75% of the compressive failure load. He also reported that the behavior of AE signals was related with a volumetric change (Rüsch 1959).

Under compressive loads on concrete, R.G. L'Hermite found a relationship between wave velocity, AE generation, and Poisson's ratio. Following observed AE activity, both Poisson's ratio and axial strain start to increase, while the wave velocity in concrete decreases (L'Hermite 1960). Robinson (1965) further compared AE behaviors with X-ray observations. The work done by Rüsch, L'Hermite, and Robinson began a much broader exploration into the AE phenomenon within engineering materials such as concrete. Future research would look into testing procedures in which acoustic emission

could be used to rate the integrity of structural elements made with these engineering materials.

3.3 Acoustic Emission in Reinforced Concrete

The increase in aging structures and catastrophic failures has caused a demand for maintenance and retrofitting of reinforced concrete structures in service. The development of nondestructive testing procedures allows engineers to test the integrity of a structure while in service. Therefore, AE techniques are a great asset to engineers (Grosse and Ohtsu 2008).

Acoustic emission waveforms and the relationship between strain measurement and acoustic emission events were studied by D. Wells in 1970. Studies exploring the fundamentals of AE activity and the effects of mixture proportioning were conducted by multiple groups of people in the late 1970s and early 1980s.   Frequency and source location analyses were performed starting in the 1970s and continued on to the late 1990s (Grosse and Ohtsu 2008). Applications to reinforced concrete were investigated in the late 1970s and continue to be researched today. The work done by Y. Niwa, S. Kobayashi, and M. Ohtsu in 1977 was some of the first work dealing with reinforced concrete. These studies have resulted in practical testing procedures to monitor cracking and assess damage in concrete structures (Grosse and Ohtsu 2008).

The results of testing have shown that there exists a potential for the prediction of failure mode of reinforced concrete beams by AE observation. In the case of under-reinforced beams, sliding between reinforcement and concrete was observed due to yielding of the reinforcement. As a results of this failure, AE count rate increases drastically. In contrast, over-reinforced beams withstand steel failure and have a constant

AE event rate until the final failure. These results show that AE events are sensitive to the type of reinforcement in a structure (Grosse and Ohtsu 2008).

The main challenge for determining the structural integrity of a test object is in the interpretation of the acoustic emission data. In order to assess the damage levels of reinforced concrete beams, many researchers have used a criterion based on two ratios associated with the Kaiser effect. Most studies have consisted of testing reinforced concrete beams which have been damaged under incremental cyclic loading. The Kaiser effect is very closely related to structural stability; therefore, AE activity is very low in a stable structure. To estimate the Kaiser effect, two ratios, most commonly the *load ratio* and *calm ratio*, are used (Grosse and Ohtsu 2008).

According to the NDIS-2421 quantitative assessment criterion, proposed by Ohtsu et al. (2002), the structure is subjected to load cycles during which AE activity is measured. The structural integrity and damage level is classified based on the load and calm ratios. NDIS-2421 defines the load ratio as the "ratio of the load at the onset of AE activity in the subsequent loading to that of the previous load." The calm ratio is defined as "the number of cumulative AE activities during the unloading process to that of the last loading cycle up to the maximum." Based on these definitions, it can be deduced that the load ratio could become larger than 1.0 in a very sound structure. As damage accumulates, the ratio drops below 1.0 due to AE events occurring at lower loading levels than before (Grosse and Ohtsu 2008).

Damage classification boundary levels can be established based on the load and calm ratios. Figure 3-1 shows a plot of the classification of damage in accordance with these two ratios.
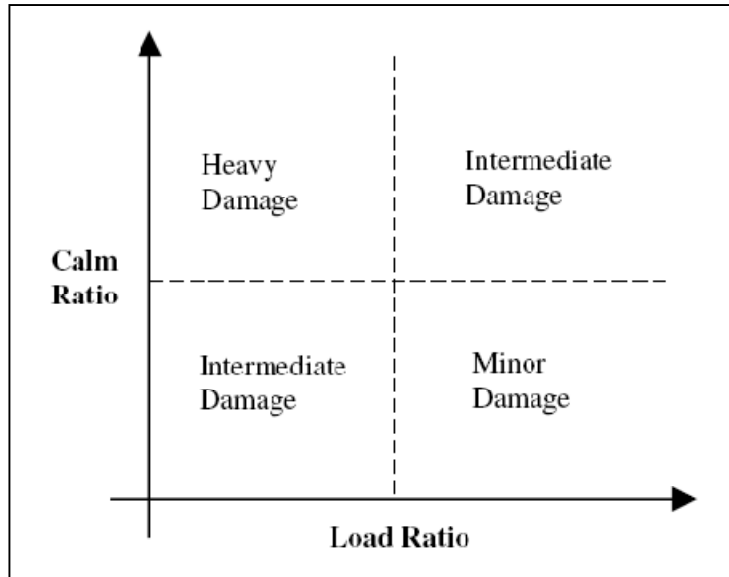
Figure 3-1: Classification of damage recommended by NDIS-2421 (Ohtsu et al.

2002)

In the research of Ohtsu et al. (2002), these boundary levels were proposed as 0.05 for the

calm ratio and 0.9 for the load ratio. To test these values, reinforced concrete beams

were tested using a cyclic load test. Crack-mouth opening displacements (CMOD) were

used to define the level of damage for each specimen. A CMOD of 0.1 mm (0.004 in.)

was selected as the transition value from "minor" to "intermediate" damage, while values

higher than 0.5 mm (0.02 in.) were deemed as "heavy" damage.

A plot of the load ratio versus the calm ratio allows for four zones to be created.

These zones specify damage levels based on the different specimens. Figure 3-2 shows a

plot for a group of specimens with the specified assessment levels.
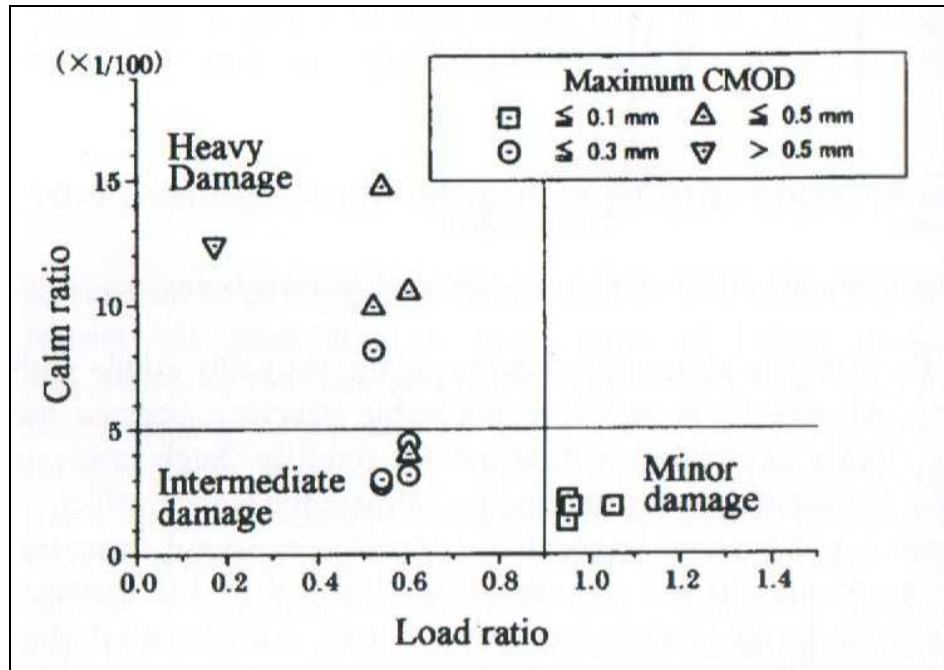
Figure 3-2: Classification of AE data by load and calm ratio (Ohtsu et al. 2002)

As can be seen in Figure 3-2, the data plotted was reasonably classified in good

agreement with the maximum CMOD values. It is, however, interesting to note that

crack widths up to 0.4 mm are described as acceptable under service loads in the

commentary (R10.6.4) to ACI 318 (2008), even though some of these points fall into the

heavy damage quadrant according to the NDIS-2421 damage assessment. According to

the commentary, crack widths in a structure are highly variable. Prior to ACI 318-99,

provisions were given for distribution of reinforcement that was based on empirical

equations using a calculated maximum crack width of 0.016 in. (0.406 mm). The current

provisions for spacing are "intended to limit surface cracks to a width that is generally

acceptable in practice but may vary widely in a given structure" (ACI 318 2008). The

general agreement between the NDIS-2421 criterion and the CMOD data indicated that

the damage levels of reinforced concrete beams can be qualified by the criterion based on

the load ratio and the calm ratio when monitoring AE activity under cyclic loading

36

(Grosse and Ohtsu 2008).

Another ratio has been used to determine the damage of reinforced concrete beams. Colombo et al. (2005) used the *relaxation ratio* and focused on the AE activity recorded during the unloading process. The relaxation ratio, in the research, was defined in terms of energy: the ratio of the average energy during unloading to the average energy during loading. The average energy was calculated by taking the cumulative acoustic emission energy recorded during each phase and dividing by the total number of recorded sensor hits. Since an average energy was taken for this assessment, there were no complications in dealing with the time of the individual processes. This research was based on the principle that AE activity during unloading is an indication of structural integrity (Grosse and Ohtsu 2008). In the case that the structure under consideration is stable, very little AE activity is observed during the unloading process. However, if the structure under consideration is not stable, there should be a considerable amount of AE activity during the unloading process. According to the results of flexural tests on several reinforced concrete beams, the relaxation ratio values were closely related to the percentage of the ultimate failure load that was reached in a specific cycle. An example figure from this research of a beam specimen can be seen in Figure 3-3.
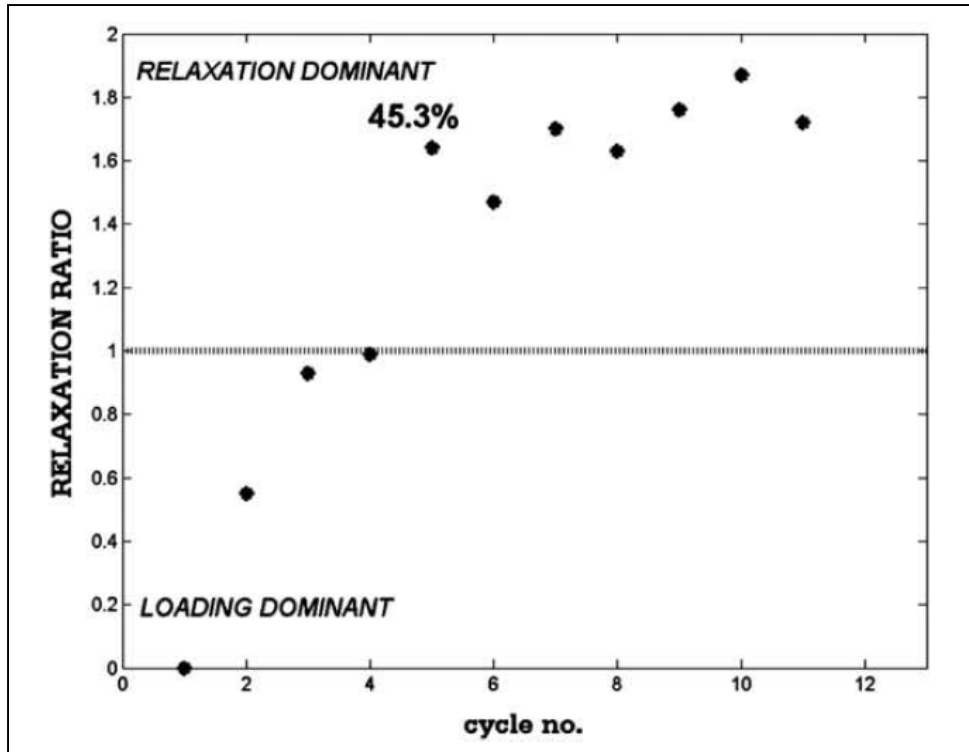
Figure 3-3: Relaxation ratio results (Colombo et al. 2005)

As seen in the figure, Colombo et al. (2005) defined two specific regions; loading dominant and relaxation dominant. Initially, the loading phase is dominant (average energy produced during loading is greater than average energy produced during unloading) and the values of the relaxation ratio all lie below the dotted line. A change of trend occurs when the load reached approximately 45% of the ultimate failure load of the specimen. At this point, the relaxation phase becomes dominant, meaning that more energy is being produced during the unloading phase compared to the loading phase. Since the change in behavior is related to a percentage of load, the relaxation ratio could be used to assess the damage in the beams. It was determined that a relaxation ratio greater than one described a beam that had experienced damage (Colombo et al. 2005).

Ridge and Ziehl (2006) proposed an evaluation criterion based on the peak

cumulative signal strength (CSS) ratio. This ratio is defined as the peak CSS at the end of the reload hold period divided by the peak CSS at the end of the initial load hold period. A sample loadset can be seen in Figure 3-4.
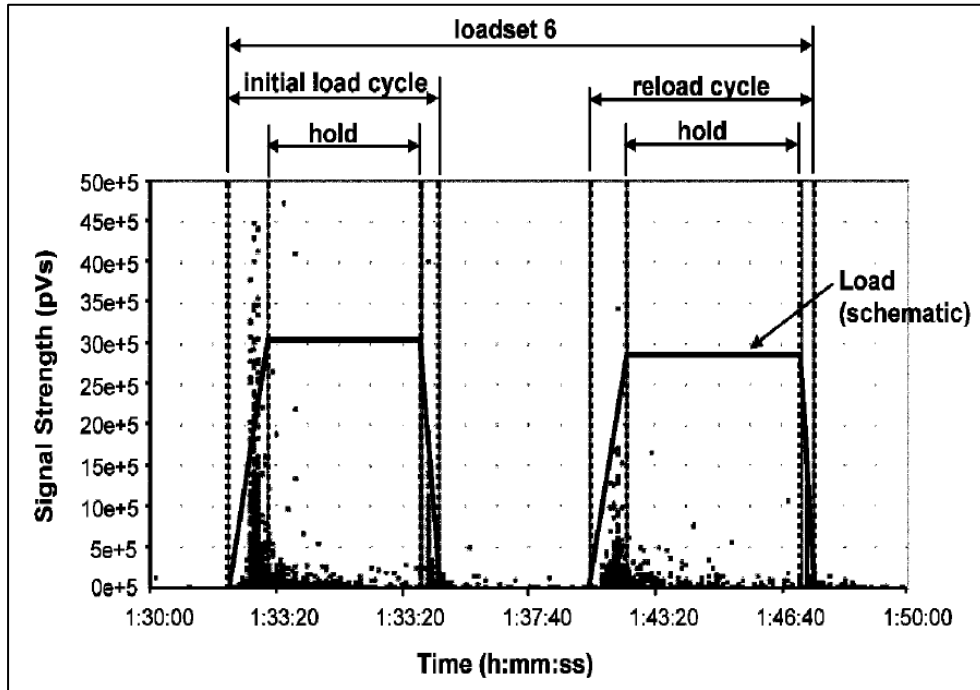
Figure 3-4: Signal strength versus time (Ridge and Ziehl 2006)

As seen in the above figure, a load hold occurs as a load was applied to a specimen and held constant for a set period of time. A reload hold period was a hold period that occurs after the magnitude of the load of the original hold period was reduced to zero and increased back to a specified load and held for a specified time. The benefit of this evaluation method was the fact that the data were taken during the load holds as opposed to during the periods of changing load intensity. Figure 3-4 also shows the signal strength of AE hits being produced due to the load applied. Loadsets, each consisting of two load cycles, were used to test six reinforced concrete beams that were strengthened with carbon-fiber-reinforced polymer (CFRP). A hold period of four minutes was used

for each loadset to provide a suitable period for evaluation of the rate of AE activity and to provide a period of evaluation that was free from "nongenuine" AE. Nongenuine AE, such as mechanical rubbing or friction, comes from secondary sources of emission and can be detrimental to post-test data analysis. The peak load used for all of the reloading sequences was slightly less than the original load to ensure that no new cracks were formed during the reloading process. The AE data were analyzed for two strengthened specimens—one strengthened with procured CFRP strips and the other with unidirectional CFRP fabric. The results of these tests showed that the ratio of peak CSS obtained during a reload hold to peak CSS obtained during an initial load hold may be a useful measure of damage. The CSS results from loadset 6 are shown in Figure 3-5.
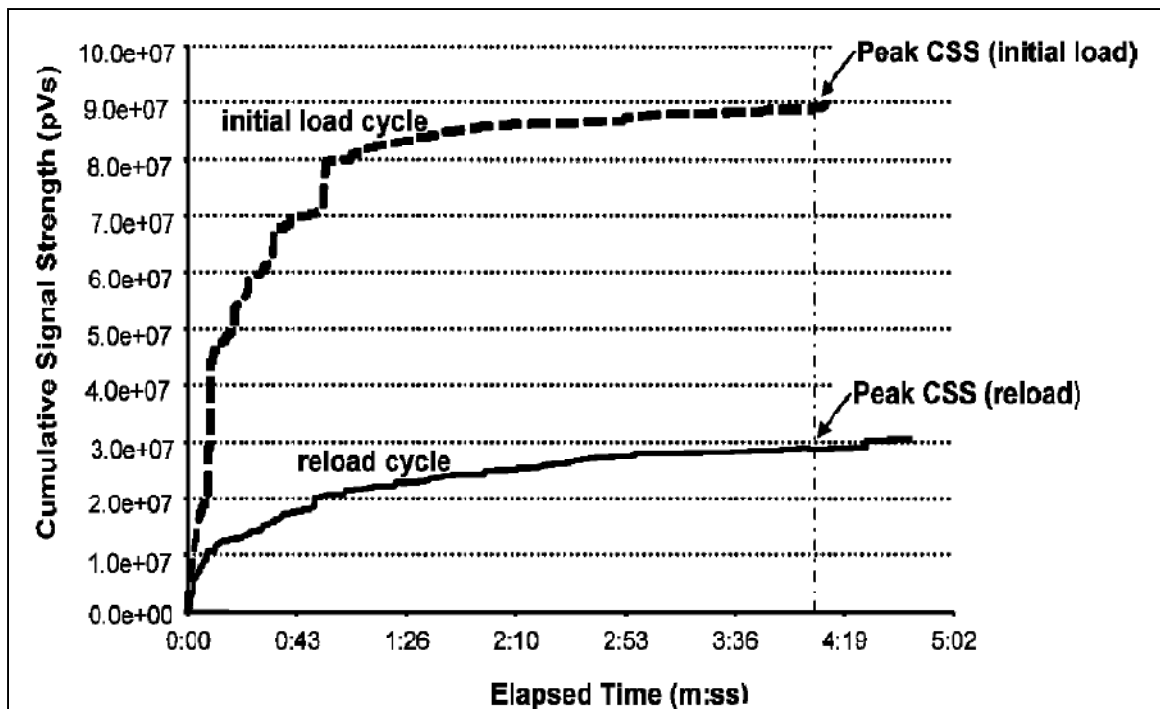
Figure 3-5: CSS during initial load hold and reload hold (Ridge and Ziehl 2006)

The results showed that for both of the strengthened specimens, a peak CSS ratio between 30 and 50% was an appropriate value to select as an indication of significant

damage. Ridge and Ziehl also stated that the evaluation criterion was purposely based on a ratio because criteria that are based on absolute measures are more heavily dependent on the sensitivity of individual sensors and attachment methods. Comparison of the cyclic load test (CLT), as described in Appendix A of ACI 437R-03, and the AE methods showed that although both methods provided an effective means of damage detection, the AE method provided increased sensitivity in some cases.

Ziehl et al. (2008) continued looking at damage assessment for other concrete structures. Their work focused on the application and interpretation of the evaluation criteria adopted for the in-situ assessment of two structures; a parking garage and a building. For each study, the evaluation criteria of interest were those associated with the CLT and AE methods. The research regarding the AE testing used two previously mentioned evaluation criterion. The first was the NDIS-2421 criterion proposed by Ohtsu et al. (2002) based on the calm ratio and load ratio. The second was the peak CSS ratio proposed by Ridge and Ziehl (2006). This study confirmed the results from the original studies. Ziehl et al. (2008) also proposed a new technique of damage assessment in which the CLT method and AE studies could be used in unison. A *global performance index* was defined based on the evaluation criteria for the CLT method; namely the permanency, repeatability, and deviation from linearity; and the AE evaluation criteria of load ratio versus calm ratio and the peak CSS ratio. The proposed global performance index was used to evaluate the ultimate capacity margin (UCM) for the load tests performed on both structures. The UCM is defined as "the margin between the ultimate capacity of a specimen and the load at which a criterion failed" (Liu and Ziehl 2009). Therefore, a specimen failed a load test once a limit on one of the criterion was reached.

41

For instance, when conducting the CLT method, once the limit for the permanency, repeatability, or deviation from linearity criterion had been reached, the specimen had failed the test. The proposed UCM index, when experimentally validated and available, would allow engineers to quantify how much reserve was left in the structure once it failed the test by reaching one of the proposed limits.

Liu and Ziehl (2009) continued the work done previously by exploring the cyclic load test and acoustic emission methods of evaluation applied to 14 reduced-scale reinforced concrete beam specimens. These specimens represented different cases in terms of failure mode (flexure and shear), loading pattern, concrete mixture design (normal and self-consolidating concrete), and resulting material properties. In addition, five acoustic emission evaluation methods were investigated to determine their ability to assess the damage level in the reinforced concrete beams. The five AE performance measures selected for this testing included the following: load ratio, calm ratio, relaxation ratio, cumulative signal strength (CSS) ratio, and a combination of load ratio and calm ratio. There were interesting test results for the different cases involved. The load ratio consistently decreased with increasing loadsets. This measure was more useful than others for assessing post-yield damage but there was some difficulty in differentiating between pre- and post-yield damage. The calm ratio was relatively stable and increased with loadsets up to yield. However, it was not compatible to post-yield evaluation. The relaxation ratio provided very similar results to the calm ratio for the flexure-critical specimens, but there was no clear trend for the shear-critical specimens. The calm ratio offered more consistent results compared to the relaxation ratio. The CSS ratio did not offer stable results like the load ratio and calm ratio. It seemed to be

affected by the concrete material type, as well. The most important conclusion was that the combination of calm ratio and load ratio offered the most consistent results, and was considered the best measure of damage for the concrete specimens. This conclusion shows that using the NDIS-2421 evaluation criterion is the best approach when determining the damage of a specimen. A general conclusion regarding the AE data was that all the measures were affected moderately by concrete material type (conventional or self-consolidating) and loading pattern (CLT or a simplified version of the CLT pattern). As found in previous studies, Liu and Ziehl concluded that the AE and CLT methods are complementary methods that provide different types of data. They suggested that an approach that combines the two methods of evaluation may be more promising than one that uses a single method.

Nair (2006) conducted research that focused on developing quantitative measures of evaluation for the structural integrity of reinforced concrete. The study applied the intensity analysis technique of quantitative assessment for other materials, such as metals and fiber-reinforced polymer, to conventional AE data parameters from reinforced concrete beam specimens. The intensity analysis generated plots using the historic index, a measure of the change in AE activity, and severity values, a measure of signal strength during load tests. Nair used this technique in determining the condition of reinforced concrete beam specimens in a laboratory setting. Post-test analysis of the AE data showed that the intensity analysis technique helped to quantify and better understand the damage intensity in the beams. The same analysis was used for two separate field tests; a concrete bridge and a steel bridge. Similar results to the laboratory research were obtained from members of the two bridges. The results from both the laboratory and

field testing emphasized the need to develop standardized intensity charts and procedures to quantify damage in reinforced concrete members (Nair 2006).

3.4 Acoustic Emission in Prestressed Concrete

The use of acoustic emission testing in prestressed concrete structures has been going on for a number of years, but most of those studies dealt with smaller specimens in controlled environments. The considerable amount of deterioration in the condition of road infrastructure has caused a demand for more realistic testing of in-service bridges and a comparison of the testing done on reinforced concrete systems to that of prestressed concrete systems.

According to Vogel et al. (2006), acoustic emission testing has more potential for fully prestressed structures than for reinforced concrete structures. This is justified by the fact that cracking in reinforced concrete structures is normal and "little matter of concern." In prestressed concrete structures, however, cracks do not normally exist due to prestressing and the formation of new cracks during service life is a key issue. These cracks may be an indicator of bad performance and other serious problems. Fowler et al. (1998) agreed with this statement based on the fact that tension zone cracking in reinforced concrete is a significant source of emission. This emission masks more significant emission associated with structural damage. Because of this, tension zone cracking has made the application of AE testing in reinforced concrete difficult.

One of the more telling experiments done in the comparison of reinforced versus prestressed concrete specimens using acoustic emission was done by Hearn and Shield (1997). Their goal was to test three conventionally reinforced and two prestressed concrete beams by cyclically loading them until failure. The crack initiation and

propagation was monitored using acoustic emission and compared to visual observation. The comparison in AE behavior between the conventionally reinforced and prestressed concrete beams was discussed and evaluated. As in reinforced concrete acoustic emission testing, the observed formation of cracks in concrete was preceded by a significant increase in AE activity rate in the prestressed specimens. The main difference between the AE activity for the two specimens took place during the unloading process. For the prestressed beams, there was extensive AE activity during the unloading process. For the reinforced beams, however, very little or no activity was recorded during the unloading cycles. These test results also indicated that there was a slight violation of the Kaiser effect at all load levels for the prestressed specimens. Hearn and Shield also suggested that, although acoustic emission testing is a viable tool for both reinforced and prestressed concrete beams, the method may be easier to develop for use with prestressed concrete structures (Hearn and Shield 1997).

A more detailed report of this research yielded more information between the differences in AE activity between the reinforced and prestressed concrete specimens. Shield (1997) graphically represented the results from the experiment in two figures. As shown in Figure 3-6, AE activity for the loading/unloading cycle for an ordinary reinforced beam began after previously applied deflection levels are exceeded. It continued during the time when the deflection was held constant, and there was no activity during unloading.
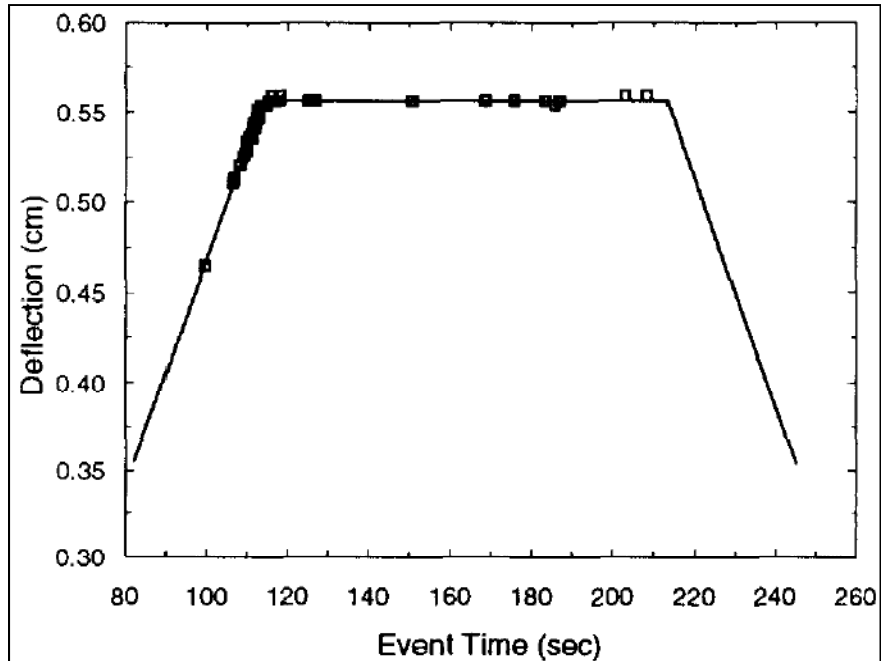
Figure 3-6: Recorded AE events versus actual loading cycle history for an ordinary reinforced beam (Shield 1997)

Figure 3-7 shows the AE activity for the loading/unloading cycle for the prestressed beam. As can be seen, AE activity began when prior deflection levels were exceeded and continued until maximum deflection level was reached. There was no activity when the deflection level was held constant, but there was activity during the unloading, or crack closure, period.
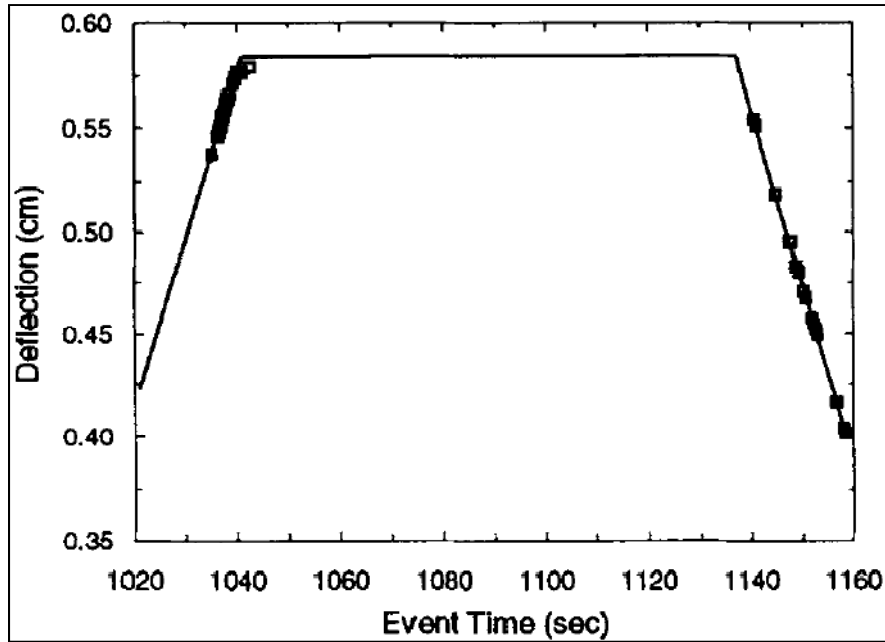
**Figure 3-7: Recorded AE events versus actual loading cycle history for a
prestressed beam (Shield 1997)**

Shield hypothesized that the differences in AE behavior were a direct consequence of the

two reinforcing methods. For the ordinary reinforced beams there was a "continuing

transfer of stress from the concrete in tension to the reinforcing steel (Shield 1997)."

This caused the AE activity during the time when the deflection was held constant. For

the prestressed beam, however, the tensile stresses were all taken by the prestressing

steel, which explained no AE activity during the hold period. During unloading, there

was significant AE activity due to the two surfaces being forced together under the effect

of the prestressing force. The force causing crack closure was much smaller in ordinary

reinforced beams and was generally not large enough to generate AE activity (Shield

1997).

Yuyama et al. (2007) explored the use of acoustic emission in the evaluation of

failures in high-strength tendons of prestressed concrete bridges. The failure was mainly

attributed to the corrosion induced in severe environments by salt attack. Some

interesting results were presented from the experiment. First, it was proven that AE was

a very useful technique in detecting and evaluating the failures of the high-strength steel

tendons. It was also shown that, in post-tensioned beams, the acoustic emission

reliability was dependent upon the grouting condition. It was shown that for unbonded

and partially grouted beams, the AE returned extremely accurate source locations for the

wire breaks. The fully grouted beams, however, did not return as accurate results due to

the complicated wave paths through the grouted ducts. This experiment also showed that

there was a clear difference in the signals transmitted by failures compared to those of

environmental and background noise (Yuyama et al. 2007).

The sources that cause AE activity in prestressed concrete are slightly different

from those in ordinary reinforced concrete. On tests of prestressed concrete girders

reported by Fowler et al. (1998), three sources of emission were investigated: shear-

induced cracking in the web, flexural cracking at the region of maximum moment, and

strand slippage at the anchorage zone. These emission sources were examined by placing

sensors in the critical areas and monitoring the emission from each area. As seen in

Figure 3-8, one sensor was located at the end of the beam to monitor strand slippage, four

were located in the shear zone, and two on the bottom of the beam to monitor flexural

cracking.
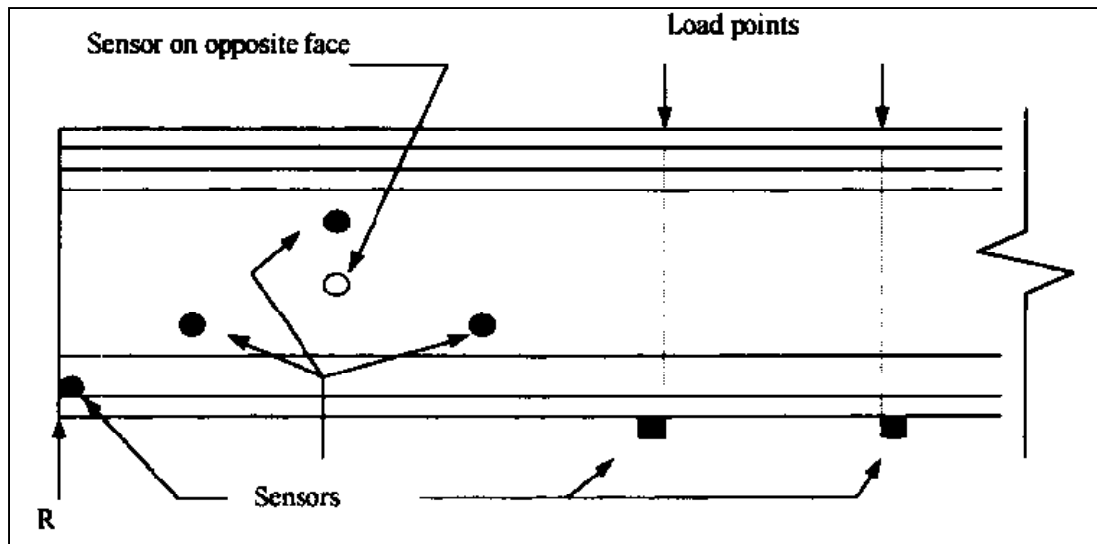
Figure 3-8: Sensor locations for load tests (Fowler et al. 1998)

During the testing, the sensors located in the flexure zone produced significant emission first, while a massive burst of emission occurred at the time of the first shear crack. The different types of AE sources need to be considered when dealing with prestressed concrete specimens. Fowler et al. (1998) contended that AE can not only be used to detect damage in a prestressed beam, but also to distinguish the difference between shear and flexural cracks.

3.5 Summary

Acoustic emission monitoring has been used on a variety of different materials in a multitude of different ways. After reviewing the relevant literature, it was seen that certain testing procedures have proven to be more effective in the field of structural concrete. Some type of cyclic loading (load and reload) should be used to evaluate the emission from certain types of failures at different load levels. Also, certain evaluation criteria have been proven to be more effective, as well as more feasible, than others. For instance, the use of the peak CSS ratio seems to be an easy way to quickly conduct a

damage assessment for a concrete specimen. The one important factor that seems to be consistent throughout most of the literature, however, is the adaptation of the acoustic emission method to the specific details of the project. In most of the research done thus far, the acoustic emission procedure has been amended to satisfy the conditions of the test. For this current research project, the AE procedure was adapted for the I-565 bridge girders to obtain useful data.

Chapter 4: Acoustic Emission Testing of Repaired Prestressed Concrete Bridge Girders

4.1 Introduction

The elevated portion of the I-565 highway in Huntsville, Alabama was constructed from January 1988 to March 1991. The structure consists of several spans supported by prestressed concrete bulb-tee girders that were designed to be continuous for live load. Soon after completion, wide cracks formed in many of the girder ends close to the continuity diaphragms. It was determined that restrained thermal deformations of the superstructure were the main cause for the cracking and that inappropriate reinforcing details in the girder ends contributed to the location and severity of the cracking (Gao 2003). The progression of the cracks has been closely monitored by the Alabama Department of Transportation (ALDOT) and several remediation techniques have been installed. False supports were installed near the bents supporting the cracked ends of the girders. This was done to prevent a total collapse in the event of girder failure. The supports are currently still in place, but add no structural strength to the bridge. They are simply there to support the structure in the event of girder failure. To try and prevent further propagation of the cracks, epoxy was injected into the existing cracks to seal them. Although this seemed to work for the existing cracks, new cracks formed adjacent to many of the epoxy-treated cracks (Swenson 2003, Fason and Barnes 2004).

Based on findings by ACI Committee 440 (2002), externally bonded fiber-reinforced polymer (FRP) reinforcement had proven effective for the strengthening of reinforced concrete structures. Therefore, Swenson (2003) proposed a repair using externally bonded, FRP reinforcement to counteract the potential strength deficiencies caused by the cracking in the bulb-tee girders. The FRP reinforcement was installed in December 2007.

Prior to the use of the FRP repair, Xu (2008) performed acoustic emission testing to determine the structural integrity of the system. Up to this point, most AE testing was done in the laboratory and not many tests had been conducted on in-service concrete bridges. Xu's main goals were to evaluate the effectiveness of the AE testing procedure in determining the structural integrity of the girders. To do this, the results of the AE testing were compared to the conventional strain-deflection testing technique (Xu 2008).

The experiment performed for this project had similar goals to Xu's testing in 2005. The testing procedure was very similar so that pre-FRP repair test results could be compared to post-FRP repair results. These results were used to determine if the AE testing indicated that the FRP repair had improved the structural integrity of the bridge girders. The relationship between the AE data and the FRP repair was also explored, and the different effects the FRP repair had on AE monitoring were identified.

4.2 Research Significance

The increasing deterioration of the civil infrastructure of the United States has greatly increased the amount of testing done on in-service roads and bridges. Since the roads and bridges are in service, non-destructive testing has become increasingly

important. Most of the deterioration can be attributed to the age of bridges, but other factors can affect the integrity of such structures.

Acoustic emission testing has proven to be a good testing procedure to determine the integrity of concrete specimens (Ohtsu et al. 2002; Ridge and Ziehl 2006). By comparing the results of the pre-repair testing to the post-repair testing, a conclusion was made about the impact the fiber-reinforced polymer repair has had on the integrity of the bridge girders. The comparison also gave insight into the different AE responses that were caused by the FRP compared to conventional reinforced or prestressed concrete girders.

This thesis research can be used as another experiment that shows the effectiveness of acoustic emission testing in concrete structures. The field testing also provided some important data that will be used to determine the similarities between laboratory and in-situ testing. Finally, this research gave an idea on the effectiveness of AE testing in determining the integrity of a structure after repair, and allowed for further experimentation in determining the effectiveness of the repair itself.

4.3 Acoustic Emission Evaluation Criteria

4.3.1 NDIS-2421 Criteria

The Japanese Society for Nondestructive Inspections adopted the NDIS-2421 quantitative assessment criterion to establish a more standard damage assessment (Ohtsu et al. 2002). The damage levels are evaluated based on two ratios related to the AE activity recorded during the testing. The load ratio is the ratio of load at the onset of AE activity to the previous load. The calm ratio is the ratio of cumulative AE activity during the unloading process to that of the last maximum loading cycle. In using these two

ratios simultaneously, a damage assessment can be accomplished by setting limits based upon laboratory testing. As seen in Figure 3-1, data points can be plotted and the type of damage can be determined by the plot. Ohtsu et al. proposed that the classification boundaries in Figure 3-1 to be 0.05 for the calm ratio and 0.9 for the load ratio. The AE data from the most active channel is used for plotting.

4.3.2 Signal Strength Moment Ratio Evaluation

The results of the pre-repair test depend on the Signal Strength Moment (SSM) Ratio evaluation criterion. A brief overview of this criterion is presented here, and a more detailed description of the method is discussed in Chapter 5. The SSM Ratio method uses a time-weighted approach for analyzing the AE signal strength during a load hold. SSM is the summation, over a period of sustained load, of the product of the signal strength associated with each hit by the time elapsed from the beginning of the load hold. In another form, the signal strength moment is defined as:

$$\text{SSM} = \sum_{i=1}^{n} t_i S_i \qquad \qquad \text{(Eq. 4-1)}$$

Where n is the total number of hits occurring during the load hold, t_i is the time from the beginning of the hold to the ith hit, and S_i is the signal strength occurring in the ith hit (Xu 2008). Based upon Xu's laboratory results, it was found that a greater SSM value is indicative of a situation in which the AE activity increases during a hold period. The SSM Ratio is defined by the following equation:

$$\text{SSM Ratio} = \frac{\text{SSM}_{\text{second night hold period}}}{\text{SSM}_{\text{first night hold period}}} \qquad \qquad \text{(Eq. 4-2)}$$

The SSM ratio provides an indication of the progression of damage as the load intensity increases (Xu 2008).

4.4 Experimental Procedure

4.4.1 Preliminary Investigation

The Interstate 565 Bridge consists of several prestressed concrete bulb-tee girders that were designed to be continuous for live load. The bridge deck is composed of cast-in-place reinforced concrete. Figure 4-1 shows a cross sectional view of the bridge structure. The bridge deck is 70.8 ft. (21.6 m) wide with a thickness of 6.5 in. (165 mm), not including the variable depth build-up over each girder. The bridge deck was designed to act compositely with the girders by extending the girder stirrups into the deck slab (Swenson 2003). The nine girders are spaced at 96 in. (2.4 m) center to center. Figure 4-2 presents the girder cross section.
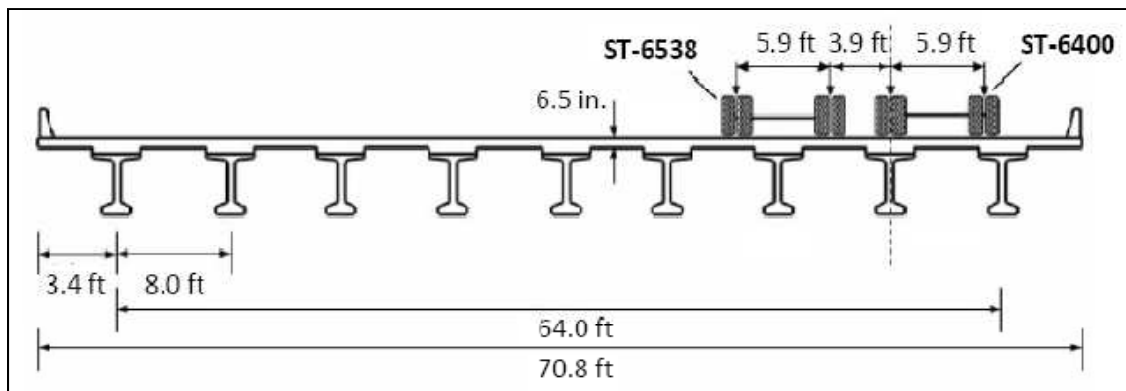
Figure 4-1: Bridge cross section and transverse position of test trucks (Fason and Barnes 2004)
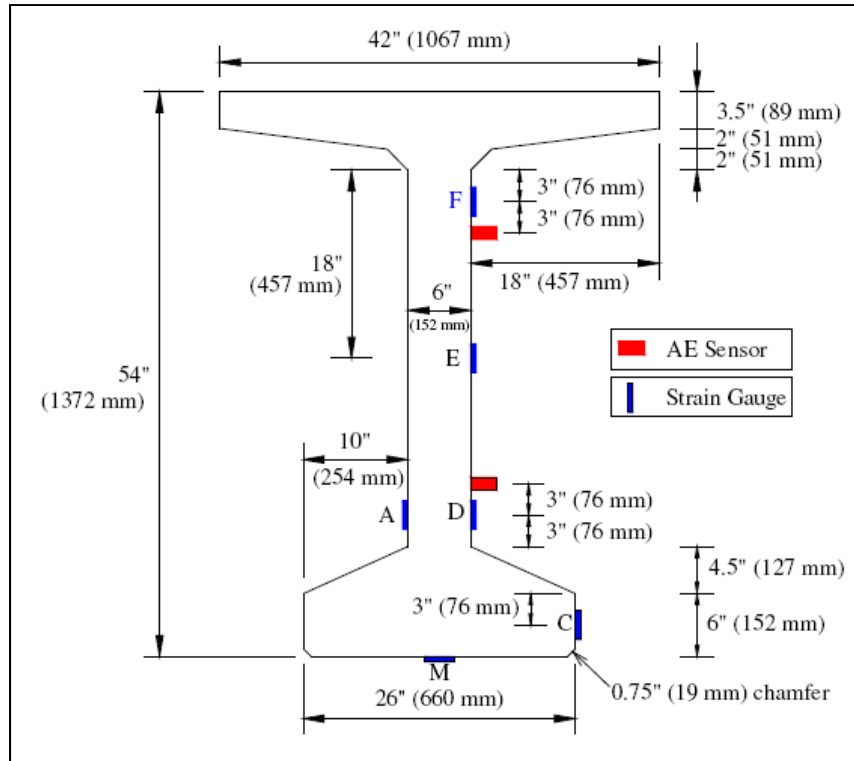
Figure 4-2: Girder cross section dimensions (Xu 2008)

A visual inspection was the first step in the testing procedure. After assessing the bridge, it was determined that the study was to focus on the most damaged girders. This included Girders 7 and 8 supported by Bent 11 connecting northbound Spans 10 and 11. Figure 4-3 shows the basic layout and orientation of the girders, spans, and bents under consideration.
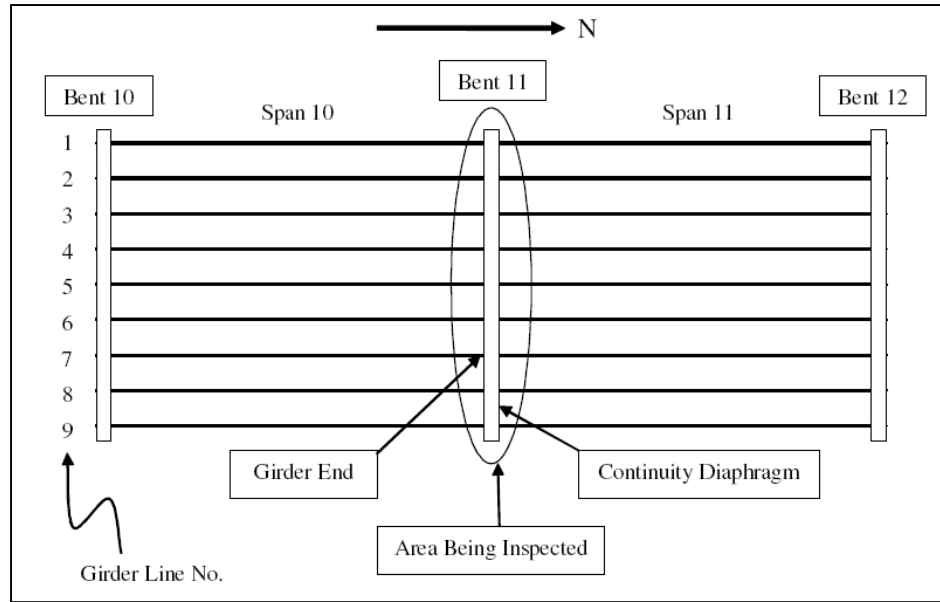
Figure 4-3: I-565 layout and numbering system (Xu 2008)

During the inspection of Girders 7 and 8 on either side of Bent 11, it was seen that

several types of cracks were present in the girder ends near the continuity diaphragm.

The first group of cracks consisted of the original cracks that had previously been

injected with an epoxy in order to seal the cracks and prevent further growth. These

cracks were large and were noticeable in many of the girders. There were also cracks

that had not been repaired with epoxy. These cracks were mostly adjacent to the

previously repaired cracks and caused concern for the bridge integrity since the girders

had cracked after the epoxy repair. There were also cracks that were present under the

fiber-reinforced polymer (for the post-repair test), which could not be seen but were

documented prior to the repair by Xu (2008). Figure 4-4 shows the cracks on the east

face of Girder 7 in Span 11. The cracks have been enhanced for clarity.

Epoxy Injected Cracks

Unrepaired Cracks

Cracks under FRP
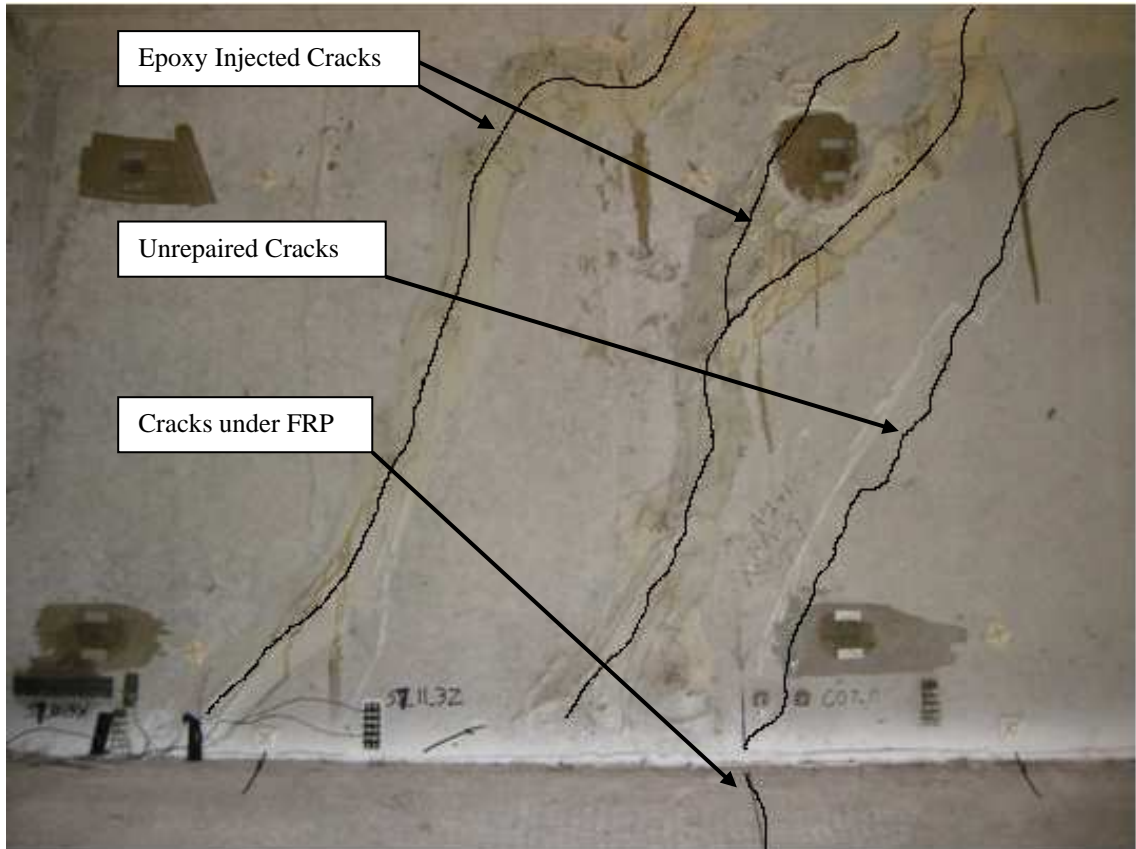
Figure 4-4: Cracks in east face of Span 11 Girder 7

As stated previously, the preliminary investigation showed that the acoustic emission

monitoring of Girders 7 and 8 would be the most insightful into the condition of the

bridge.

4.4.2 Testing Equipment

The equipment used for processing acoustic emission signals is available in a

variety of forms. Components common to all systems are transducers, preamplifiers,

filters, and amplifiers to make the signal measurable.

When an acoustic emission wave encroaches on the surface of a test object, very

small movements occur on the surface. The transducer's function is to detect this

movement and convert it into a usable signal. The transducers used for acoustic emission

testing generally use a piezoelectric sensor as the electromechanical conversion device. The transducers may be resonant or broadband and the main considerations in transducer selection are operating frequency, sensitivity, and environment and physical characteristics (ASNT 2005).

In this testing, PAC R6I-AST 50 kHz integral resonant transducers were chosen for use with the acoustic emission equipment. Table 4-1 summarizes the PAC R6I-AST characteristics. These sensors have a preamplifier built in and therefore eliminate the need for a separate preamplifier. This choice was made with the purpose of attaining high sensitivity as well as the ability to utilize long cables without the need for a separate amplifier. This choice also decreases equipment cost and setup time in the field. The preamplifier present within the transducer housing provides filtering, gain, and cable drive capability (ASNT 2005). Filtering in the preamplifier is the primary means of defining monitoring frequency for the acoustic emission test.

Table 4-1: PAC R6I-AST Sensor summary information (Adapted from PCI 2002)

Characteristic	Value
Dimensions (Diameter x Height) (mm)	29 x 40
Weight (g)	98
Operating Temperature (˚C)	-35 to 75
Case Material	Stainless Steel (304)
Face Material	Ceramic
Connector Type	BNC
Connection Location	Side
Peak Sensitivity (dB)	117
Operating Frequency Range (kHz)	40-100
Resonant Frequency (kHz)	55
Directionality (dB)	±1.5
Seal Type	Epoxy
Comments	40 dB gain Integral Pre-amp for 50 ohm load
Recommended Accessories	1234-x Cable, MHR6I Hold-Down

The system computer used was a 24-channel "Sensor-based Acoustic Multi-channel Operation Systems" (SAMOS) manufactured by Physical Acoustics Corporation (PAC). This system controls the main amplifiers and thresholds, which are adjusted to determine the test sensitivity. SAMOS multi-channel systems are driven by the Windows AE-Win Software. Standard coaxial RG-58 A/U cables were used to connect the PAC R6I-AST sensors and the SAMOS operating system.

4.4.3 Instrumentation Setup

The preparation for the I-565 bridge testing took place for one week. The acoustic emission installation and setup took one day (May 24, 2010) and AE testing took place over two nights (May 25-26, 2010). In order to save time on site, preliminary testing was performed in the Auburn University Structural Engineering Laboratory prior to travelling to Huntsville. Information including hardware, filter, and acquisition setup is summarized in Table 4-2.

Table 4-2: AE test parameters

Parameters	Values
Hit Definition Time (HDT)	200
Peak Definition Time (PDT)	50
Hit Lockout Time (HLT)	300
Threshold	60 dB
Preamplifier (R6I-AST)	40 dB

The setup for the AE monitoring began with the cleaning of the concrete surface. The girder surface was cleaned and sanded until it was smooth. Dirty surfaces can cause a reduction in the acoustic contact and allow for poor data. A high-silicone vacuum grease produced by Dow Corning was used as the coupling medium between the sensor and the concrete surface.

Before placing the sensor on the girder face, the sensor was connected to the cable running to the acquisition system. To place the sensor on the girder face, a small amount of the coupling medium was placed on the face of the sensor and the sensor was pressed against the concrete surface. This minimized the air entrapped at the interface, ensuring good acoustic continuity. The coupling medium oozed from all sides as the sensor was pushed against the surface. After placement, the sensor was held in place by the coupling medium until a magnetic hold-down device was installed. The magnetic hold-down device was slipped over the sensor, and it maintained a small amount of pressure against the sensor.

The magnetic hold-down device was secured in place by two steel sheets that were glued to the concrete surface. The two steel sheets (1.25 in. x 0.5 in. x 0.02 in.) were glued to the girder face as shown in Figure 4-5. The magnetic hold-down device allowed for a considerable amount of flexibility in placing the sensors since the sensors could be placed in any desired position. However, care was taken in securing the magnetic hold-down device to ensure that the sensor was not moved after being placed on the concrete surface. The hold-down devices also offered some protection for the sensors from environmental hazards. They also acted as insulators against any external noise that may otherwise have affected the testing.
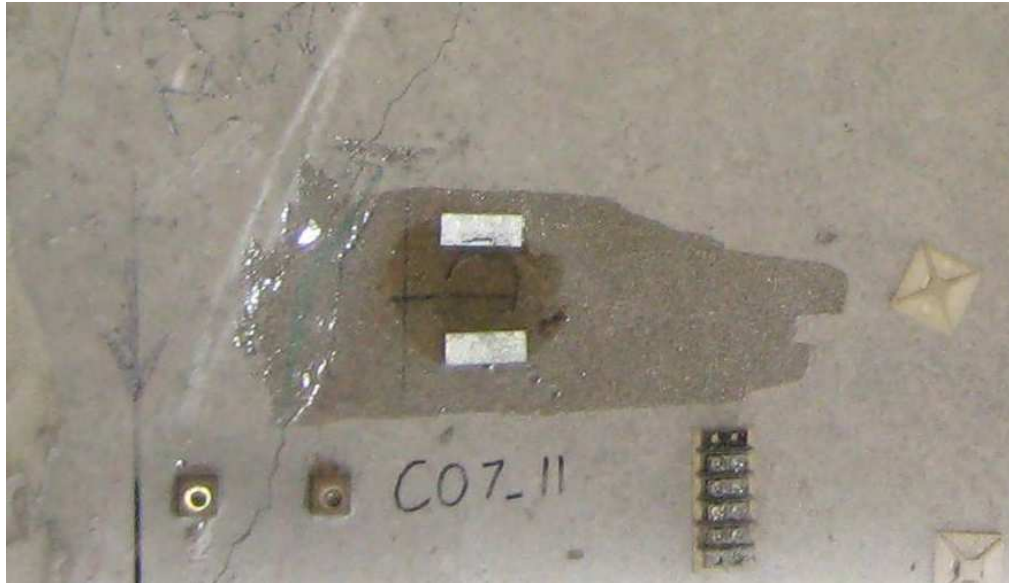
Figure 4-5: Steel sheets on girder face

Once the magnetic hold-down device was properly placed over the sensor, the cable was
secured using cable ties and mounting pads. This was done to prevent any movement and
interference. The sensor was restricted so no movement caused by the weight of the
cable occurred. Once the cables were tied down, the sensor installation was complete.
The entire sensor setup can be seen in Figure 4-6.

Figure 4-6: Sensor installation

The sensors were arranged in grids in order to capture the AE events occurring during the testing process. Twenty-four sensors, in groups of six sensors each, were placed in rectangular grids on the east faces of both Girders 7 and 8 along Spans 10 and 11. There was one group of sensors on each girder end. There were a number of unsealed and sealed cracks on these faces which allowed for quality AE data to be accumulated and verified.

Based on the preliminary investigation, Girder 8 had a number of sealed cracks along both Spans 10 and 11. Girder 8 in Span 11 had a very long unsealed crack close to the continuity diaphragm, while smaller unsealed cracks were present in Span 10. Figure 4-7 shows the configuration of sensors along Girder 8 and Figure 4-8 shows the arrangement of Sensors 13-18. Six sensors (1 through 6) were installed on the east face of Span 10 on Girder 8 (S10G8) near the continuity diaphragm. The grid of AE sensors was 24 in. (0.61 m) high x 72 in. (1.82 m) wide. Likewise, another 6 sensors (13 through 18) were installed on the east face of Span 11 on Girder 8 (S11G8). This grid also had dimensions of 24 in. (0.61 m) x 72 in. (1.82 m).
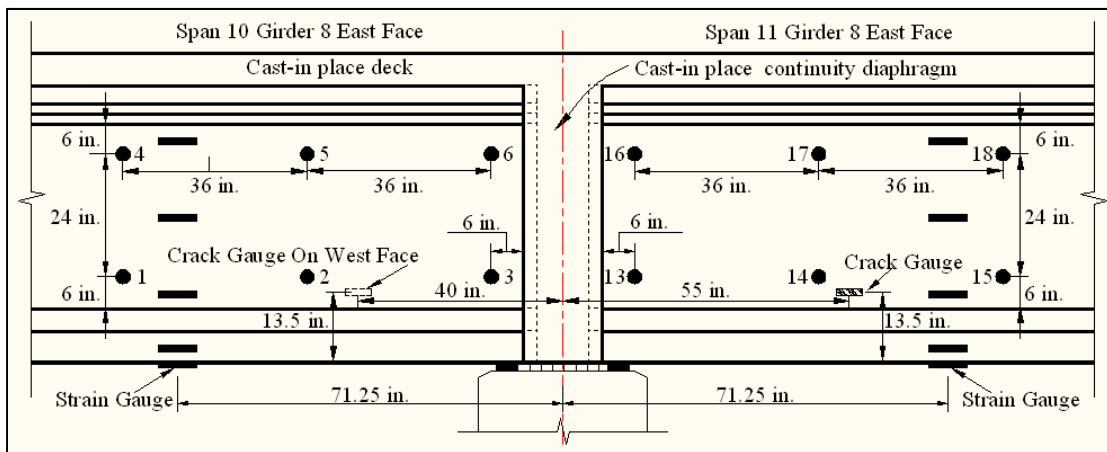
Figure 4-7: Sensor configuration on east face of Girder 8 (Xu 2008)

Figure 4-8: Arrangement of Sensors 13-18 on Girder 8

A large number of both sealed and unsealed cracks were visible in Girder 7.

Girder 7 in Span 11 (S11G7) had unsealed cracks that ran nearly the entire depth of the

beam adjacent to sealed cracks. Like Girder 8, Girder 7 in Span 10 (S10G7) had shorter

unsealed cracks on the east face. Six sensors (7 through 12) were placed on the east face

of S10G7 near the continuity diaphragm as shown in Figure 4-9. As seen in this figure,

Sensor 11 was moved down 2 in. (51 mm) to avoid being placed over a crack. Six

sensors (19 through 24) were also placed on the adjacent end of S11G7 as shown in

Figure 4-9. Sensors 20 and 23 were shifted 1 in. (25 mm) to the right to avoid being

placed over a crack. The configuration of sensors 19-24 can be seen in Figure 4-10.
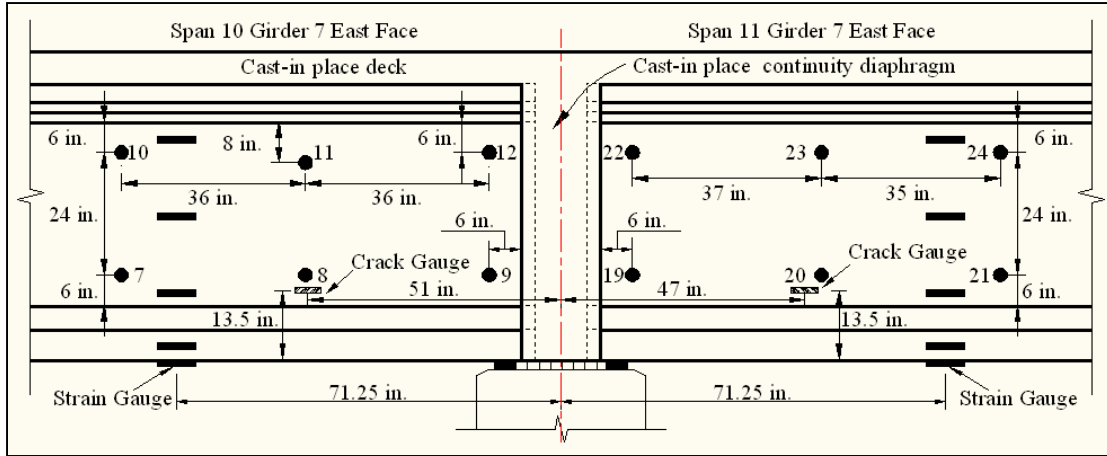
Figure 4-9: Sensor configuration on east face of Girder 7 (Xu 2008)
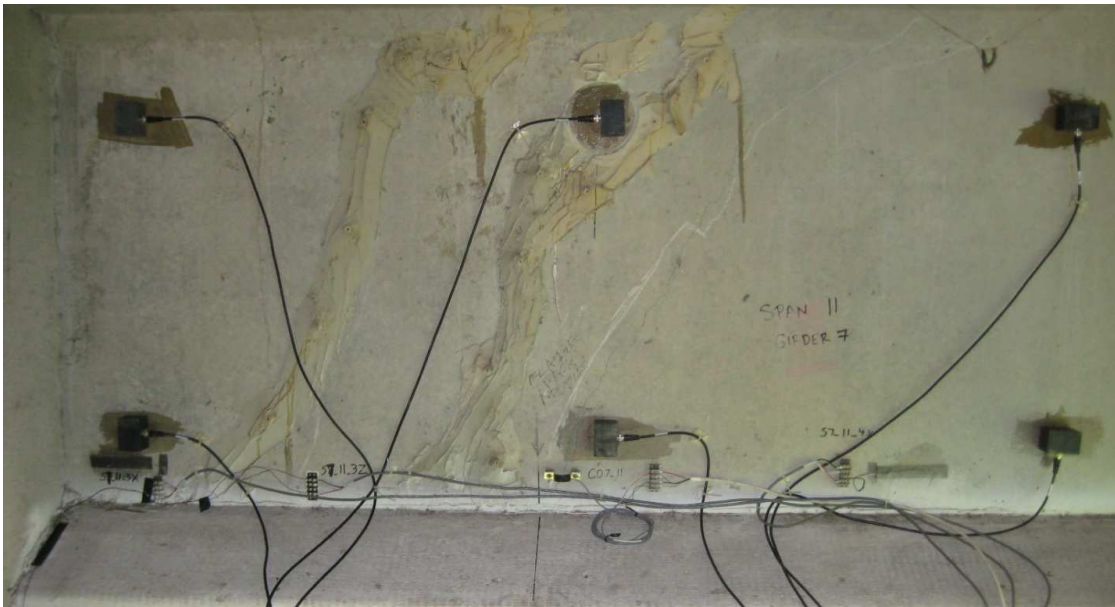
Figure 4-10: Arrangement of Sensors 19-24 on Girder 7

4.4.4 Conventional Measurements

To fully evaluate the integrity of the I-565 bridge structure, other data were
collected and compared to the AE data. The strains at the concrete surface were
measured by using electrical-resistance strain gauges (ERSGs), which were bonded
directly to the concrete surface using epoxy. The strain gauges used were 2.5 in. (60

mm) strain gauges with a resistance of 350 Ω and temperature compensation appropriate for concrete (Texas Measurements MFLA-60•350-1L). Strain gauge locations can be seen in Figure 4-7 and Figure 4-9.

The amount of vertical displacement that the bridge experienced under loads was measured using deflectometers. Along with the AE data, these measurements were used to understand the general behavior of the bridge. For this testing, twelve deflectometers were placed at six different locations along each girder.

Under loading, the existing cracks can generate AE due to the rubbing of the cracked surfaces as they open and close in response to changing traffic loads. Four crack-opening measurement devices (COMDs) were used to measure the crack-opening displacements (CODs) during the load tests. These devices were attached on either side of the cracks on the west face of S10G8 and on the east face of S11G8, S10G7, and S11G7. Each of the crack-opening measurement devices was installed 13.5 in. (0.34 m) above the bottom of the girder. The crack-opening device locations relative to the AE sensors can be seen in Figure 4-2, Figure 4-7, and Figure 4-9.

4.4.5 Bridge Loading for Acoustic Emission Testing

After the sensors and cables were installed, the channel sensitivities were checked to make sure they were consistent for each sensor. The hardware was initially checked in the Auburn University Structural Research Laboratory prior to the week of testing to ensure that all of the sensors were working properly. After the sensors were mounted on the concrete girders in the field, a system performance check was completed using the pencil-lead break technique (Pollock 1995). As seen in Figure 2-4, a 0.02-in. (0.5-mm) HB pencil lead was broken on the concrete surface a set distance from each sensor. This

was done to check that each sensor was working properly and to identify any weak channels in the system. All significant data concerning weak channels were noted in the test log. After the testing was completed, sensor sensitivities were checked again to confirm there was no loss of sensitivity during the test period.

During the nights of testing, one lane of the bridge was open to traffic. This lane of traffic was over Girders 1 and 2 which are the farthest from Girders 7 and 8. An acoustic emission calibration test was performed on Girders 7 and 8 during 6 minutes of ambient traffic flow prior to the testing period. During the calibration test, it was seen that very few AE signals were caused by the open lane of traffic, which indicated that the traffic had no significant effect on the results of the load tests.

Loading of the bridge girders was performed by moving load trucks onto the bridge. Since the AE testing method is a measure of damage growth, it is dependent on load history. Therefore, loading patterns were designed to produce useful data and utilize the AE method to evaluate the integrity of the concrete girders. Two different load test trucks, provided by the Alabama Department of Transportation (ALDOT), were used for the test. The trucks, ST-6400 and ST-6538, can be seen in Figure 4-11 and Figure 4-12.

Figure 4-11: Standard load truck ST-6400 (pre-repair and post-repair)

Figure 4-12: Standard load truck ST-6538 (post-repair)

On the first night of testing, truck load configuration LC-6.5 was used to induce

load effects slightly larger than values corresponding to the full service-level live load for

which the bridge was designed. The load configuration LC-6.5 for both trucks can be

seen in Figure 4-13 and Figure 4-14. The solid arrows represent the actual load being

applied to the structure acting through the three axles of the truck. The dotted arrows

represent the total resultant load being applied from the trucks. The footprint of ST-6400

and ST-6538 can be seen in Figure 4-15. The first night of testing was completed in two

parts due to the four loading positions.
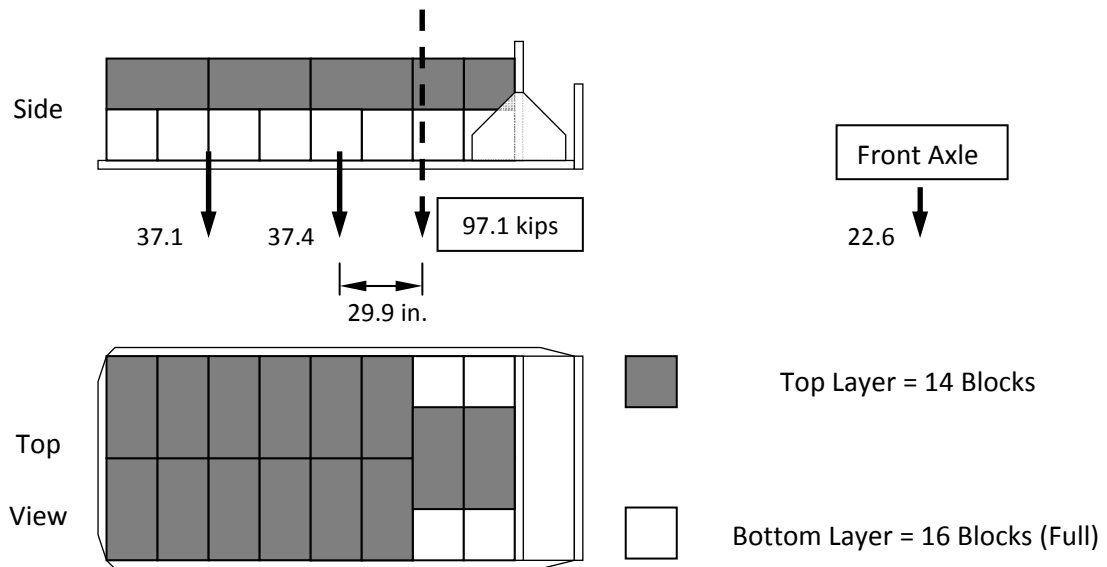
Figure 4-13: Truck ST-6400 load configuration LC-6.5 for pre- and post-repair

Side View

39.1 kips   39.5 kips   94.7 kips

14.2 in.

Front Axle

16.1 kips

Top View

Top Layer = 8 Blocks

Middle Layer = 9 Blocks

Bottom Layer = 12 Blocks
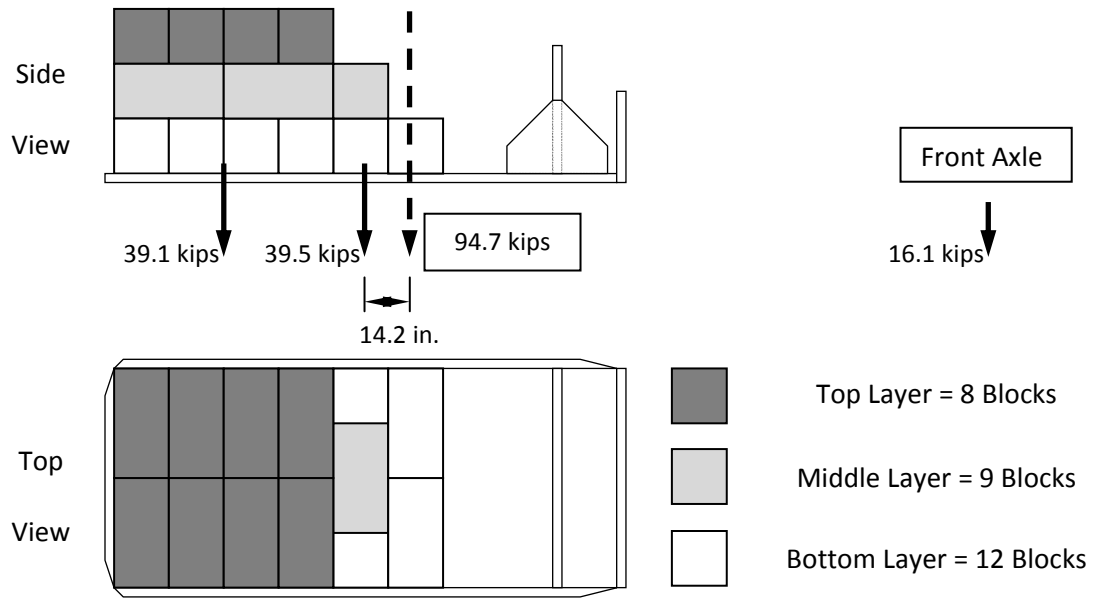
Figure 4-14: Truck ST-6538 load configuration LC-6.5 for post-repair
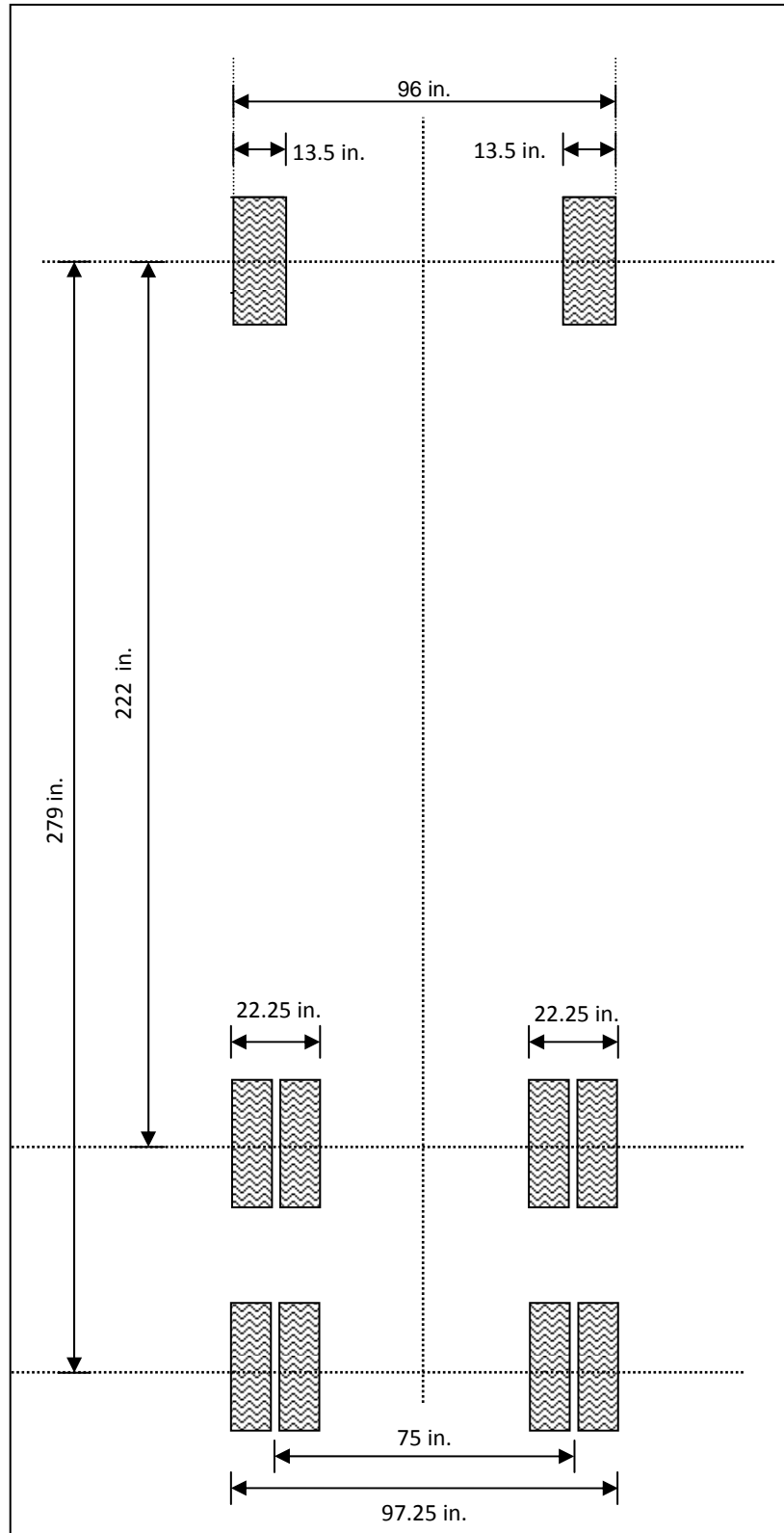
Figure 4-15: Footprint of ALDOT load trucks (ST-6400 and ST-6538)

As can be seen in the above figures, the blocks on each truck were designed to achieve

similar loadings to the bridge under the back of the trucks. This was done to replicate the

pre-repair test done on this bridge in 2005 (Xu 2008). The pre-repair loading schemes

were designed to maximize the combined influence of shear and positive bending. An

elevation view of the testing setup and the truck stop position locations is shown in

Figure 4-16.

Figure 4-16: AE testing stop position locations

As stated before, initial readings for all sensors were recorded for six minutes prior to the load trucks being driven into position. Part one of testing during the first night consisted of using both trucks to load Span 10. The first truck, ST-6400, with load configuration LC-6.5 (Figure 4-13), was backed onto the bridge gradually and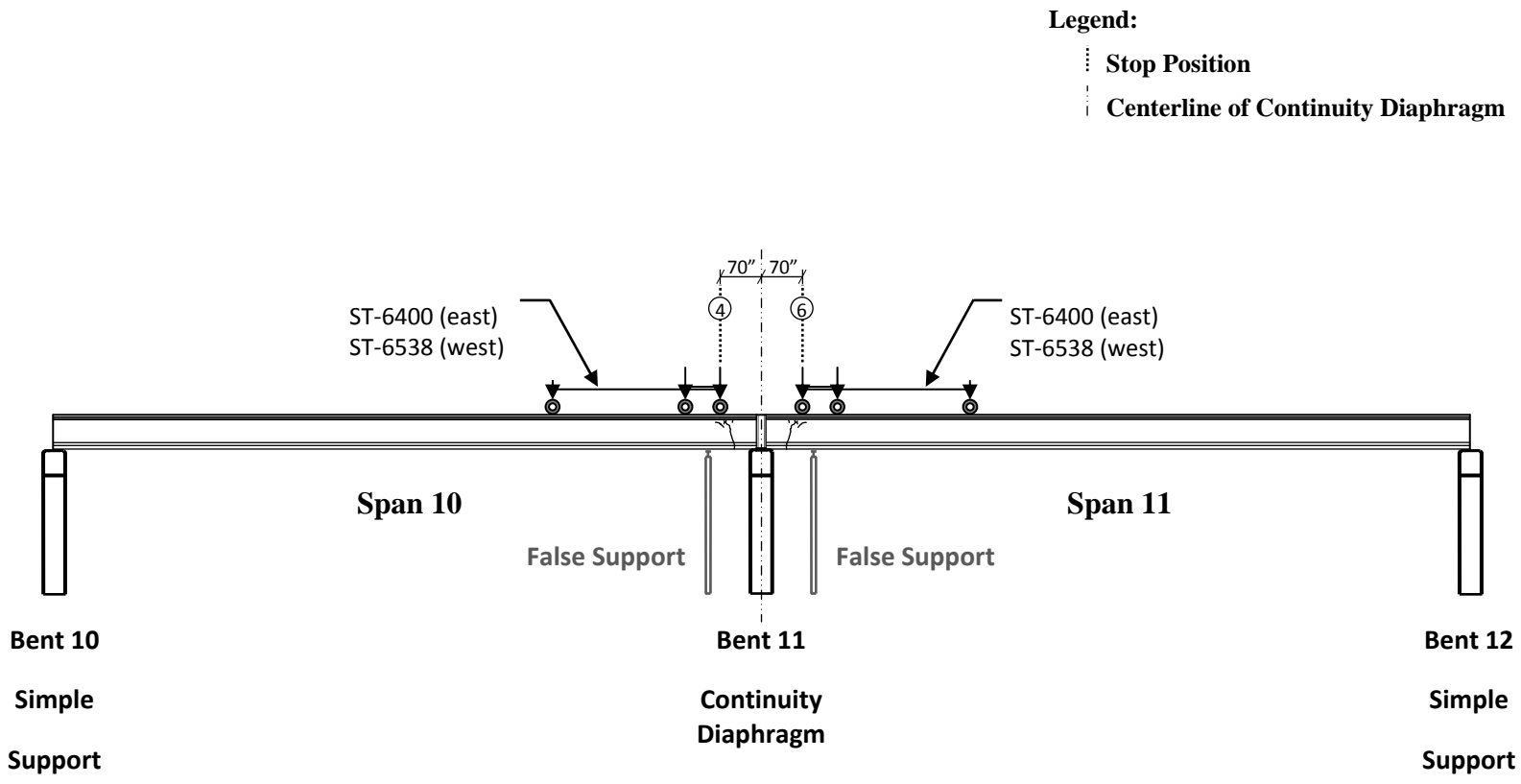 placed at its predetermined position. The transverse positions of the test trucks are shown in Figure 4-1. As seen in Figure 4-17, the first longitudinal stop position for the test truck was where the third axle of the truck aligned with Line 4 (70 inches from the centerline of the continuity diaphragm). Once the first truck was in position and a two-minute hold was completed, the second test truck, ST-6538, with load combination LC-6.5, was gradually backed into its predetermined position. Once both trucks were in the positions shown in Figure 4-17, they remained still for approximately nine minutes. The trucks were then driven off the bridge simultaneously, and the structure was observed for seven minutes.
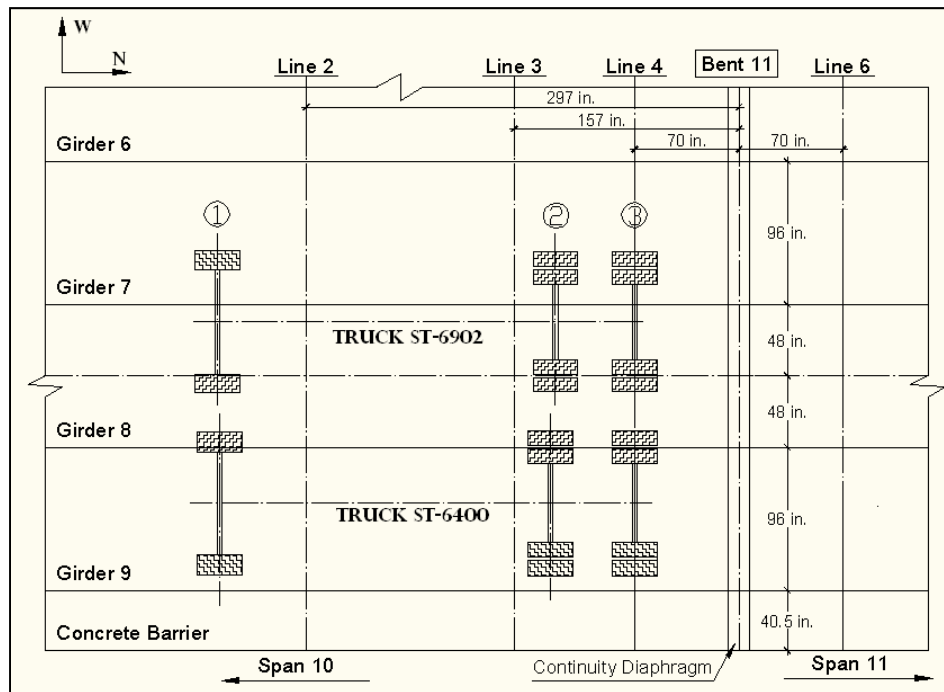

Figure 4-17: Longitudinal test positions for Span 10 loading

74

Part Two of the first night's testing used the same test trucks but loaded Span 11. The load application process was almost identical to Part one. Once again, six minutes of testing were conducted while the bridge was under no load. After the six minutes, the first test truck, ST-6400 with LC-6.5, was moved into its predetermined position, seen in Figure 4-18. For this testing, the third axle of both trucks coincided with Line 6 (70 inches from the centerline of the continuity diaphragm). After the first truck was in position and two minutes of monitoring was completed, the second test truck, ST-6538 with LC-6.5, was moved into its predetermined position (Figure 4-18). After both trucks were in position, the bridge was monitored for nine minutes. After nine minutes, the trucks were driven off Span 11 simultaneously and the bridge was observed for seven minutes.
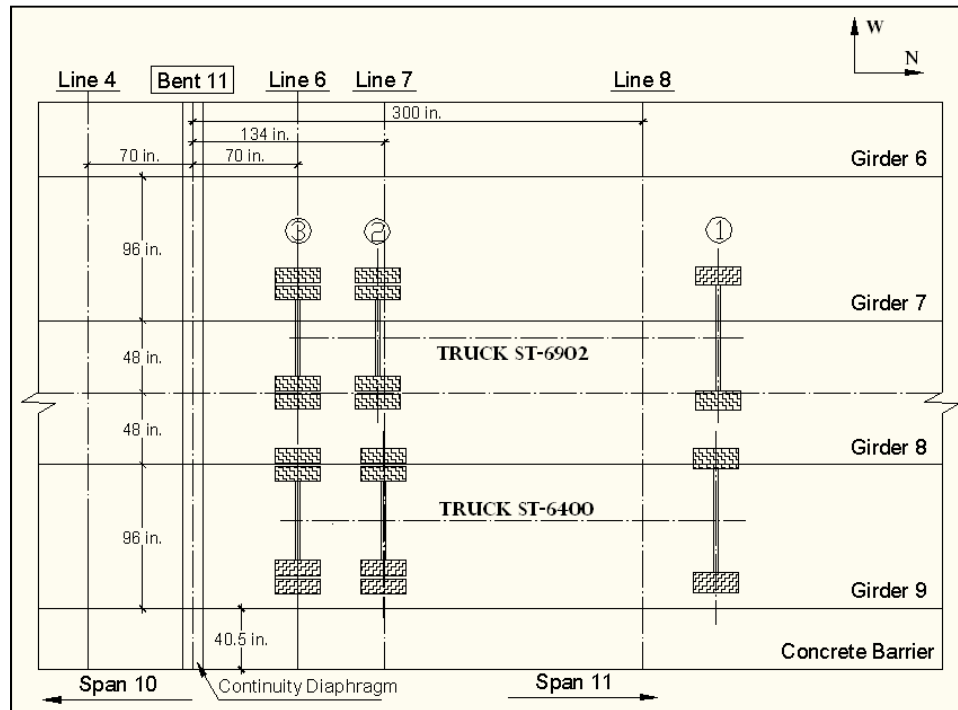
Figure 4-18: Longitudinal test positions for Span 11 loading

For the second night of testing, the first night's testing was repeated exactly except for the load configuration. Load configuration LC-6.0 was used for the second night's testing. LC-6.0 represented roughly 96 percent of the first night's load. This load combination was implemented to make sure that the first night loading was not exceeded. Figure 4-19 and Figure 4-20 show the load combination LC-6.0. Once again, the solid arrows represent the loads being applied to the structure through the truck's three axles and the dotted arrow represents the total resultant load being applied to the structure.
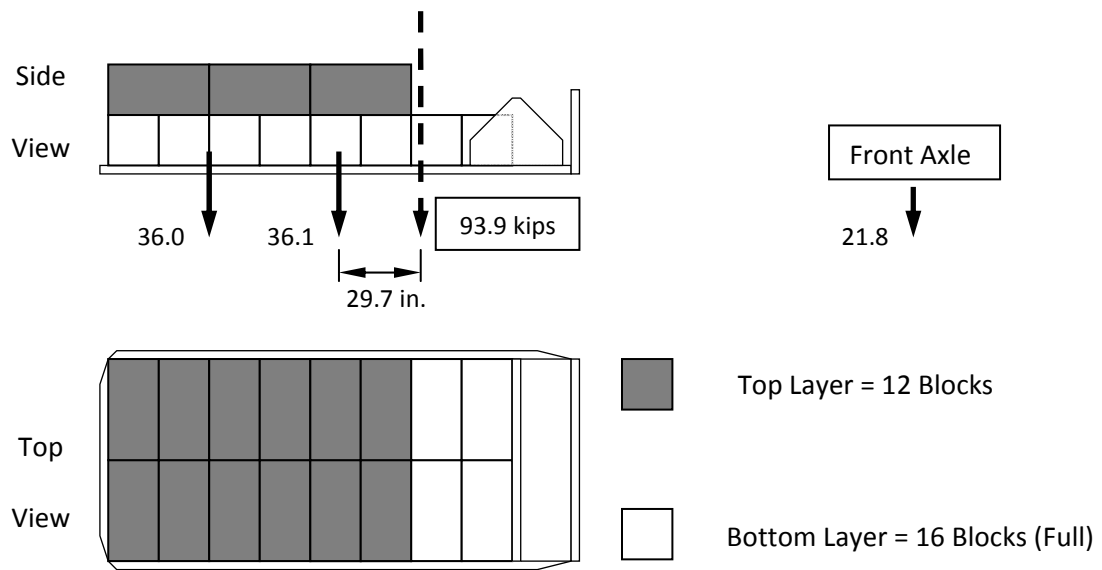
Figure 4-19: Truck ST-6400 load configuration LC-6.0 for pre- and post-repair
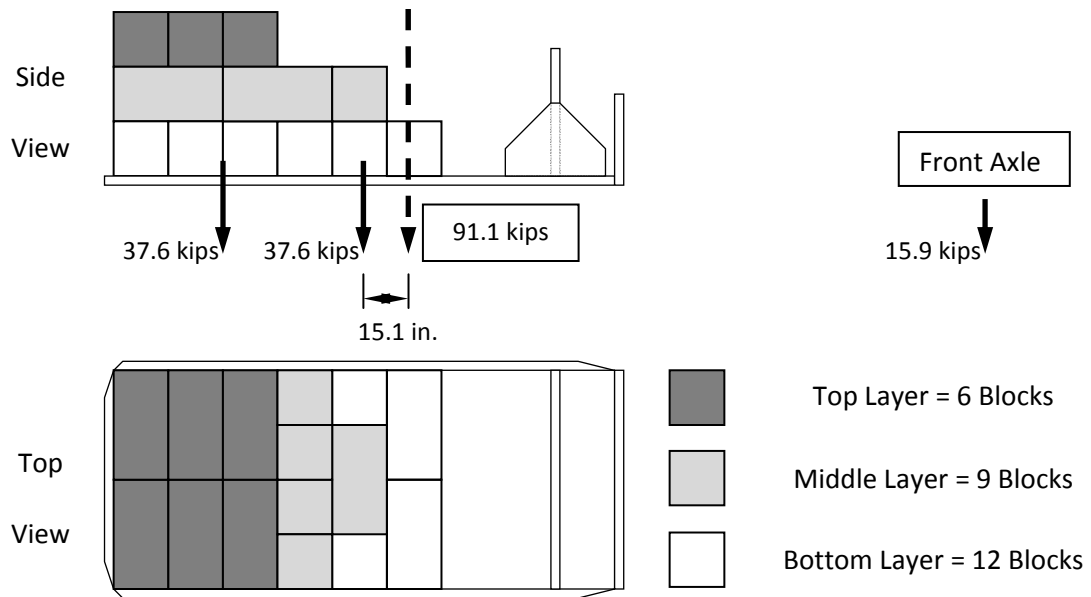
Figure 4-20: Truck ST-6538 load configuration LC-6.0 for post-repair

After testing was completed, the sensors were removed from the face of the girders and the hold-down devices and cables were stored. Pictures were taken to make comparisons between visible cracks before and after the testing.

The acoustic emission procedure described in this chapter was designed for this specific research project. As stated in Chapter 2, there are many different testing procedures that can be used for acoustic emission testing. The most important aspect of any acoustic emission procedure is keeping track of all events that occur during the test. Everything should be noted by the operator, including temperature changes, adverse weather, changes in traffic patterns, etc. These notes should be used during the data analysis to sort out any anomalies in the results.

Chapter 5: Experimental Results and Discussion

5.1 Organization of Results and Discussion

One of the objectives of the post-repair testing was to determine the structural integrity of four prestressed girders in the elevated portion of the I-565 highway. This information was compared to the pre-repair test results to see if the condition of the girders had improved over the time period between the two tests. This comparison also shed light on the impact of the FRP-repair that was installed in between the two tests.

In this chapter, the pre-repair test results are presented first. The crack-opening displacements for the pre-repair tests are shown to give a representation of the behavior of the girders during the loading process. This information was also used in conjunction with the AE data to better understand AE behavior during the loading process. Two evaluation criteria are presented following the crack-opening displacement analysis. The NDIS-2421 criterion was used to determine the structural integrity of each girder based upon damage levels. The signal strength moment (SSM) ratio evaluation was another way the damage level of the girders was assessed. Finally, the AE 2D-LOC software was used to determine the source locations of the AE events produced during the load test. This data was compared to the visible cracks on the surface of the girders.

Following the pre-repair test results, a brief summary of the differences between the pre-repair and post-repair tests is presented. This is shown so that any difference in

test results can be addressed and possibly explained by the few changes made between the two tests.

Finally, the post-repair test results are presented. In order to effectively compare the two tests, similar evaluations were performed, including the crack-opening displacements, the NDIS-2421 evaluation criterion, and the SSM ratio evaluation. Some of these criteria were amended to better represent the data. Additional evaluations are also presented to validate the results from the other assessments.

5.2 Pre-FRP Repair Results and Discussion

5.2.1 Crack-opening Displacement Analysis

The results from the crack-opening displacement (COD) measurements can be seen in Figure 5-1. This figure represents the crack width changes at the four gauge locations during the first night's loading. A positive value of COD indicates an opening of the crack relative to the original reading; a negative value indicates a relative closing of the crack. The crack-opening device on Span 10, Girder 8 (S10G8) was on the west face of the girder; the other three were on the east face of each girder. The SP10G8 COD was located on the opposite face (relative to the other CODs) because this crack did not extend all the way through the beam. According to Xu (2008), the behavior of the SP10G8 COD was different from the other three CODs because of out-of-plane bending. Also seen in Figure 5-1 are the CODs relative to each other. The behavior of each crack is shown through the entire loading sequence. For instance, the crack located in Girder 7 of Span 10 (S10G7) was much more sensitive when the loading was being performed on Span 10. Likewise, for Span 11, the most sensitive COD was S11G7. This also leads into another interesting point: the Girder 7 CODs were much more sensitive than the

Girder 8 CODs. Both S10G7 and S11G7 had a range of about 0.04 mm, which was much larger than S10G8 and S11G8 with ranges of 0.005 and 0.02 mm, respectively. Considering that the position of the crack-opening devices and the dimensions of the girders were the same, Xu (2008) hypothesized that Girder 7 was more damaged than Girder 8 based of the increased COD values. Xu (2008) also showed that the values for the COD in S10G7 and S11G7 produced during the load hold in their respective spans were almost the same, indicating that Girder 7 had similar characteristics and condition in Spans 10 and 11.
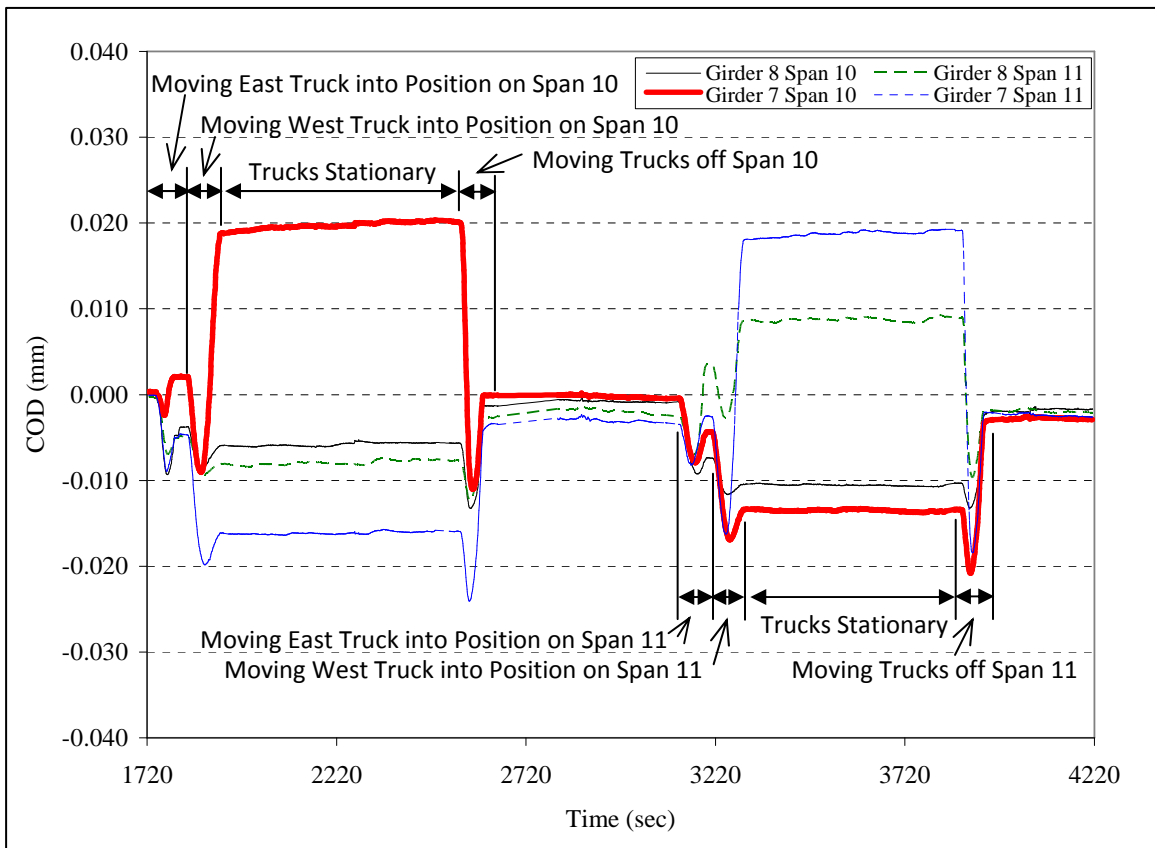

Figure 5-1: Crack-opening displacement during first night loading (Xu 2008)

The COD data were also used in relation to the AE activity. Similar to previous findings, it was shown that an increase in AE activity was directly related to a change in

COD values. Figure 5-2 shows the AE activity generated from all six sensors on S10G8

on the first night of loading. SP10G8 was chosen to show the general trend that occurred

in all four girders. The markers in the figure represent the AE amplitude of an individual

hit that occurred during the test. The COD values are also shown on this plot. It can be

seen in this plot that most AE activity took place when a large *change* in COD occurred.

This shows that the opening and closing of cracks in the concrete girders was associated

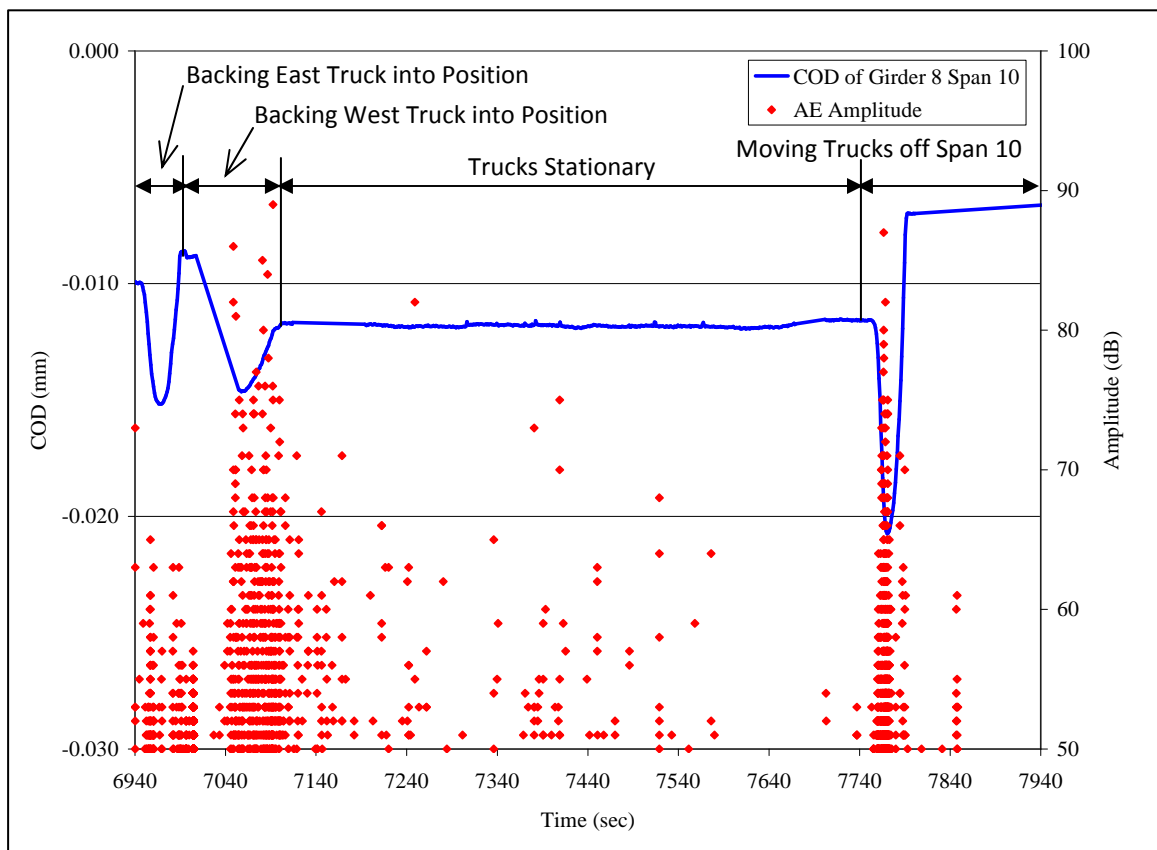with a significant increase in AE activity (Xu 2008).

Figure 5-2: COD and AE activity of Span 10 Girder 8 during second night (Xu 2008)

It should be noted that not all AE activity was associated with a significant change in

COD values. Some AE activity could have been caused by ambient noise, such as traffic

or other environmental factors. However, it could in fact be genuine acoustic emission.

It could represent damage that was occurring at nearby cross sections other than the one

where the COD was located. It is important to note that AE has extreme sensitivity and

microscopic crack growth that is undetectable by COD gages can and does cause

significant amounts of AE activity.

5.2.2 Pre-FRP Repair AE Evaluation Criteria Results

5.2.2.1 NDIS-2421 Criterion

According to Ohtsu et al. (2002), the load ratio used in the NDIS-2421 criterion

requires accurate control of loading because inaccuracies can render the method useless.

Because of the fact that the truck loading varies in location rather than in magnitude, Xu

(2008) concluded that the load ratio could not be used for the evaluation of the in-service

bridge. However, it could be assumed that the measured strain at a location in the girder

is closely related to the *load effect* (bending moment, shear, etc.) at that particular cross

section that results from a moving truck load. Therefore, Xu proposed that a *strain ratio*

could be used as an effective replacement for the load ratio in the evaluation criteria.

Shown in Figure 4-2, the strain used for the analysis was near the top of the girder (Strain

Location F). Since it was impractical to know the previous maximum strain the bridge

had experienced during its service life, Xu used the relative maximum strain for the

testing period. This is a commonly cited difficulty with application of AE to in-service

structures. However, it should be noted that load testing is typically conducted with

strategically placed and purposely heavy loads and therefore it is likely that the load test

represents the first loading to a given level. Xu defined the strain ratio as "the ratio of the

strain at the onset of AE activity during the period where both trucks moved off the

bridge to the relative maximum strain for the testing period" (Xu 2008). The strain ratio

is represented as:

$$\text{Strain Ratio} = \frac{\text{Strain}_{\text{onset of AE activity}}}{\text{Strain}_{\text{relative max}}} \qquad \text{(Eq. 5-1)}$$

The calm ratio was calculated using the cumulative signal strength during the

period that both trucks moved off the bridge. It can be represented as follows:

$$\text{Calm Ratio} = \frac{\text{Cumulative AE Signal Strength}_{\text{from max of strain to end}}}{\text{Cumulative AE Signal Strength}_{\text{from beginning to max strain}}} \qquad \text{(Eq. 5-2)}$$

Figure 5-3 is a plot that shows a set of data used to calculate the two ratios for Girder 8 in

Span 10. The strain was superimposed on a plot of AE cumulative signal strength (CSS)

versus time. The CSS data were generated from all six sensors on Girder 8 of Span 10.

As seen in the plot, the compressive strain gradually increased to a maximum value as the

trucks drove away from the Span 10 loading position, but while they were still on the

span. The strain magnitude then decreased until the trucks were completely off the

structure. The "loading" and "unloading" phases of cross sectional effects due to this

truck moving operation were identified based on the measured strain change indicated in

Figure 5-3. The point labeled "onset of AE" actually indicates the point at which

significant AE activity occurred during the loading process. The actual onset of AE

occurred immediately after the loading began, indicated by the first rise in the CSS data.
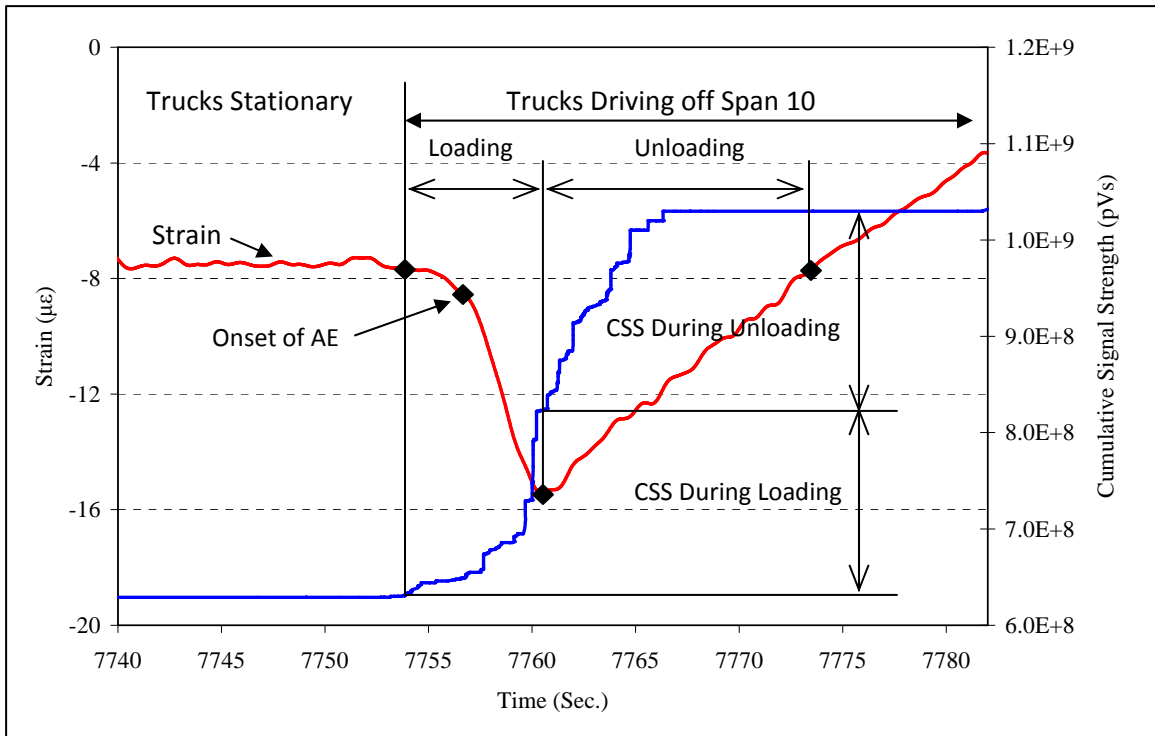
Figure 5-3: Plot used in determining strain and calm ratios for Span 10 Girder 8

(Xu 2008)

Once the strain and calm ratios were determined based on the data for each girder,

the degree of damage of the girders was determined using the NDIS-2421 criterion.

These damage levels are plotted in Figure 5-4. The strain and calm ratios are indicated

on the horizontal and vertical axes, respectively. The solid markers represent data from

the first night, while the hollow markers represent data from the second night. Based on

previous laboratory tests of prestressed concrete beams (Xu 2008), the damage

classification limits for prestressed concrete were set at 0.7 for the strain ratio and 0.5 for
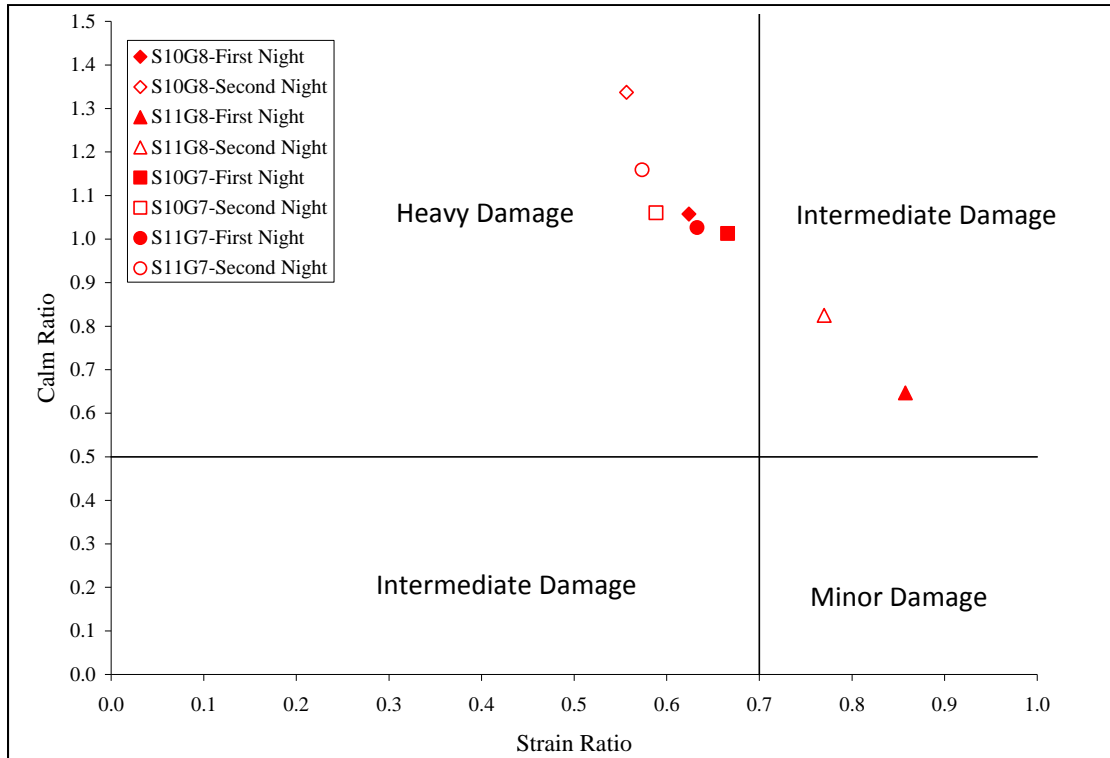
the calm ratio.

Figure 5-4: Damage qualification based on NDIS-2421 method (Xu 2008)

According to the limits provided and the data shown, Xu concluded that S10G8, S10G7 and S11G7 were classified as "heavy damage" and S11G8 was classified as "intermediate damage." These classifications showed a reasonable agreement with the crack-opening displacement data. Based on this agreement, Xu stated that the damage level of prestressed concrete girders could be reasonably qualified by the NDIS-2421 criterion based on the strain ratio and the calm ratio (Xu 2008).

5.2.2.2 Signal Strength Moment Ratio Evaluation

The ratio of signal strength moment (SSM) was employed by Xu to evaluate the damage levels in each girder. This evaluation was proposed based on a laboratory testing program, and time lengths were chosen based on experimental data and previous research. Although the actual load hold time used in the bridge testing was nine minutes,

a duration of 240 seconds was used for this evaluation. The SSM ratio is expressed as a
percentage as follows:

$$\text{SSM Ratio} = \frac{\text{SSM}_{\text{second night hold period}}}{\text{SSM}_{\text{first night hold period}}} \times 100\% \qquad \text{(Eq. 5-3)}$$

The results of the SSM ratio evaluation are shown in Figure 5-5. The ratio is shown
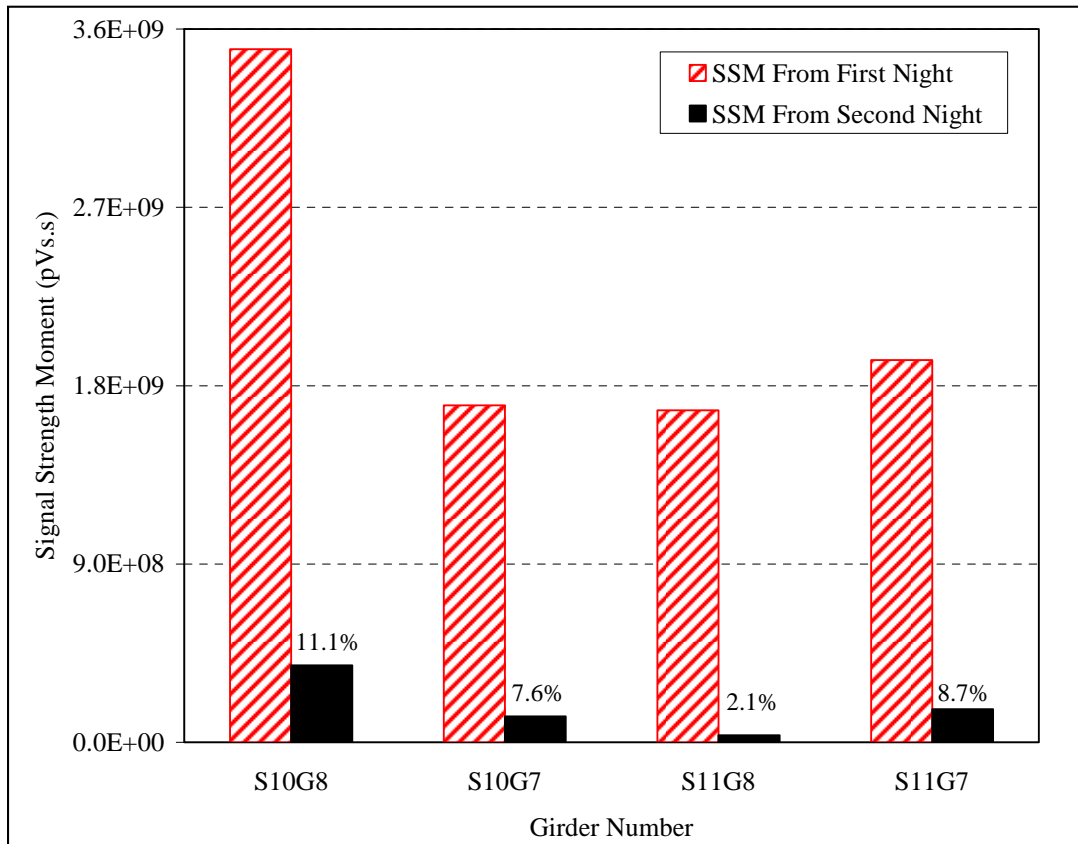above each second night SSM.

Figure 5-5: Signal strength moment (SSM) ratio during holds (Xu 2008)

As can be seen in Figure 5-5, the respective SSM ratio values indicate the different
damage levels. The results showed that S10G8 was the most damaged with an SSM ratio
of 11.1%. According to the results, S11G8 was damaged the least. Xu combined these
results with laboratory test results and concluded that prestressed beams were heavily

damaged when the SSM ratio exceeded 4%. Based on this, S10G8, S10G7 and S11G7 were heavily damaged and S11G8 was not heavily damaged (Xu 2008).

Xu compared the results from the NDIS-2421 and SSM Ratio evaluation methods and produced Table 5-1. As shown in this table, the SSM ratio results agreed with the results from the NDIS-2421 method.

Table 5-1: AE evaluation results (Xu 2008)

Girder	NDIS-2421	SSM Ratio
SP10G8	Heavy Damage	Heavily Damaged
SP11G8	Intermediate Damage	Not Heavily Damaged
SP10G7	Heavy Damage	Heavily Damaged
SP11G7	Heavy Damage	Heavily Damaged

According to both methods, Girders S10G7, S10G8, and S11G7 were "heavily" damaged while S11G8 was not heavily damaged. The results from both methods are in agreement, showing that the SSM ratio evaluation criterion is a good way to assess the present structural integrity of a bridge girder (Xu 2008).

5.2.3 Crack Location using AE 2D-LOC Analysis Technique

One of the many important aspects of AE testing is the ability to locate sources of emission. In concrete engineering, this means that by using acoustic emission, one can triangulate the location of a source using a grid of sensors. By doing this, each source can be plotted and crack patterns can be formed. These AE crack patterns can be compared to visible cracks on the concrete surface. Although this technology is used in a planar, 2D form for this research, it has been developed into a 3D form and can locate and plot cracks and inconsistencies within the concrete. Xu (2008) used this technology

to assess the accuracy of the two-dimensional source location analysis by comparing the results to the actual crack patterns visible on the surface of the girders.

The AE data presented in these results were generated on the first night of load testing. The data were processed using the AE 2D-LOC source location software provided by Physical Acoustic Corporation (PAC). Locating is the "process of collecting incoming hits into events and analyzing the arrival times of the hits in an event to produce a source location (PCI-8 Based AE System User's Manual 2002)." The fundamental basis for the location calculation is the simple time-distance relationship. The arrival time of a transient stress wave can be combined with velocity to yield the distance from the sensor to the source.

The resulting event locations produced using AE 2D-LOC for the end of Girder 8 in Span 11 can be seen in Figure 5-6. Each triangulated source location is represented by a small square marker. The larger, numbered square markers are the sensor locations. For comparison, the actual visible crack pattern was superimposed on this plot. Cracks from both the east and west face of the girder are shown.
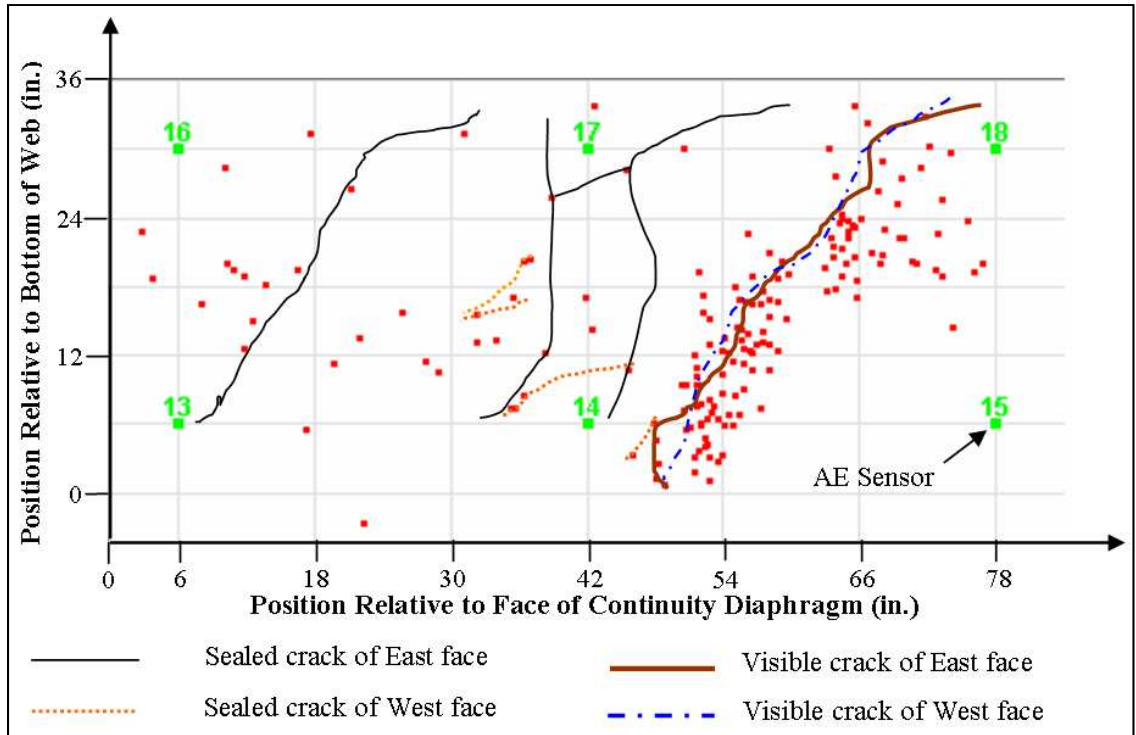
Figure 5-6: AE event location and crack pattern of Span 11 Girder 8 (Xu 2008)

The plot of event locations for the end of Girder 7 of Span 11 is shown in Figure 5-7. The visible crack pattern is superimposed to compare the results. For Xu's testing, the events plotted were restricted to the beginning of the testing trucks moving onto Span 11 and end with the testing trucks moving off the bridge. As seen in Figure 5-6 and Figure 5-7, the event locations correlate well with the crack patterns visible on the surface of the girder. It should be noted that the AE is most concentrated at the "active," unrepaired cracks, rather than the ones that were sealed previously.
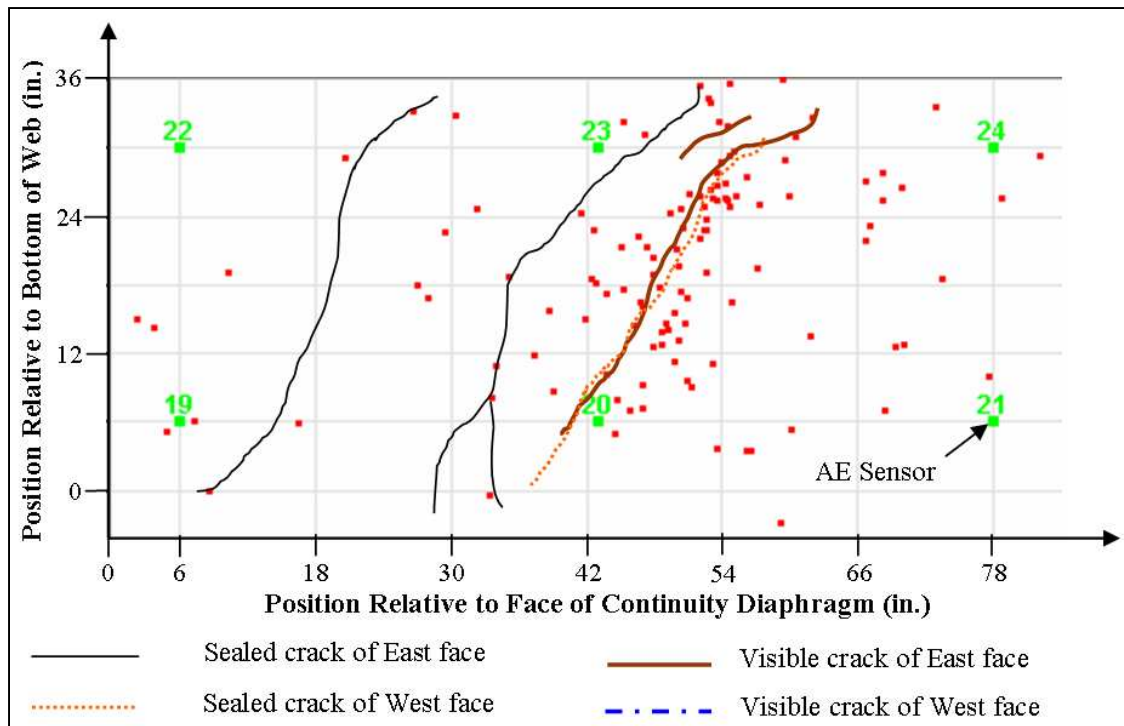
Figure 5-7: AE event location and crack pattern of Span 11 Girder 7 (Xu 2008)

It is also seen that some of the events are scattered in the figures. Xu contends that this may have been caused by errors in the selection of the events due to friction; either between the prestressing strands and the concrete or due to the elongation and slip of the strands (Xu 2008). Reflections from the boundaries of the girders may have also played a role. It is possible to optimize the source location capability by focusing on the 'first arrival' of the waveforms, discrimination of waveform types, and moment-tensor techniques. However, these topics are focused on advanced source location which lies beyond the scope of this work. It was also a point of emphasis that most of the observed events were concentrated in the middle region of the sensor grid. Very few events were assigned locations near the edges of the sensor grid. This can be attributed to the attenuation of signals traveling from one extreme to the other. Once a crack developed in

90

the extreme of the monitored area, the signal was strong in the sensors near the extreme, but weakened as it traveled to the other sensors (Xu 2008).

5.2.4 Summary and Conclusions

Xu's pre-repair testing in 2005 provided an evaluation of AE testing procedures under field testing of prestressed concrete bridge girders. Evaluation criteria were developed and the results were compared to visual inspection of the bridge. Specific conclusions were drawn from the testing and results.

First, the AE method showed that it was a promising technique for nondestructive field testing of prestressed concrete girders (Xu 2008). The data were processed and provided substantial results regarding the structural integrity of the girders tested. The testing procedure was sound and easily carried out.

The damage levels of the prestressed concrete girders were reasonably qualified by a modified NDIS-2421 criterion. This criterion was based on the strain ratio and the calm ratio. The critical values of 0.7 for the strain ratio and 0.5 for the calm ratio seemed to give accurate results of damage compared to the interpretation of the crack-opening displacements (Xu 2008).

The proposed evaluation criterion based on the ratio of signal strength moment (SSM) seemed to be validated by the modified NDIS-2421 assessment and the COD measurements. The proposed critical threshold value of 4% for the SSM ratio seemed to be accurate (Xu 2008).

The AE 2D-LOC software returned accurate source locations when compared to the visible cracks on the surface of the girders. This AE technique is a very useful tool

that has been developed to locate cracks on the surface of concrete structures or within

mass concrete systems with reasonable accuracy (Xu 2008).

Xu concluded that the AE method is a promising and effective means of

investigating the condition of prestressed concrete bridges. Because of its nondestructive

nature, it can be used to obtain valuable information on in-service bridges with minimal

effect on traffic patterns. Drawbacks of using AE monitoring include the potential for

background noise that may affect the data that is collected and processed. However, it

should be pointed out that background checks of 10 minutes in length were conducted

prior to loading and after the load was removed. The background checks did not show

significant background noise for the pre-repair test. Xu concludes by stating that further

research should focus on the implementation of evaluation criteria for in-situ testing of

prestressed concrete girders (Xu 2008).

5.3 Differences in Pre- and Post-repair Testing

5.3.1 Bearing Pad Installation

To evaluate the effectiveness of the fiber-reinforced polymer repair on the four

girders, the same tests were performed on the bridge after the installation of the FRP

repair. However, certain aspects were modified to accommodate certain changes in the

state of the bridge.

Soon after the first observation of cracking in the girders, the Alabama

Department of Transportation installed false supports under spans containing cracked

girders. This was done long before any of the testing associated with this study. The steel

false supports were installed within ten feet of the bents, which allowed the cracked

sections of the girders to be contained between a false support and a bent. These false

supports were installed with the intention of leaving a gap of at least one inch between the bottom of the girder and the top of the false support. Bearing pads were then used to partially fill the gap between each girder and the steel frame beneath. At the onset of pre-repair testing, researchers discovered that the gaps under several girders had closed to the point that no visible space remained.

5.3.2 Pre-Repair Bearing Pad Conditions

During the pre-repair test preparation, a temporary strain gauge was mounted to one column of a false support to determine if the false supports were partially supporting normal traffic loads due to the bearing pads being in direct contact with the girders. Based on measured transient strains, it was determined that the bearing pads were transmitting some load through the false supports during normal traffic conditions (Fason 2008). It was decided by the research team that it was best to test the bridge under conditions as close to its original design as possible. However, due to complications with the removal of the bearing pads, the complete removal of all bearing pads was not possible with the available equipment and materials. After realizing that the complete removal of all bearing pads was not an option, holes were drilled in the bearing pads to reduce the effective stiffness of the pads (Fason 2008).

The pre-repair tests were conducted without the complete removal of the bearing pads. Fason (2008) reported that, prior to the pre-repair tests, one bearing pad was completely removed (SP10G8), one half of another bearing pad was removed (east half of SP10G7), and holes were drilled in the remaining bearing pads to reduce their effectiveness (west half of SP10G7, SP11G7, and SP11G8). Following the pre-repair

tests, it was suggested that the presence of the bearing pads could have had an effect on the recorded results.

5.3.3 Post-Repair Bearing Pad Conditions

All bearing pads were required to be completely removed due to the installation of the FRP reinforcement.   Following installation of the FRP reinforcement, the bearing pads were not replaced, allowing for test conditions that were desired during the pre-repair tests. This change in support conditions during the FRP installation complicates the direct comparison of pre-repair and post-repair test results.

5.3.4 Post-Repair Procedural Changes

Some changes were also made to the procedure used for post-repair testing. These changes were made to account for different testing conditions as well as availability of testing materials.

The first of these changes was the location of some strain gauges. In Figure 4-2, the pre-repair locations of the AE sensors and strain gauges can be seen. For the post-repair testing, Strain Gauge F was moved to measure the strain at the cracks located under the FRP repair. This was done to measure the FRP strains at the cracks to determine how the FRP repair was interacting with the crack. Due to this change, the strain location used for Xu's AE evaluation was not available for the post-repair testing. This strain was used to determine the strain ratio used for the NDIS-2421 evaluation criteria. Figure 5-8 shows the post-repair cross section used for testing and an updated gauge notation system.
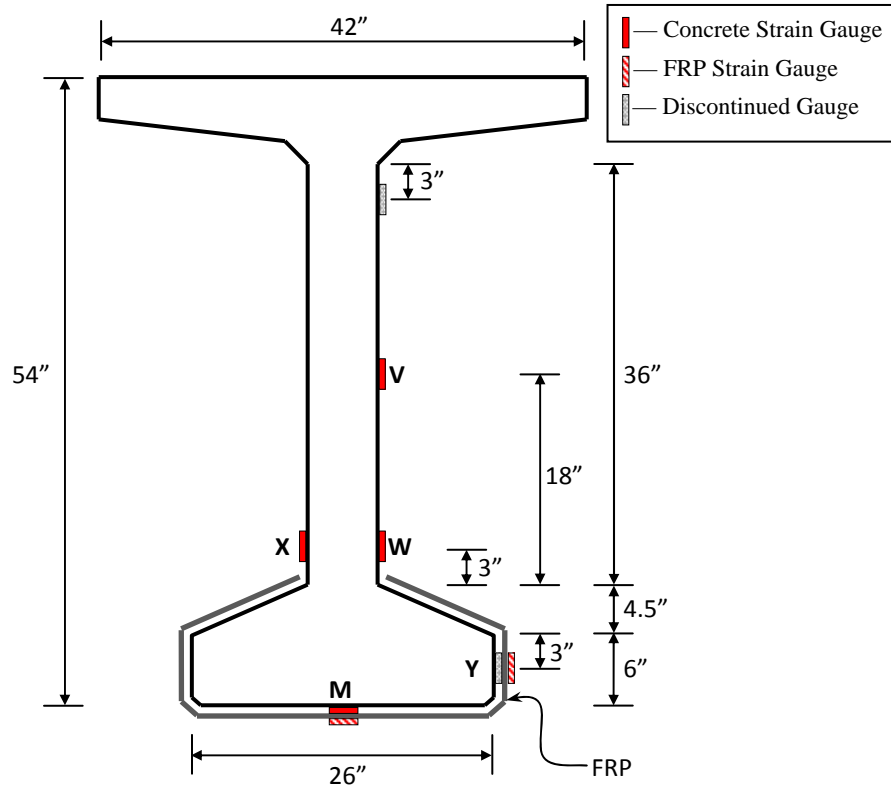
Figure 5-8: Post-repair cross section dimensions and strain gauge locations

Two trucks were used for the pre-repair and post-repair testing. For the pre-repair testing, one of the standard trucks was out of service, so a nonstandard truck was used for testing. The replacement truck was an ALDOT tool trailer truck (ST-6902), shown in Figure 5-9.

Figure 5-9: Load truck ST-6902 (pre-repair unconventional truck)

The other truck used was a standard ALDOT load truck (ST-6400). For the post-repair

testing, both trucks were standard ALDOT load trucks (ST-6400 and ST-6538), shown in

Figure 4-11 and Figure 4-12. The following tables show the comparison between the

testing trucks. Table 5-2 shows the weight distributions from the pre-repair test and

Table 5-3 shows the weight distributions from the post-repair test.

Table 5-2: Load truck weight distributions—pre-repair test (Bullock 2011)

Axle	Group	Tires	ST-6400		ST-6902	
			LC-6.5 (lbs)	LC-6 (lbs)	LC-6.5 (lbs)	LC-6 (lbs)
Front	Left	Single	11500	10750	7575	7850
	Right	Single	11500	10900	7200	7450
Rear 1	Left	Double	19450	18900	20300	19350
	Right	Double	19150	18350	19500	18750
Rear 2	Left	Double	18000	17200	19450	18600
	Right	Double	17850	17500	20150	19250
Total Weight (lbs)			**97450**	**93600**	**94175**	**91250**

Table 5-3: Load truck weight distributions—post-repair test (Bullock 2011)

Axle	Group	Tires	ST-6400		ST-6538	
			LC-6.5 (lbs)	LC-6 (lbs)	LC-6.5 (lbs)	LC-6 (lbs)
Front	Left	Single	10950	10800	8150	7750
	Right	Single	11600	11000	7950	8100
Rear 1	Left	Double	18050	17500	20200	19200
	Right	Double	19300	18600	19300	18400
Rear 2	Left	Double	18000	17250	20450	19850
	Right	Double	19100	18750	18650	17700
Total Weight (lbs)			**97000**	**93900**	**94700**	**91000**

Since two different trucks were used in the testing of the bridge, there may be some slight

effect on the testing results. Table 5-4 shows the comparison of weight distributions

between the unconventional truck (ST-6902) used for the pre-repair test and the

conventional truck (ST-6538) used for the post-repair test. Although there are small

differences in the weights of these two different trucks, these differences are of

approximately the same size as the differences in the pre- and post-repair weights of the

standard ST-6400 truck.

Table 5-4: Comparison of trucks ST-6902 and ST-6538 (Bullock 2011)

Axle	Group	Tires	ST-6902 (pre-repair)		ST-6538 (post-repair)	
			LC-6.5 (lbs)	LC-6 (lbs)	LC-6.5 (lbs)	LC-6 (lbs)
Front	Left	Single	7575	7850	8150	7750
	Right	Single	7200	7450	7950	8100
Rear 1	Left	Double	20300	19350	20200	19200
	Right	Double	19500	18750	19300	18400
Rear 2	Left	Double	19450	18600	20450	19850
	Right	Double	20150	19250	18650	17700
Total Weight (lbs)			**94175**	**91250**	**94700**	**91000**

Finally, a different threshold level was used for the post-repair testing. This was done because too many events were being detected by the sensors during the calibration test prior to the load test. By increasing the threshold level from 55 dB, used in the pre-repair test, to 60 dB, there were fewer events being detected by the sensors. This decreased the amount of data that was recorded during testing.

5.3.5 Effects on Pre- and Post-repair Comparison

One of the objectives of this research was to explore the structural integrity of the repaired concrete girders. The FRP repair should have given the girders additional strength, and the goal was to assess the sensitivity of existing AE evaluation procedures to detect that change in behavior. If needed, a secondary goal was to develop new AE evaluation procedures. However, the different support conditions (bearing pads) and the introduction of a new material (FRP repair) complicated a direct comparison of the pre- and post-repair response of the bridge itself. Therefore, these changes needed to be

carefully considered when comparing the pre-repair and post-repair response. The FRP repair should have introduced a difference in the AE response between the two tests. Again, however, this relationship was hard to determine because of the differences in the bridge support conditions.

Additionally, since a different strain gauge was used in the NDIS-2421 analysis, different results were obtained. However, the NDIS-2421 evaluation criterion does not rely on strain but rather ratios of strain. Since it was properly selected, the strain gauge used in the post-test did yield valid results that could be compared to the pre-repair test. A more valid comparison, however, was made after adjusting the NDIS-2421 evaluation criteria to better fit the post-repair test. This adjusted procedure, which will be presented later in this chapter, was then used to assess the pre-repair testing data.

The differences in the load trucks may have also introduced some variability in the results. However, by looking at Table 5-4, it can be seen that there was very little change between the two trucks used in the pre-repair and post-repair testing. This difference probably caused only minimal variability in the results.

The change in threshold level does not affect the testing procedure, but it does affect the analysis and comparison between the pre-repair and post-repair results. A straight comparison between some of the results will not be possible because of this change.

As a start to the comparison of the pre- and post-repair testing, the pre-repair analysis was extended to the post-repair data to see if any differences arose in the test results. This provided insight into any changes to the structural integrity of the bridge girders and resulted in some conclusions as to the effectiveness of the FRP repair.

99

5.4 Post-FRP Repair Results and Discussion

5.4.1 Crack-opening Displacement Analysis

Using conventional measurements is a good way to obtain a better understanding of the present structural integrity of a bridge. Apart from visual inspection, conventional measurements, such as deflections, strains, and crack-opening displacements, are easy ways to classify the condition of a bridge. As in the pre-repair test, the crack-opening devices were used in conjunction with the acoustic emission monitoring to determine if there was a correlation between the two.

Figure 5-10 shows the results of crack-opening displacement measurements produced in four gauge locations during the Span 10 loading on the first night. The crack-opening devices were placed in the same position as the pre-repair testing, with the S10G8 device (COD8_10) placed on the west face of the girder, and the other three (COD7_10, COD7_11, COD8_11) placed on the east face of the girders. Because of this, the S10G8 COD data showed significantly different behavior compared to the other COD data. Like the pre-repair testing, this was most likely due to out-of-plane bending. The SP10G8 COD behavior was also different due to the nature of the crack itself. Unlike the other cracks that extended all the way through the girder, the SP10G8 crack was only visible on the west face. Therefore, the only location for the COD device was on the west face. This crack was also located closer to the bent, which may have caused some different behavior.
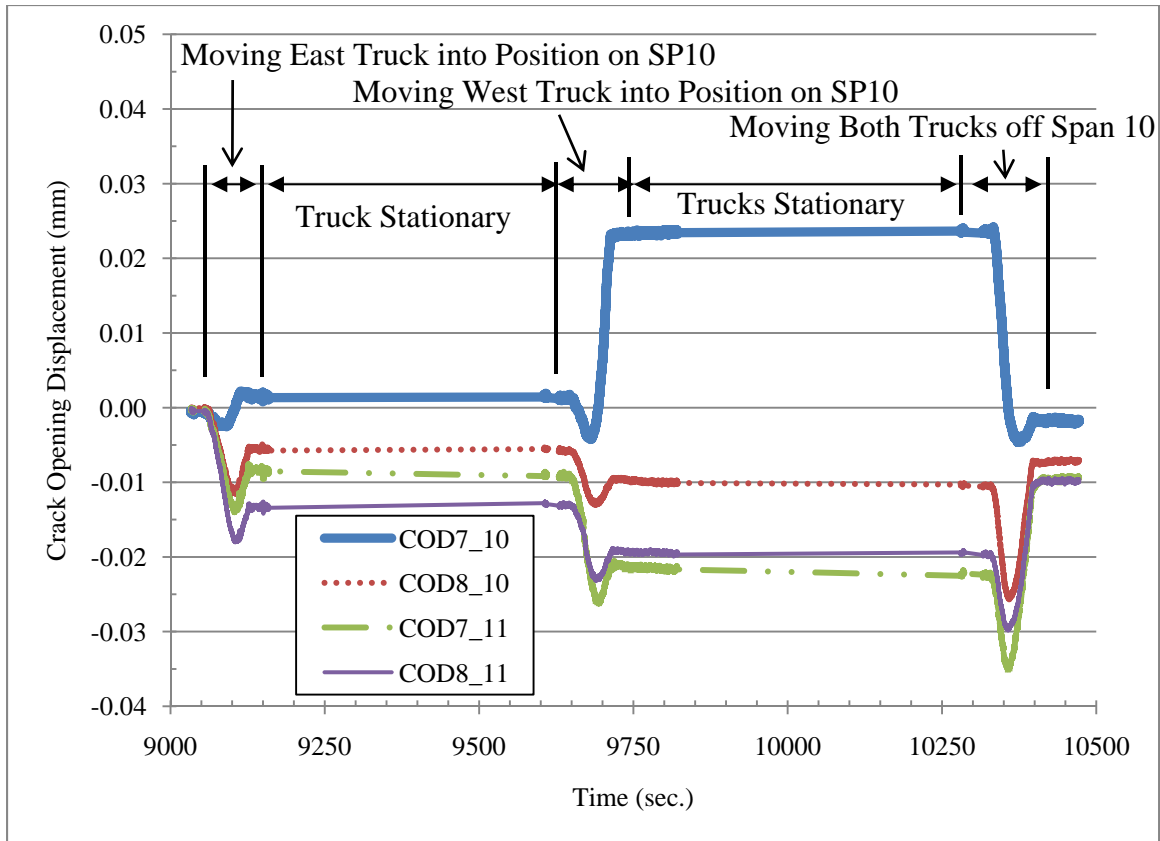
Figure 5-10: Crack-opening displacement during Night 1 loading of Span 10

The Span 10 and Span 11 loading COD data were split up to see more detail of the data and loading process. As can be seen in Figure 5-10, the COD data for S10G7 and S11G7 produced the maximum values for the Span 10 loading. Figure 5-11 shows the rest of the first night loading sequence of Span 11. Much like the pre-repair data, it can be seen that SP11G7 yields the maximum COD value for Span 11 loading. This information strengthens the argument that the cracks in Girder 7 were more flexible than in Girder 8 in both Span 10 and Span 11.
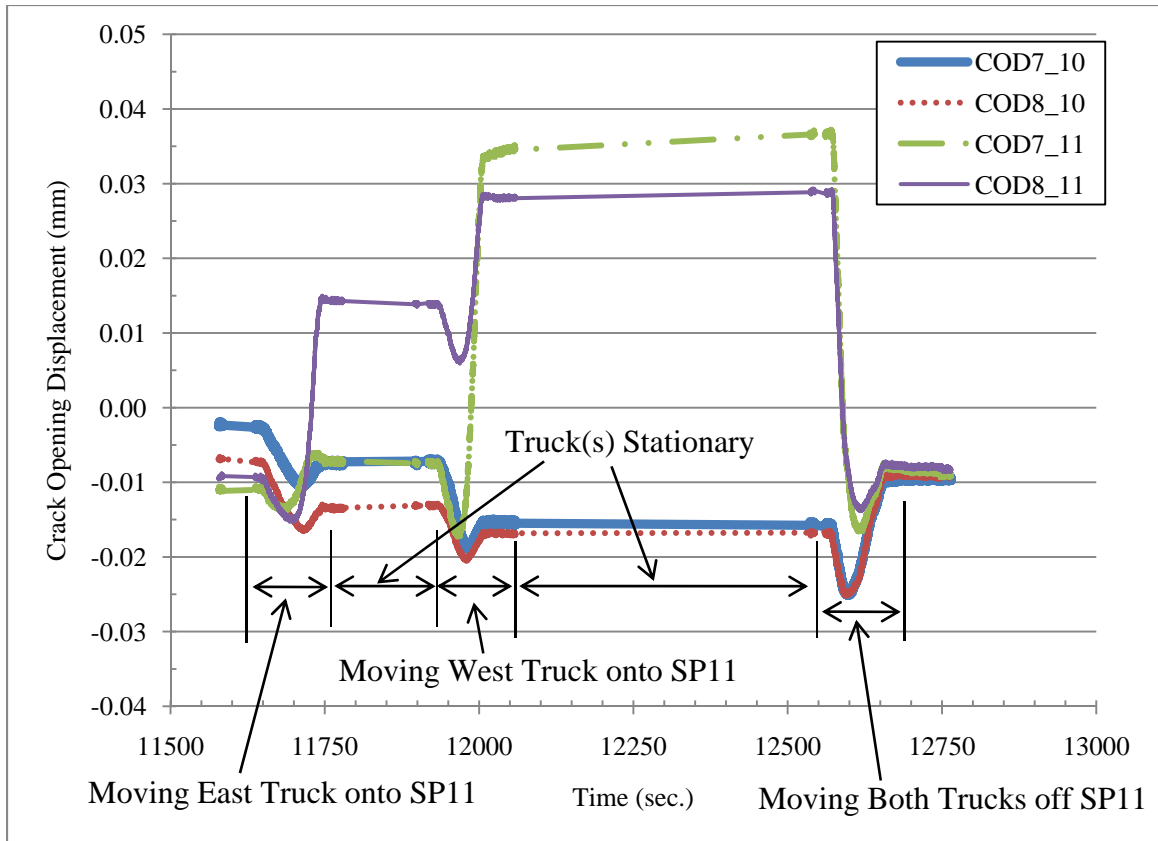
Figure 5-11: Crack-opening displacement during Night 1 loading of Span 11

It should be noted that in the pre-repair testing, it was found that the COD data for Girder 7 in both Span 10 and 11 were very similar. The maximum values for the COD were roughly the same for both the Span 10 and Span 11 loading. This was not the case for the post-repair testing. For the Span 10 testing, the maximum COD value for Girder 7 was 0.024 mm. For the Span 11 testing, the maximum COD value for Girder 7 was 0.037 mm. This shows that the pre-repair conclusion that the condition of Girder 7 was similar in Spans 10 and 11 did not hold true for this testing. It shows that the cracks in Span 11 opened more, which indicates that Girder 7 of Span 11 was in a different condition than Girder 7 of Span 10.

These data also show that the loading had some effect on the condition of the bridge. All of the COD devices were zeroed prior to testing. As shown in Figure 5-10 and Figure 5-11, the ending COD values were not at zero, indicating that there may have been some sort of inelastic response. The Span 10 and Span 11 testing was done in succession, and the total decrease in the COD data was on the magnitude of 0.01 mm (0.00 mm at the beginning of Span 10 loading, -0.01 mm at the end of Span 11 loading). For the pre-repair testing, the COD values began at 0.00 mm and ended around 0.002 mm, a much smaller decrease in value. It should also be noted that during the load holdings, there seemed to be some propagation of cracks. During each of the load holds, there seems to be an increase in magnitude from the start of the hold to the end of the hold. The pre-repair data showed more of a consistent value throughout the hold.

These discrepancies between the pre- and post-repair testing are not necessarily indicative of a degrading structure. It should be emphasized that the presence of the bearing pads and steel support frames during the pre-repair testing could have had a large effect on the difference in the data. The difference in the two tests is most likely due to the presence of the bearing pads in the pre-repair test, which caused the CODs to hold a constant displacement during the load holds. The post-repair behavior (an increase in magnitude of the COD data during the load holds) is more typical than the pre-repair response of a consistent value throughout the load hold. Environmental factors may have had some effect on the differing results, as well. The temperature effects on the concrete over the course of the testing, differing traffic patterns, and other conditions all could have contributed.

As in the pre-repair testing, the AE activity was measured during the loading sequences. As in most AE testing, an increase in AE activity is directly correlated to a propagation of damage. The AE amplitude generated from all sensors during the first night loading of Span 10 is shown in Figure 5-12.
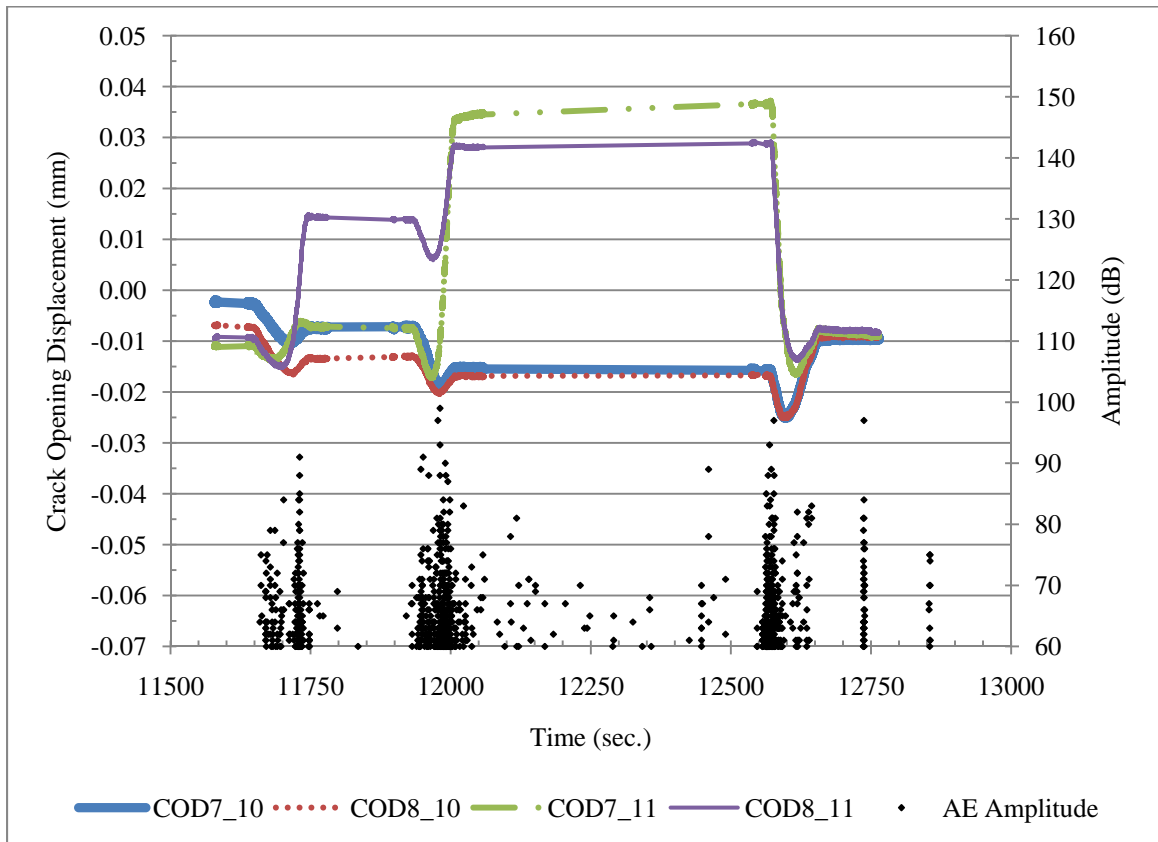
Figure 5-12: AE amplitude and COD versus time of Span 11 loading on Night 1

It is seen that most AE activity took place when a large change in COD occurred within the girders. The clusters of AE events correlate well with the peaks in the COD measurements, showing that the formation or propagation of cracks in prestressed concrete girders is associated by a significant increase in AE activity. The "random" bursts of AE activity (two instances) that occurred after the trucks move off the bridge may be due to traffic patterns on the bridge or other ambient noise causing an AE event

to occur. However, it is also possible that the cracks were closing and therefore creating frictional emission. The crack closure process is not immediate and redistribution of stresses takes place over a period measured in tens of minutes (recovery period). During the load hold, however, the scattered AE activity may be attributed to the slightly increasing COD measurement of SP11G7. There seems to be a correlation between the opening of this crack and the AE activity being produced during the process.

Figure 5-12 gives good agreement between the pre- and post-repair testing. It also reemphasizes the experimental observation that an increase in AE activity is correlated to some form of increasing damage of the structure; in this case, crack growth.

5.4.2 AE Evaluation Criteria Results

5.4.2.1 NDIS-2421 Criterion

As in the pre-repair testing and analysis, the load effects at a particular cross section varied due to the *location* of the truck loads, not due to the *magnitude* of the truck loads. Therefore, the load ratio was not used in the evaluation of the in-service bridge directly. Instead, the girder strain was more closely related to the load effect at a location. The strain ratio was used to represent the variation of the load effect induced at the instrumented section by moving truck loads. The process used to determine the NDIS-2421 evaluation criterion was altered for the post-repair testing. Instead of determining the damage of each girder for each night of the tests, a single damage assessment for each girder was found using both nights of testing. The procedure to determine the critical values was also changed for the post-repair data analysis.

As discussed previously, the strain gauge used in the pre-repair testing was not used for the post-repair testing. The strain gauges used for the post-repair testing were

located on the FRP directly above cracks on each of the girders. These strains were selected to get the best representation of the strain occurring at an already damaged part of the girder. It also provided some insight into the relationship between the strain in the concrete and the FRP.

In replacing the conventional load ratio with the strain ratio, certain steps must be taken to ensure that proper values are used for the NDIS-2421 criterion. The first of these steps is determining the initial onset of significant AE that occurs during a loading period. An attempt was made to objectively determine the onset of significant acoustic emission. The onset of significant acoustic emission has been defined in the past as the first time the *historic index* exceeds a particular value. The strain corresponding to that time is the strain at the onset of AE. According to ASTM E2478-06, the historic index is a form of trend analysis with the objective of locating significant changes in the slope of the cumulative signal strength versus time curve. The definition of historic index is given by:

$$H(t) = \frac{N(\sum_{i=K+1}^{N} S_{oi})}{(N-K)\sum_{i=1}^{N} S_{oi}}$$ (Eq. 5-4)

where:

$$K = \begin{cases} 0 & N < 200 \\ 0.8N & 200 \leq N < 1000 \\ N - 200 & N \geq 1000 \end{cases}$$

where $H(t)$ is the historic index at time t; N is the number of hits up to and including time t; S_{oi} is the signal strength of the ith event; and K is an empirically derived factor varying with the number of hits.

To use the historic index, one must determine the correct threshold levels for the derived factor, K. This was accomplished with trial and error using the data collected

from the load testing. Using the limits presented in Eq. 5-4, the K-factor can be
represented in Figure 5-13.
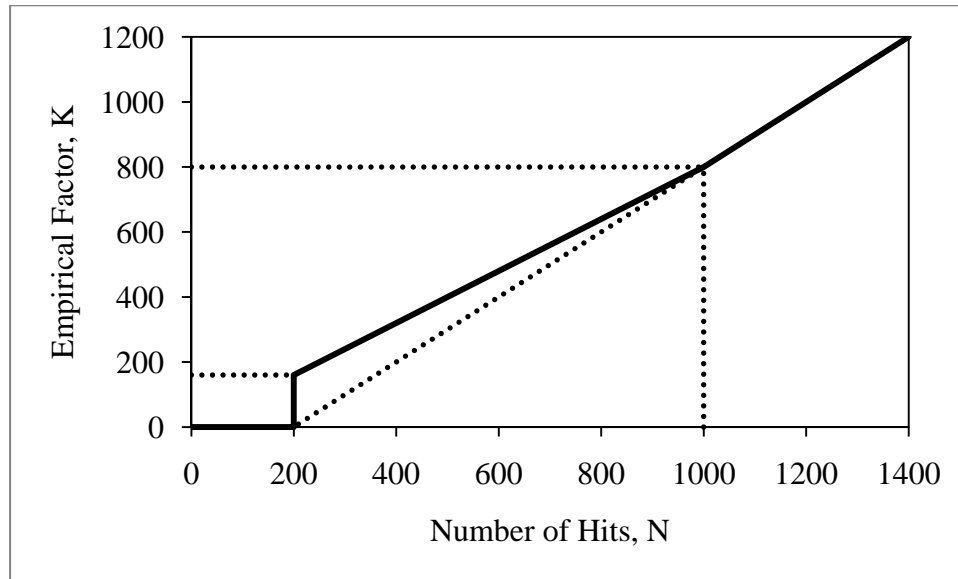
Figure 5-13: K-factor based on original historic index equation

The K-factor is determined by the number of hits that are being produced during the
loading/unloading sequence. Therefore, the threshold levels should be adjusted based
upon the loading procedure and conditions. For the post-repair testing, different K-factor
threshold levels were used for all four of the girders being tested. This was done to
obtain accurate values that could be used in the NDIS-2421 criterion.

To determine the correct historic index threshold values for the K-factor, an
iterative process was used to look at the historic index plot for varying limits. As can be
seen in Figure 5-14, the historic index plot begins with a value of one until a certain
number of hits occurs, at which time the historic index plot jumps to a value either
greater than or less than one.
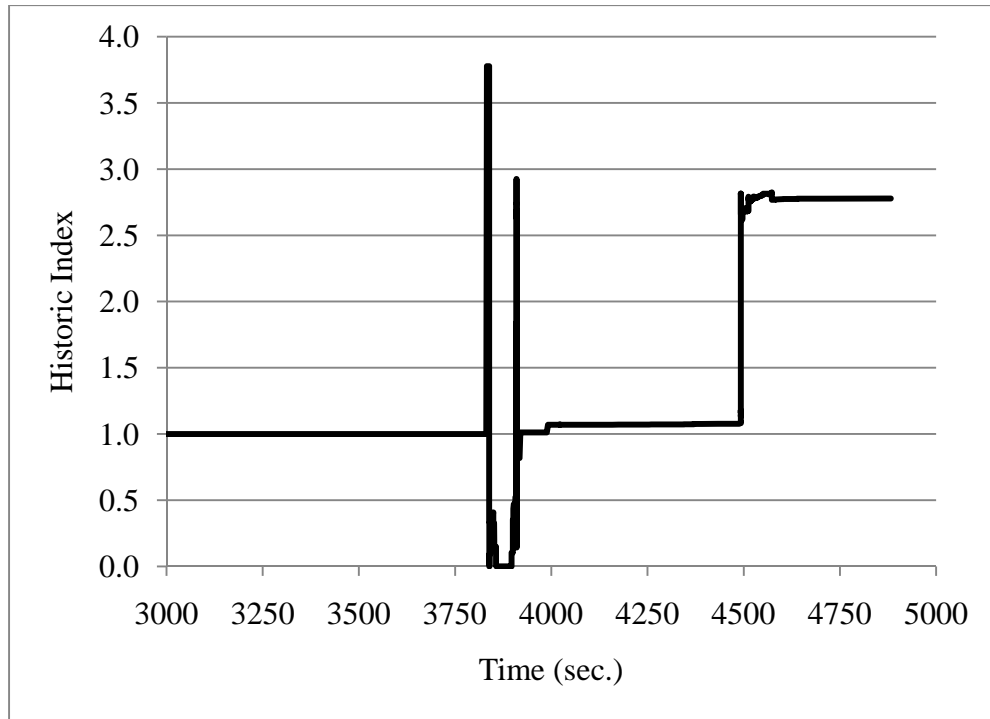
Figure 5-14: Historic index plot for SP10G7 on Night 2

To determine the threshold value for N to determine the K-factor, multiple plots were

produced with different N values. The correct N value was determined by a positive

increase in the first peak that corresponded with a change in the strain plot for that

loading sequence. By varying the number of hits before the spike in the historic index

plot, one could move the plot rather easily. However, a different choice in the number of

hits, N, to be used to determine K would cause different values for the NDIS-2421

results. Figure 5-15 shows a plot of the historic index overlaid with the strain from

SP10G7 on Night 2.
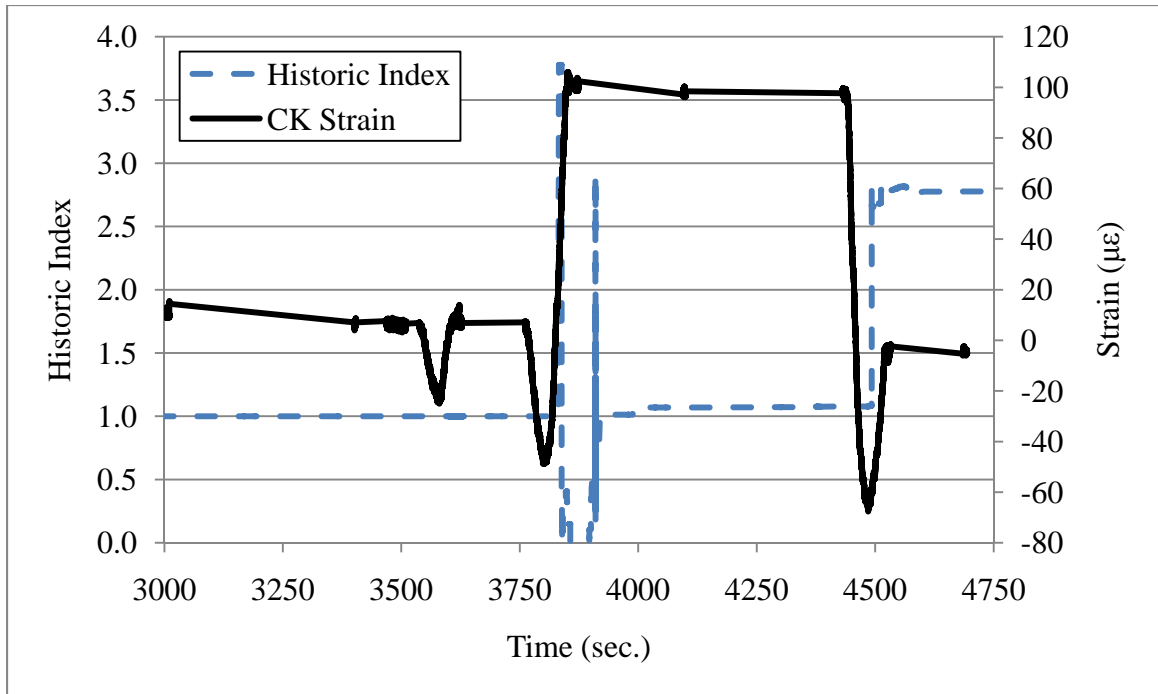
Figure 5-15: Historic index and strain versus time for SP10G7 on Night 2

As seen in the above figure, the peak that occurs using an adapted threshold of N=90 for

the first step of the piecewise function for K coincides with the increase in strain due to

the second truck being loaded onto the bridge. This process was repeated for all four

girders that were being tested. It was seen that for SP10G7, the empirically derived

factor, K was given by the following piecewise function:

$$K = \begin{cases} 0 & N < 90 \\ 0.8N & 90 \le N < 1000 \\ N - 200 & N \ge 1000 \end{cases}$$

Figure 5-16 shows the adjusted K curve for SP10G7. It should be noted that the

empirically derived K-value was only adjusted for the first and second steps of the

piecewise function. Future research should focus on the adjustment of the entire curve,

but this study is beyond the scope of this project. The third step of the function does not

affect the first spike in the historic index curve, which is the only indicator that is being used to develop a basis for the NDIS-2421 criterion.
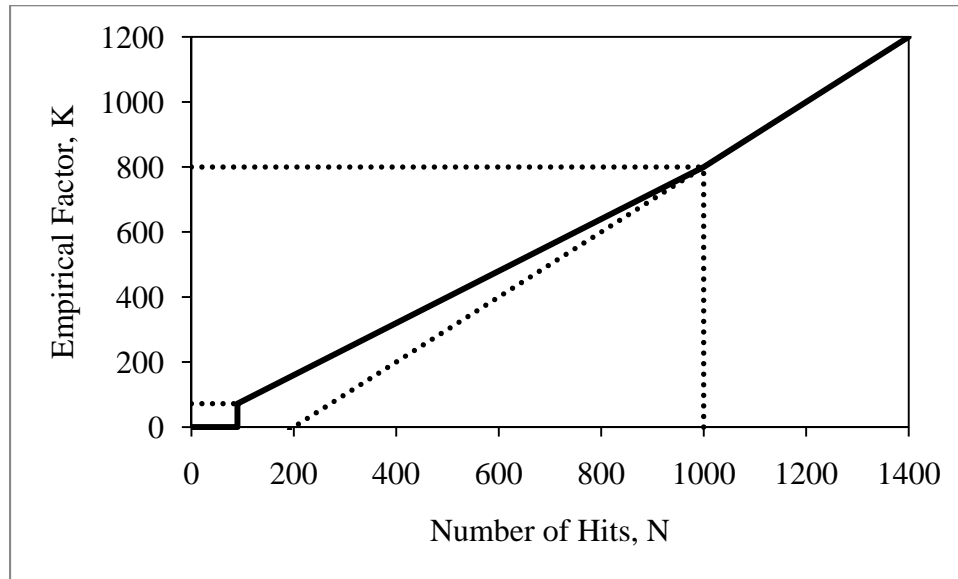
Figure 5-16: Derived K-factor for SP10G7 (N=90)

The other three girders all produced independent K curves based upon the number of hits that occurred during the loading phase of Night 2. It was necessary to determine independent K curves for each of the girders to ensure that the "spike" in the historic index curve occurred during a loading cycle. The historic index and K curves can be seen in Appendix B. The N threshold values for SP10G8, SP11G7, and SP11G8 were 110, 120, and 110, respectively.

After developing the historic index with a corrected K value based upon the number of hits occurring, the NDIS-2421 plots were developed by looking at the Night 1 and Night 2 strain, CSS, and historic index curves. For the explanation of this process, SP10G7 will be used to show the steps involved in determining the critical values. The plots for the other girders can be seen in Appendix B. To determine the strain at the

onset of AE, the historic index versus strain plot was used, which can be seen in Figure

5-15. The strain ratio for this process was redefined as follows:

$$\text{Strain Ratio} = \frac{\text{Strain at the onset of significant AE on Night 2}}{\text{Maximum Strain on Night 1}} \qquad \text{(Eq. 5-5)}$$

Using this equation incorporated the loading from Night 1 and Night 2, which seemed to

give the best representation of the damage that occurred in the girder.

Using Figure 5-17, it can be seen that the onset of AE occurs at the point (3833

sec., 29 με).
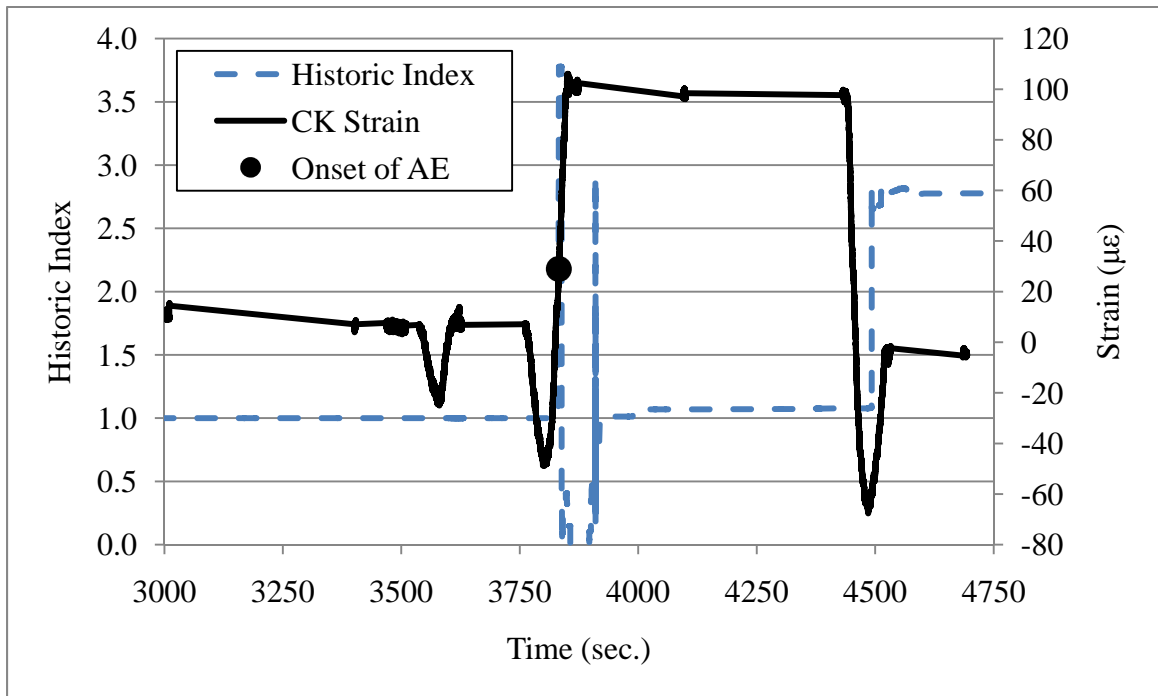
Figure 5-17: Onset of AE for SP10G7 on Night 2

Figure 5-18 shows the strain from Night 1. From this plot, the maximum strain from

Night 1 loading can be determined to be 100 με. It should be noted that the transient

spikes occurring just after the maximum labeled in Figure 5-18 were neglected.
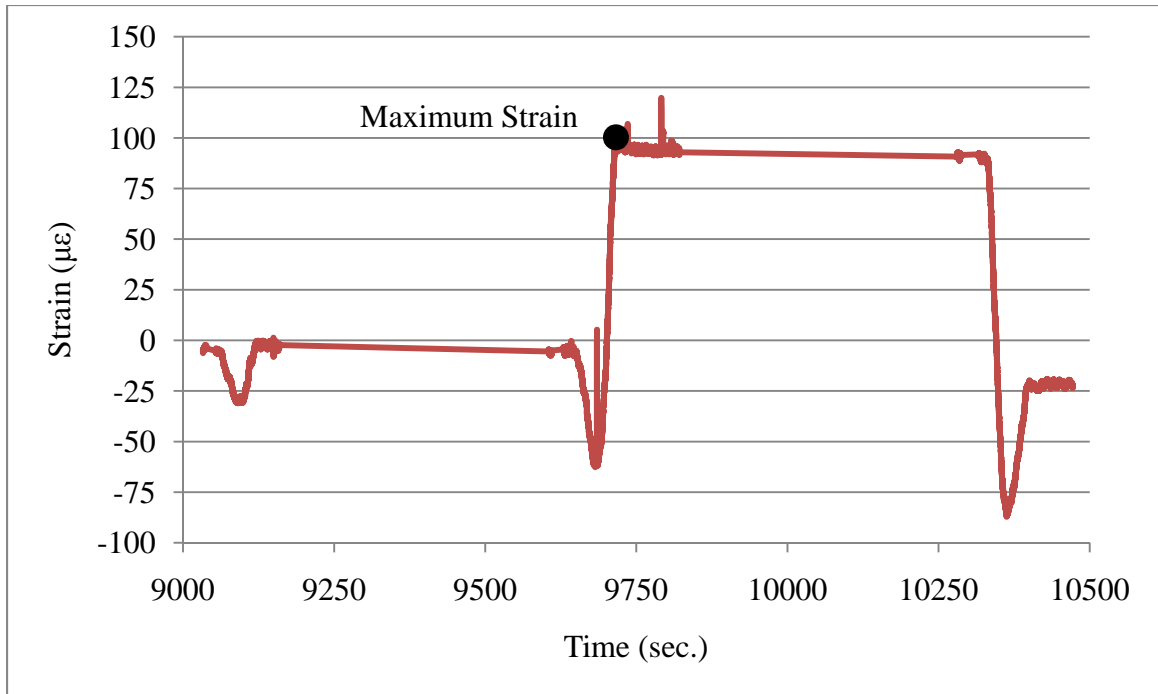
Figure 5-18: Maximum strain from Night 1 for SP10G7

Using these two strain values, the strain ratio for SP10G7 can be calculated as 29/100 =

0.29.   Although this ratio seems to be reasonable, it should be noted that this process was

somewhat subjective in the determination of the newly formed K piecewise function.

This process has seemed to return reasonable results for all four girders, but the process

should be refined through further laboratory testing.

The next step in the NDIS-2421 damage assessment was determining the calm

ratio for the girders. This process was completed by looking at the CSS during both

nights of testing. The general equation for the calm ratio deals with the ratio between the

CSS during the unloading process versus the CSS during the loading process. Due to the

complex loading sequences of this project and the lack of prior research using this type of

loading, three possible equations were looked at to determine the most suitable calm

ratio:

$$\text{Calm Ratio} = \frac{\text{CSS during unloading on Night 2}}{\text{CSS during loading on Night 1}} \qquad \text{(Eq. 5-6)}$$

$$\text{Calm Ratio} = \frac{\text{CSS during unloading on Night 1}}{\text{CSS during loading on Night 1}} \qquad \text{(Eq. 5-7)}$$

$$\text{Calm Ratio} = \frac{\text{CSS during unloading on Night 2}}{\text{CSS during loading on Night 2}} \qquad \text{(Eq. 5-8)}$$

All three of these equations could satisfy the general calm ratio concept. However, Eq. 5-6 was originally based on a cyclic load testing where there was a reloading process. Since this project did not have a conventional reloading process where the reload occurs immediately after the load, Eq. 5-7 and Eq. 5-8 seemed to be more fitting for this analysis. Figure 5-19 and Figure 5-20 show the SP10G7 CSS plots for Night 1 and Night 2. The loading and unloading portions are indicated on each plot.
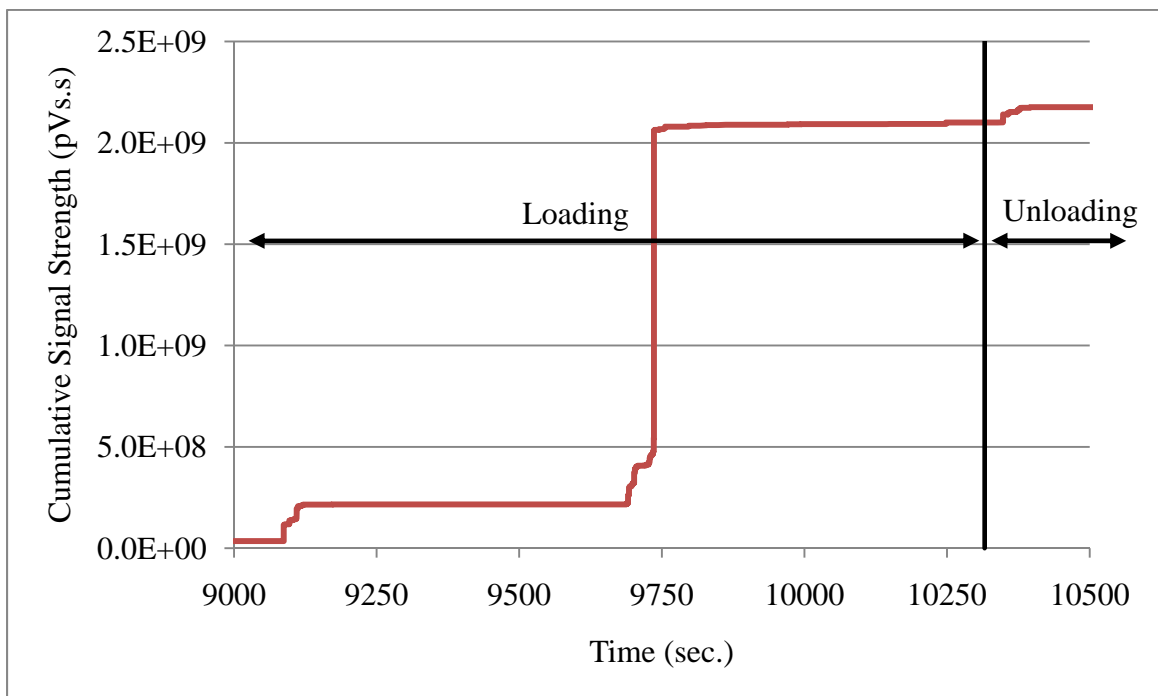
Figure 5-19: CSS from SP10G7 loading on Night 1
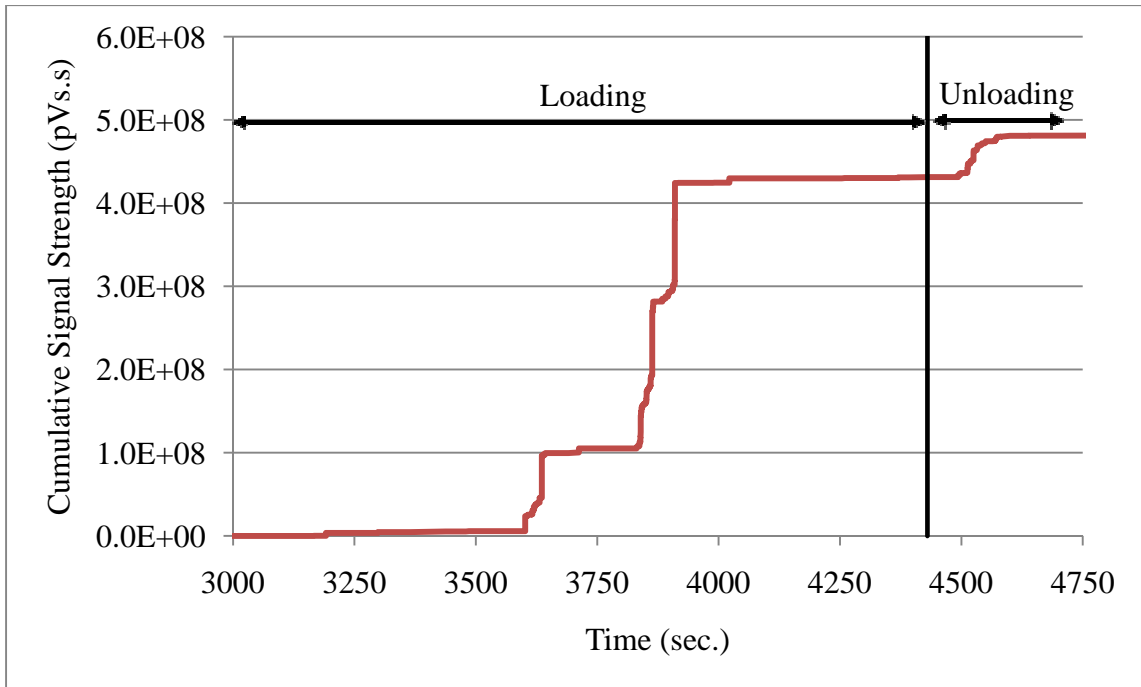
Figure 5-20: CSS from SP10G7 loading on Night 2

The calm ratio was calculated to be 0.024 using Equation 5-6, 0.04 using Equation 5-7, and 0.12 using Equation 5-8. Since all three of these values were similar in magnitude and choosing one over the other would not change the NDIS-2421 damage classification, it seemed that any one of these equations could be used to calculate the calm ratio. After reviewing the other four girders, similar results were obtained. Equation 5-7 was chosen because of two reasons: using a single night's loading/unloading cycle seemed more consistent than combining two nights' cycles, and Night 1 produced more AE data than Night 2.

Once the strain and calm ratios were determined, the NDIS-2421 plot was produced for each of the four girders. Figure 5-21 shows the NDIS plot for SP10G7. It can be seen that, according to the NDIS-2421 criterion, SP10G7 falls into the quadrant of intermediate damage.
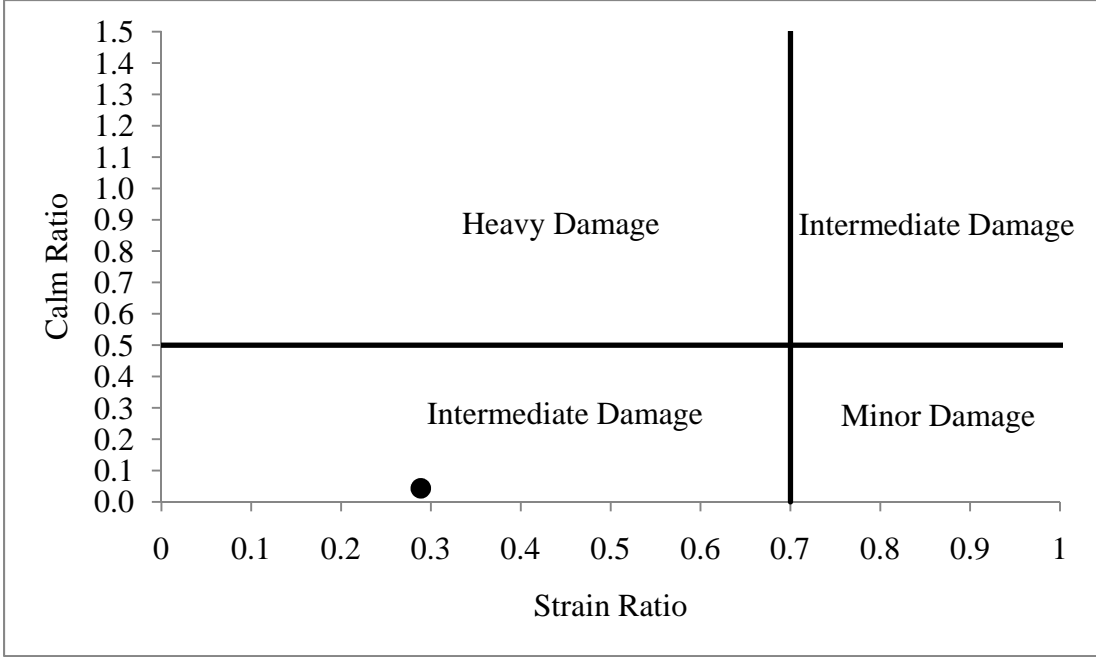
Figure 5-21: Damage qualification based on NDIS-2421 for SP10G7

After looking at all four girders, the damage qualifications based on the NDIS-2421

criterion were plotted in Figure 5-22. It should be noted that a higher strain ratio means

that the onset of AE is occurring at a strain that is close to the previous maximum strain.

A lower strain ratio indicates a breakdown of the Kaiser effect, in that AE is occurring at

a strain much less than the previous maximum strain.
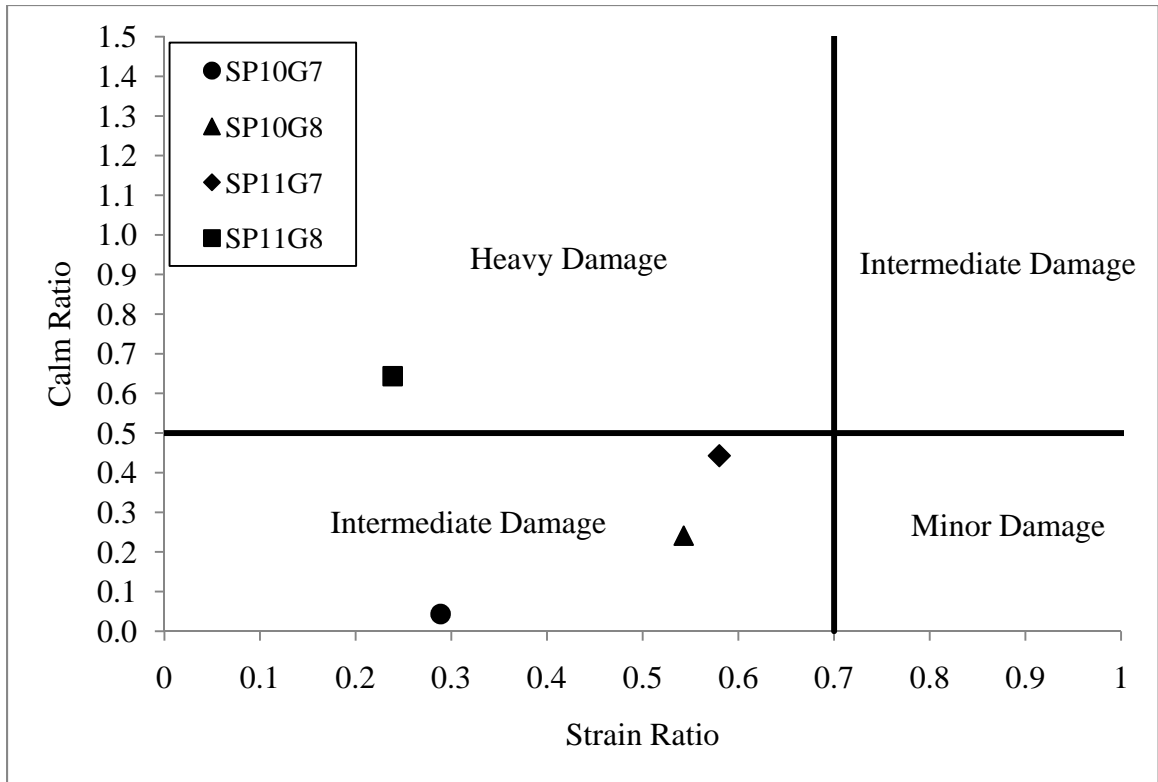
Figure 5-22: Damage qualification based on NDIS-2421 for all four girders

Figure 5-22 shows that SP10G7, SP10G8, and SP11G7 all fell into the quadrant associated with intermediate damage, while SP11G8 was classified in the heavy damage quadrant.

5.4.2.2 Signal Strength Moment Ratio Evaluation

The Signal Strength Moment (SSM) Ratio was proposed as a way to determine the propagation of damage within a girder. A larger SSM ratio indicates a breakdown of the Kaiser effect which, in turn, describes increasing damage in a structure. Based on laboratory testing done by Xu (2008), it was seen that the SSM threshold for damage in prestressed concrete beams was 4%; that is, a value greater than 4% indicated a specimen that was heavily damaged.

A better understanding of the SSM ratio analysis was needed before accepting the procedure proposed by Xu (2008). Data analysis was used with the AE data from Night 1 and Night 2 of the post-repair testing to verify the procedure used in the pre-repair testing. The first analysis was used to determine the validity of the 240-second hold proposed by Xu. Figure 5-23 shows the SSM ratio for SP10G8 for six different hold times: 60, 120, 180, 240, 300, and 360 seconds—each beginning at the start of the load hold.
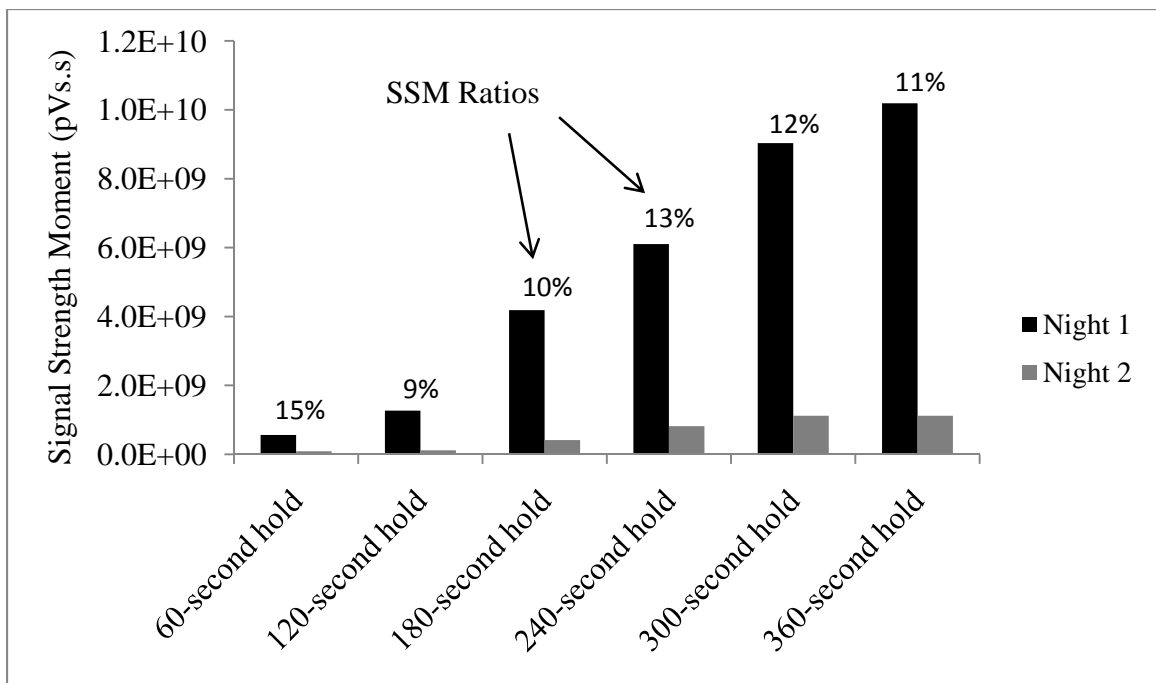
Figure 5-23: SSM ratios for different data time frames for SP10G8

Figure 5-23 shows that the SSM ratio is more sensitive to hold times at smaller durations (less than 240 seconds). As the hold time increases, the SSM ratio begins to level out. This conclusion was confirmed by similar results found from the other three girders tested. The 240-second time frame seemed to be the best option for the SSM ratio.

Figure 5-23 shows different durations, each starting at the beginning of a load hold. However, the researchers also investigated whether it was important that the SSM

ratio duration started at the beginning of the load hold. This issue was explored to see if different 240-second time spans throughout the nine-minute load hold would yield similar results. Figure 5-24 shows six different 240-second time spans for SP10G8. Each time span begins 60 seconds after the previous time span; i.e. Time Span 1 starts at the beginning of the load hold and lasts for 240 seconds, Time Span 2 begins 60 seconds after the beginning of Time Span 1 and lasts for 240 seconds.
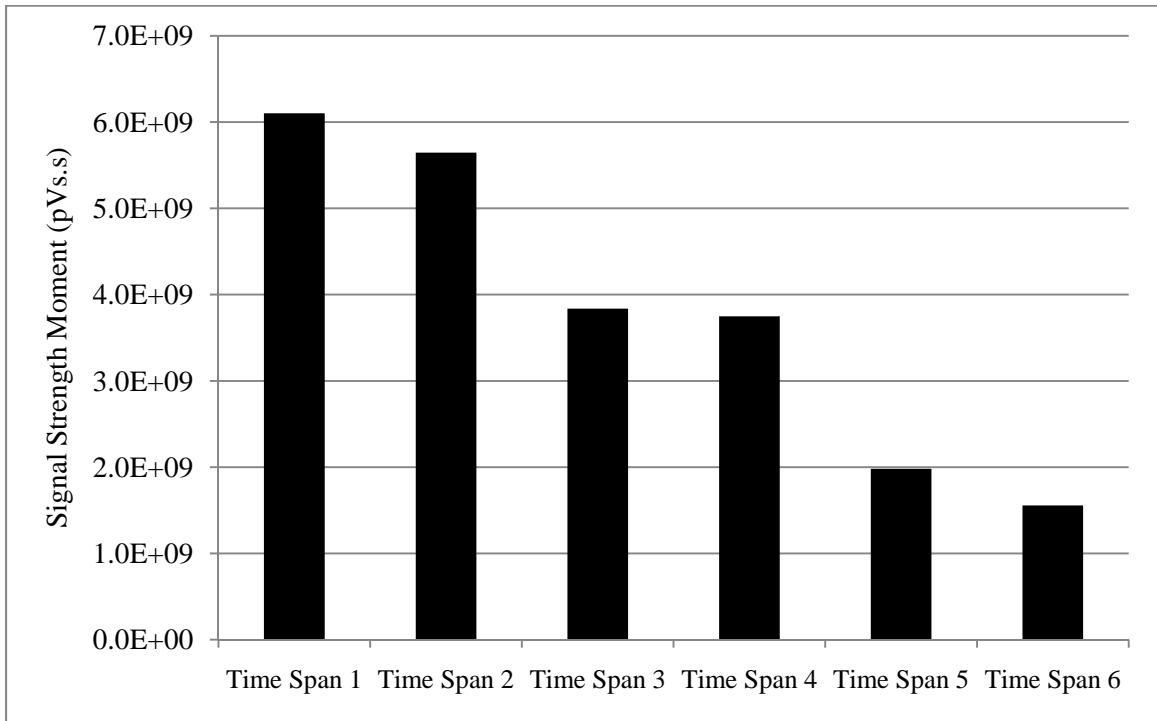
Figure 5-24: SSM for different 240 second time spans for SP10G8 on Night 1

Figure 5-24 shows that most AE activity occurs in the first 240-second time span. This seems to be evident since AE data should be occurring for a brief time after the trucks are in place. Any AE occurring throughout the rest of the nine minute load hold is caused by environmental/ambient noise or the continuing propagation of damage. The first 240-second time span seems to be the best option for the SSM ratio since the most data are being collected during that time.

After determining that the first 240 seconds produced the most AE data, the SSM ratios for each of the six time spans were found to see if there were similarities in the different time spans. Figure 5-25 shows the SSM ratios from the six different time spans for SP10G8.
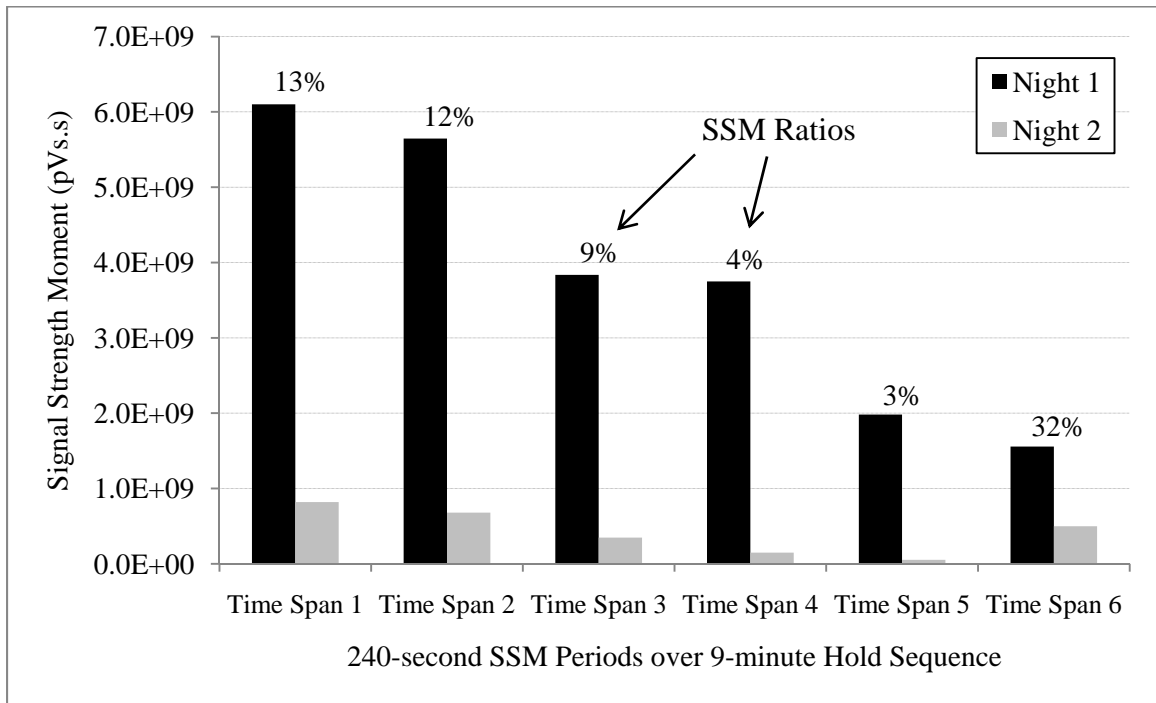
Figure 5-25: SSM ratios for different 240-second time spans for SP10G8

It can be seen that the 240-second time span chosen for the SSM ratio analysis does have an effect on the SSM ratio. According to Xu's 4% threshold, Time Spans 1, 2, 3, and 6 would have resulted in a classification of "heavily damaged" girders, while Time Spans 4 and 5 would have indicated "not heavily damaged" girders. This is a concern for the SSM ratio analysis, and it should be noted that more testing should be done to improve the selection of which 240-second time span should be used in the analysis. However, since it has been seen that the most AE data occurs right after the trucks are in position, further analysis for this study was conducted using Time Span 1.

119

An interesting deduction can be made from Figure 5-25 and similar figures for

SP10G7, SP11G7, and SP11G8. Looking at Time Span 1 and Time Span 2, it can be

seen that the overall SSM ratio from the two time spans do not differ greatly; 13% and

12%, respectively. An analysis was used to show that during the testing procedure, the

240-second time span does not need to start immediately after the trucks are in place.

This is useful in that it gives the AE operator a delay time that allows for some error in

the communication of the exact moment when the trucks are in place. A recommended

delay time is between 10 and 15 seconds. Both of these delay times seemed to agree with

the SSM ratio that was obtained by using the time span starting immediately after the

trucks were in place.

After repeating the SSM ratio process used by Xu (2008) on the post-repair

girders, the following conclusions were made about the girders. Based on the data from

Night 1 and Night 2 testing, all of the SSM ratios for the four girders were over 4%.

Figure 5-26 shows the Night 1 and Night 2 signal strength moment and their relative

ratios.
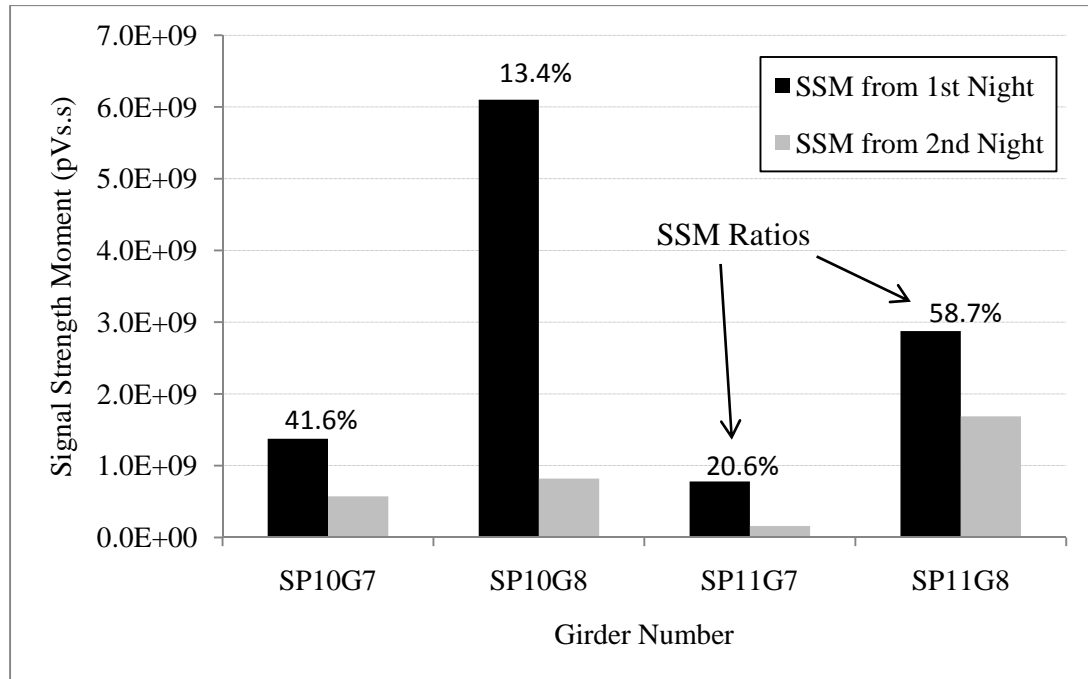
Figure 5-26: Signal strength moment (SSM) ratio during holds

According to Xu's 4% threshold, all four girders are "heavily damaged." However, according to the SSM ratio analysis, there is no indication of what "heavily damaged" actually means. More extensive testing should be done to see if the 4% that was obtained using laboratory tests does indeed carry over to be applicable to prestressed girders with an FRP repair. Also, the testing should be done in such a way as to determine the actual damage level associated with a 4% SSM ratio value.

There were some similarities between the pre-repair and post-repair results for the SSM ratio analysis. For both tests, SP10G8 gave the largest magnitude of signal strength moment. However, the SP10G8 signal strength moment from Night 1 of the pre-repair test was 3.5×10^9 pVs.s while the post-repair returned a value of 6.1×10^9 pVs.s. This discrepancy may be explained by the increased AE emission due to the interaction between the concrete and the FRP repair. This general trend was seen in all four girders.

5.4.3 Crack Location using AE 2D-LOC Analysis Technique

As in the pre-repair testing, the AE 2D-LOC Software was used to compare

source locations to the actual cracks in the concrete girders. This software uses

triangulation to determine source location given the magnitude and "speed" of the

emission signal. The pre-repair testing gave fairly accurate results with minimal

interference from environmental and ambient noise.

Figure 5-27 shows the source locations from both nights of testing. Sensors 13—

18 can be seen in the prescribed pattern (with a threshold limit of 60 dB). As can be seen

in the plot, there seems to be a cluster of events that occurs near Sensor 14 and moves up

the face toward Sensor 18. An estimated crack pattern was drawn based on this AE data

to compare to the visible cracks on the face of the girder.
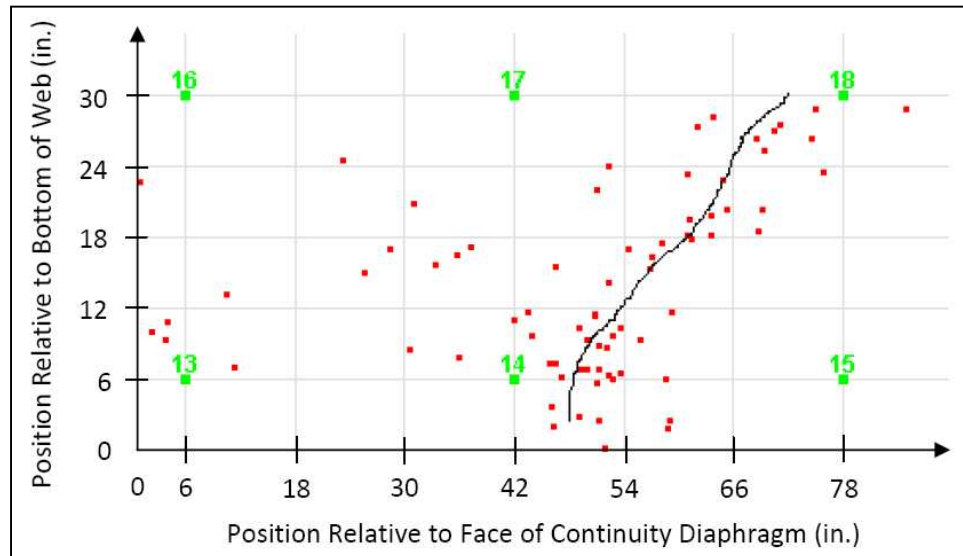
Figure 5-27: AE 2D-LOC source locations for SP11G8

The actual visible cracks on the face of SP11G8 can be seen in Figure 5-28. In

this figure, two types of cracks can be seen. First, the repaired cracks can easily be seen

due to the epoxy used to seal them. However, there was a new crack that had formed

after the epoxy was injected, which has been traced and labeled. Comparing Figure 5-27 and Figure 5-28, an agreement can be seen between the source locations and the visible, unsealed crack. This agreement shows that the AE 2D-LOC software can give fairly accurate results when trying to locate active cracks in the concrete. This also matches the results found by Xu (2008).
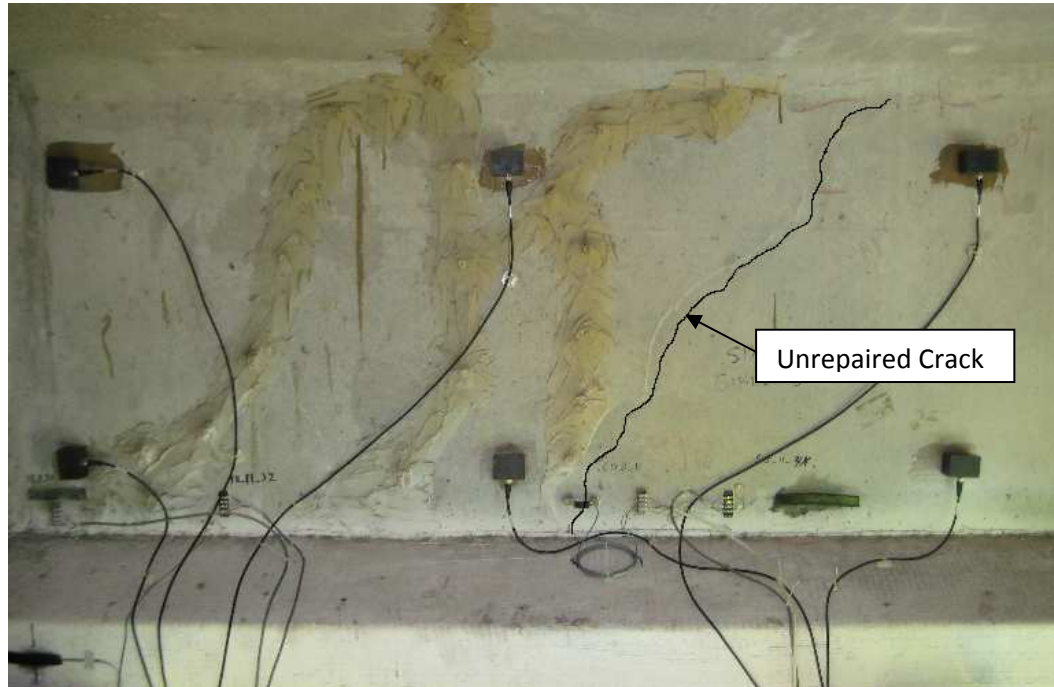
Figure 5-28: Visible cracks on face of SP11G8

To verify the results from SP11G8, another girder was evaluated to see if similar results could be replicated. The source locations for SP11G7 (Sensors 19—24) are shown in Figure 5-29. Once again, a general pattern of event locations can be seen moving from the left of Sensor 20 to the right side of Sensor 23.
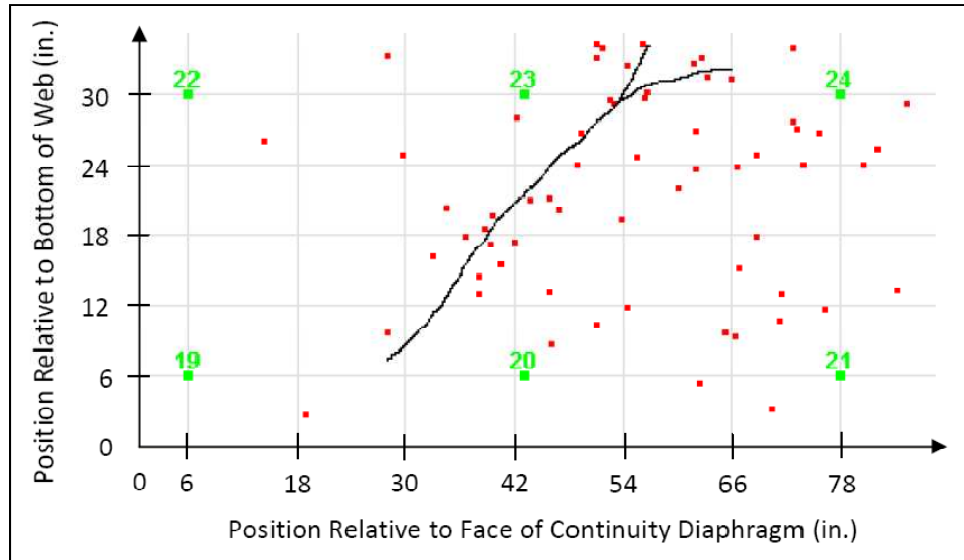
Figure 5-29: AE 2D-LOC source locations for SP11G7

For comparison purposes, Figure 5-30 shows the actual cracks located on the face of SP11G7. Like SP11G8, this girder has two types of cracks; the epoxied cracks and a new crack that formed after the epoxy hardened. Once again, there exists a general agreement between the event source locations in Figure 5-29 and the unsealed crack in Figure 5-30.

Figure 5-30: Visible cracks on face of SP11G7

The AE 2D-LOC software was also used to determine any crack patterns located in SP10G7 and SP10G8. The source location patterns and the actual crack patterns can be seen in Appendix D. No conclusions were made about the effectiveness of the AE 2D-LOC software on these girders. There was no indication of a clear pattern in the source location plot that correlated well with the actual crack pattern in the girder. This may have been caused by the increase in threshold level. The increase in threshold level also explains why the pre-repair AE 2D-LOC results show much more AE data being produced during the load test compared to the post-repair results. More AE data were being filtered during the post-repair test.

It should be noted that there seem to be "random" event source locations plotted in Figure 5-27 and Figure 5-29. Like the pre-repair testing, this can be attributed to the friction caused by the concrete and prestressing strands, from environmental or ambient noise, or reflections of the AE. Another possibility for the random source locations could

be the interaction between the FRP and the concrete. Compared to the pre-repair test, the post-repair test did not yield significantly more AE events occurring in the bottom of the girder where the FRP was located. However, this could have been caused by the change in the threshold level used for the post-repair testing (previously discussed in Section 5.3). More AE testing should be done on FRP repaired specimens to see if a relationship exists between the FRP repair and any acoustic emission. If there is some interaction between the FRP repair and the concrete that causes random emission to occur, the operator should be conscious of this relationship and adjust the procedure accordingly.

5.4.4 Additional Evaluation Criteria

5.4.4.1 Channel Hit Frequency

Information can be gained by looking at some very simple plots that show the nature of the acoustic emission signals. First and foremost, a simple bar graph showing the frequency of hits per channel can give information about which channels were more active than others. The channel hit frequency for the Span 11 loading on Night 1 is shown in Figure 5-31.
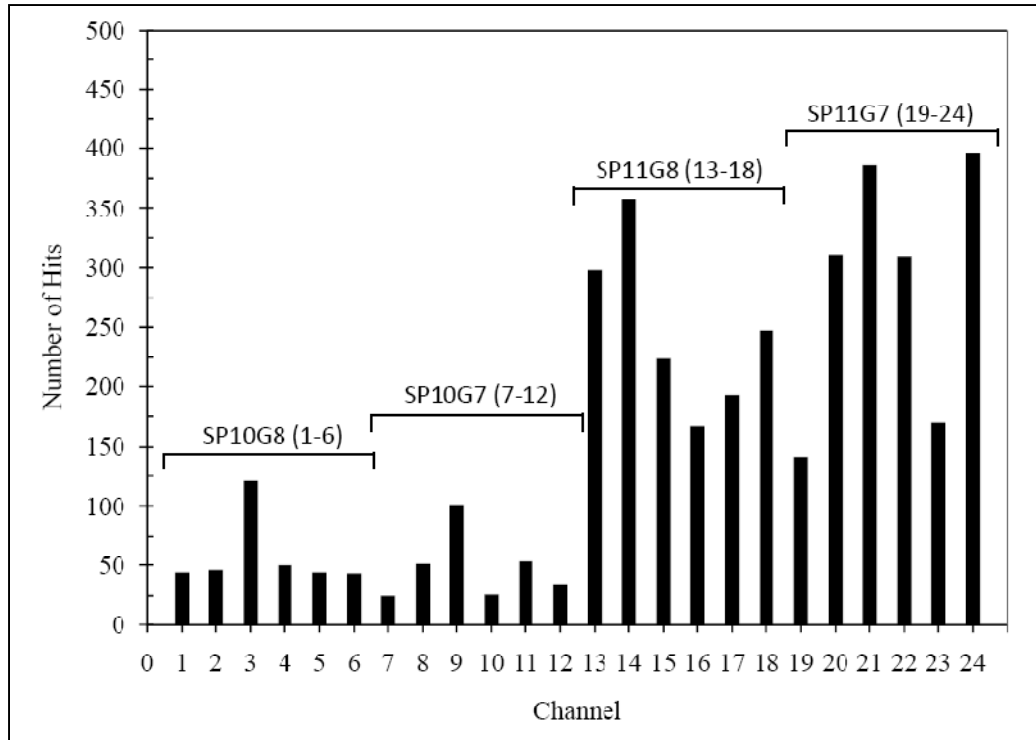
Figure 5-31: Channel hit frequency for Span 11 loading on Night 1

It can be seen that the sensors (channels) located on the Span 11 girders (channels 13-24) were much more active than those on Span 10 (channels 1-12). However, Span 11 loading did produce AE in Span 10, as well. It should be noted that Channels 3 and 9, the two channels located closest to the interior bent (and Span 11) produced the most Span 10 AE hits during the Span 11 loading. Figure 5-31 also shows that the most active channels in Span 11 correspond to the sensors located closest to the AE-2D LOC crack locations.

5.4.4.2 Peak CSS Ratio

The peak CSS ratio can be used as another indication of damage that is occurring in the bridge girders. The peak CSS ratio is expressed as:

$$\text{Peak CSS Ratio} = \frac{\text{Peak CSS at the end of reload hold period}}{\text{Peak CSS at the end of initial hold period}} \times 100\% \qquad \text{(Eq. 5-9)}$$

According to Ridge and Ziehl (2006), a Peak CSS Ratio between 30% and 50% indicates significant damage. Figure 5-32 shows the CSS plotted from SP10G7 on Night 1.
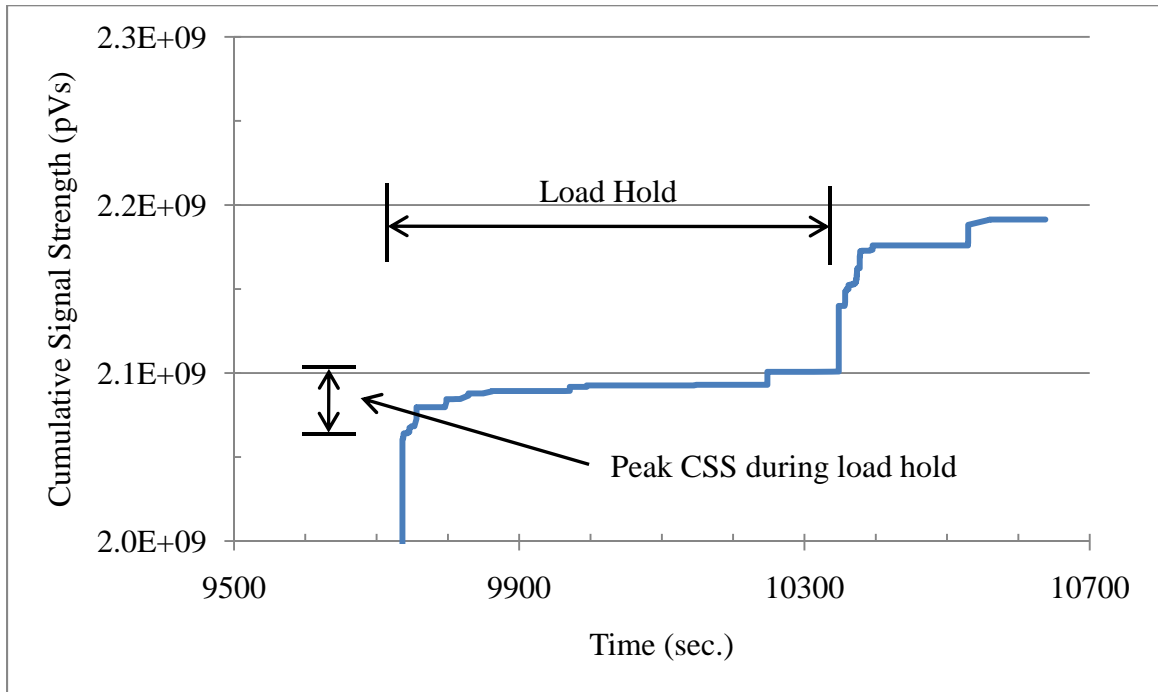
Figure 5-32: CSS from SP10G7 on Night 1

The peak CSS for Night 1 would be defined as the CSS accumulated during the load hold right before both trucks began driving off of Span 10. This hold period is labeled on Figure 5-32. The CSS plot from SP10G7 on Night 2 is plotted in Figure 5-33.
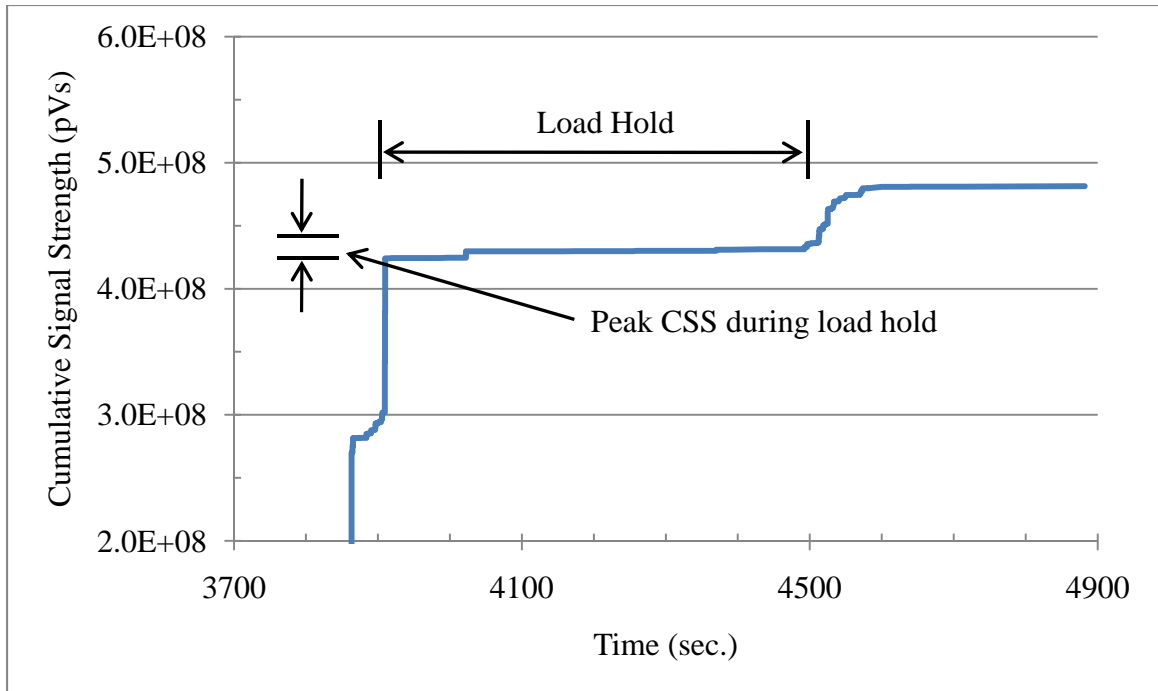
Figure 5-33: CSS from SP10G7 on Night 2

The reload period was defined as the Night 2 loading and the initial load period was

defined as Night 1. After dividing the Peak CSS from Figure 5-33 by the Peak CSS in

Figure 5-32 and multiplying by 100%, the Peak CSS ratio was calculated to be 8%.

Table 5-5 shows the Peak CSS ratios for all four girders.

Table 5-5: Peak CSS ratios for post-repair test

Girder	Peak CSS at end of reload hold period (pVs)	Peak CSS at end of initial hold period (pVs)	Peak CSS Ratio (%)
SP10G7	2.31×10^6	2.89×10^7	8
SP10G8	1.00×10^7	1.12×10^8	9
SP11G7	5.45×10^6	2.02×10^7	27
SP11G8	6.51×10^7	1.67×10^8	39

Table 5-5 shows that only SP11G8 of the Peak CSS ratios was in the 30-50% significant

damage level, meaning it was the only one with significant damage according to this

evaluation criterion. The Span 11 girders, it should be noted, are much larger than the Span 10 girders. These two girders both had significant, active cracks present in the web. On the other hand, SP10G8 had an active crack present on only one side of the girder. The COD data agree with these results in that the Span 11 girders produced the largest range of COD values. Therefore, the Peak CSS ratios seem to line up with the visible damage in the girders and the COD data.

5.5 Post-Repair Analysis Applied to Pre-Repair Data

To draw a proper comparison between the pre- and post-repair test results, it was necessary to apply the adapted analysis used for the post-repair data to the pre-repair data. This re-evaluation of the pre-repair AE data allowed for a more direct comparison between the two tests.

The adapted NDIS-2421 criterion procedure used for the post-repair analysis was applied to the data gathered during the pre-repair test. The results from the adapted NDIS-2421 analysis are shown in Figure 5-34.
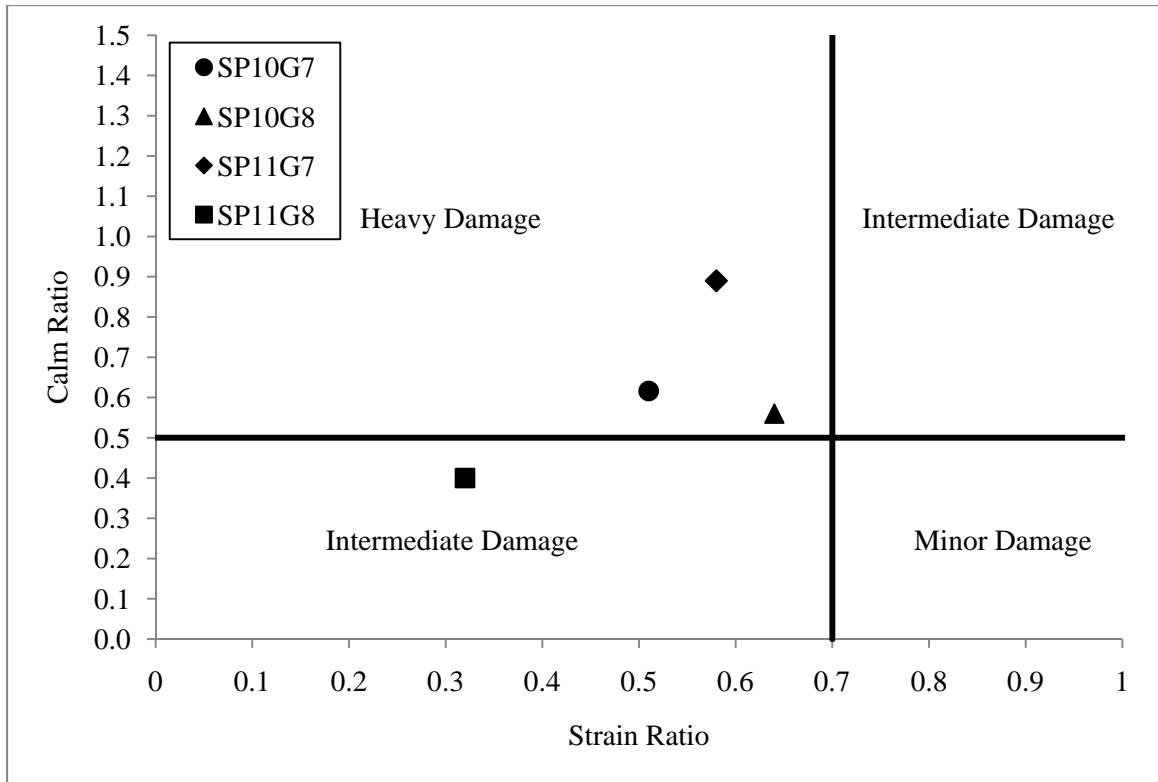
Figure 5-34: Damage classification based on adapted NDIS-2421 for pre-repair

As seen in the above figure, the adapted NDIS-2421 criterion classified SP10G7,

SP10G8, and SP11G7 in the "heavy damage" quadrant, while classifying SP11G8 in the

"intermediate damage" quadrant. These results actually agree with the results from the

pre-repair NDIS analysis performed by Xu (2008), presented in Section 5.2.2.1.

However, the values used to plot the NDIS-2421 results were different between the two

tests. Comparing the pre-repair results in Figure 5-4 to the adapted pre-repair results in

Figure 5-34, all three of the girders classified as "heavy damage" (SP10G7, SP10G8, and

SP11G7) had calm ratios of one or more for the pre-repair and less than one for the

adapted pre-repair results. For the lone "intermediate damage" girder (SP11G8), it was

greater than the strain ratio limit of 0.7 and greater than the calm ratio limit of 0.5 in the

pre-repair results and was the complete opposite for the adapted pre-repair results (lower

131

than the strain and calm ratio limits). Although the analyses returned similar results as far as damage classification, the strain and calm ratios calculated for each of the girders were quite different.

The Peak CSS Ratio analysis was not performed for the original pre-repair evaluation. To draw some comparisons between the two tests, it was necessary to complete this analysis for the pre-repair test. The same procedure used for the Peak CSS Ratio analysis of the post-repair data was implemented for the pre-repair data. Table 5-6 shows the results from this analysis.

Table 5-6: Peak CSS ratios for pre-repair test

Girder	Peak CSS at end of reload hold period (pVs)	Peak CSS at end of initial hold period (pVs)	Peak CSS Ratio (%)
SP10G7	4.73×10^5	2.20×10^7	2
SP10G8	5.13×10^6	5.32×10^7	10
SP11G7	9.34×10^6	3.71×10^7	25
SP11G8	2.74×10^6	9.10×10^7	3

As seen in the table, the Peak CSS Ratio analysis indicates that all four of the girders have no significant damage (based on the 30% critical value proposed by Ridge and Ziehl (2006)). This conclusion certainly contradicts the NDIS-2421 results, but some similarities do exist between the two analyses. First of all, according to the NDIS-2421 criterion, SP11G8 was classified as "intermediate damage," while the Peak CSS analysis returned a value of 3%, signifying very little damage. Likewise, SP11G7 seems to be the most damaged girder of the four according to the NDIS-2421 criterion, and it yielded the highest Peak CSS ratio.

The SSM Ratio analysis used for the post-repair testing was the same analysis used for the pre-repair analysis, so the results of these two analyses can be compared without adaptation.

5.6 Summary and Conclusions

There has been considerable research done on acoustic emission monitoring of bridges. However, specific evaluation criteria and testing techniques are still being researched when it comes to prestressed concrete bridge girders. This in-field study provided insight into testing techniques that need to be improved upon, as well as possible problems with evaluation criteria that have been proposed for prestressed concrete girders. This study also gave insight into the current integrity of the I-565 bridge structure in Huntsville, Alabama and the effectiveness of the fiber-reinforced polymer repair.

In comparison to the pre-repair testing results, the post-repair results showed a slight change in the damage levels of the prestressed concrete bridge girders. Figure 5-35 shows the adapted pre-repair and post-repair results from the NDIS-2421 criterion. The hollow markers represent the adapted pre-repair results and the solid markers represent the post-repair results.
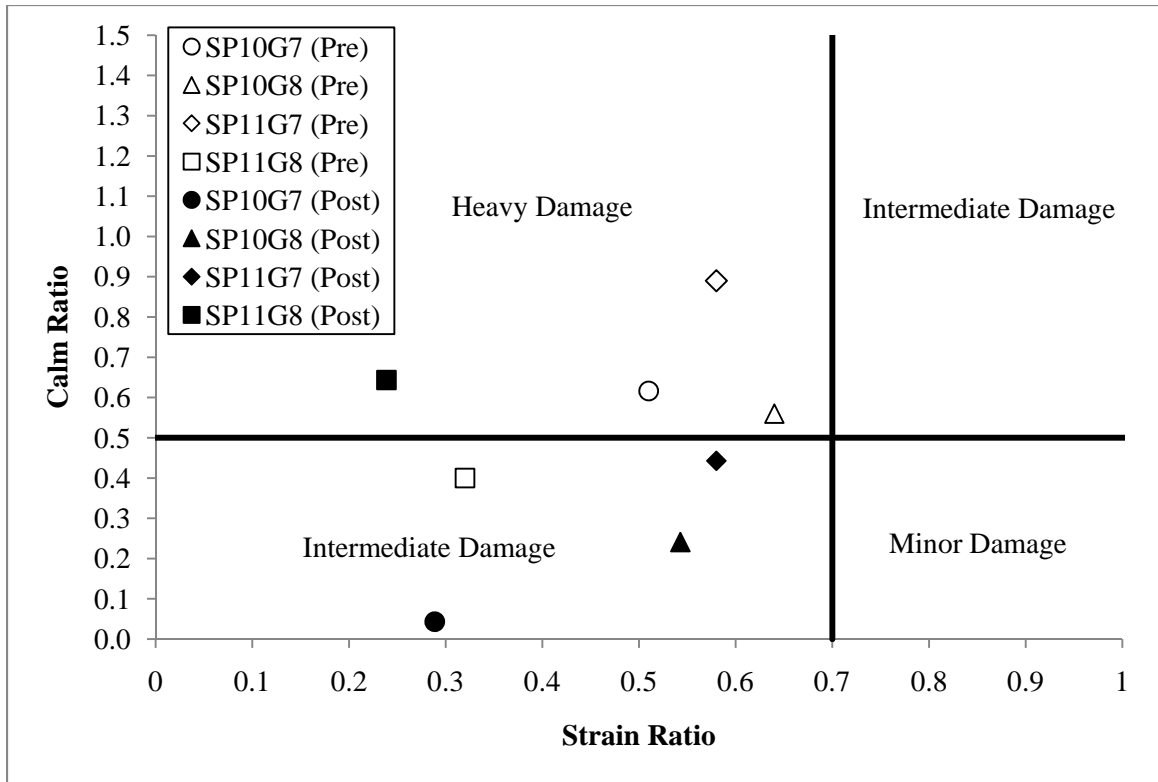
Figure 5-35: Adapted pre-repair and post-repair NDIS-2421 results

As can be seen from the NDIS-2421 results, SP10G7, SP10G8, and SP11G7 showed

improvement by moving from the "heavy damage" to the "intermediate damage"

quadrants. SP11G8, on the other hand, moved from the "intermediate" to the "heavy"

quadrant, indicating a decrease in condition. No direct conclusions can be made from

this plot because of the difference between the support conditions for the two tests.

However, some conclusions can be made once all the evaluation analyses are compared.

The following tables summarize the damage classification results of both the

modified pre-repair analysis and the post-repair analysis:

Table 5-7: Adapted pre-repair test results

Girder	NDIS-2421	SSM Ratio*	Peak CSS Ratio**
SP10G7	Heavy Damage	Heavily Damaged (8%)	No Significant Damage (2%)
SP10G8	Heavy Damage	Heavily Damaged (11%)	No Significant Damage (10%)
SP11G7	Heavy Damage	Heavily Damaged (9%)	No Significant Damage (25%)
SP11G8	Intermediate Damage	Not Heavily Damaged (2%)	No Significant Damage (3%)

*Percentage in parentheses represents SSM ratio (4% critical damage threshold)
**Percentage in parentheses represents peak CSS ratio (30% critical damage threshold)

Table 5-8: Post-repair test results

Girder	NDIS-2421	SSM Ratio*	Peak CSS Ratio**
SP10G7	Intermediate Damage	Heavily Damaged (42%)	No Significant Damage (8%)
SP10G8	Intermediate Damage	Heavily Damaged (13%)	No Significant Damage (9%)
SP11G7	Intermediate Damage	Heavily Damaged (21%)	No Significant Damage (27%)
SP11G8	Heavy Damage	Heavily Damaged (59%)	Significant Damage (39%)

*Percentage in parentheses represents SSM ratio (4% critical damage threshold)
**Percentage in parentheses represents peak CSS ratio (30% critical damage threshold)

As can be seen from Table 5-7 and Table 5-8, the results differ in the degree of damage, which is a concern with most evaluation criteria for acoustic emission testing. Since there is no specific amount of damage associated with "heavy damage," this statement is slightly subjective to the reader's interpretation of damage. From previous reinforced concrete beam research, most damage levels are determined based upon the crack-opening widths (Ohtsu et al. 2002). Based on visual inspection alone, the SP11G7, SP11G8, and SP10G7 girders appeared the most damaged since there were extensive, unsealed cracks extending all the way through the girder. The post-repair test results

agreed with this because SP11G8 was categorized as "heavy damage" by the NDIS-2421 criterion, and had the worst results (by percentage) for the SSM ratio and peak CSS ratio criteria. As for the pre-repair results, SP11G8 actually "performed" the best of all the girders, receiving an "intermediate damage" classification for the NDIS-2421 criterion and lower ratios for the SSM Ratio and Peak CSS analyses. The drastic change from the pre-repair to the post-repair results would have indicated a decline in the integrity of SP11G8. However, the support conditions must be taken into account. For the pre-repair test, SP11G8 still had aid from the bearing pad/false support. According to the research team, this bearing pad was the hardest to remove prior to the FRP repair being installed. This may be an indication that, compared to the other three girders, SP11G8 was receiving the most support from the false supports during the pre-repair test. This may be why SP11G8 had the biggest change from the pre- to post-repair behavior. It could have allowed SP11G8 to actually yield better results for the pre-repair testing. For the post-repair test, however, all bearing pads were removed so that no extra support was given to the girders. Because of this reason, the post-repair test probably yielded more accurate results regarding the actual damage state of the girders.

The SSM Ratio evaluation used the same procedure for the pre- and post-repair. Once again looking at trends in the results, a significant increase in the SSM Ratio from the pre-repair test to the post-repair test did not mean a significant increase in the Peak CSS Ratio from one test to the other. For example, SP10G7 showed an increase from 8% (pre-repair) to 42% (post-repair) in SSM Ratio. For the Peak CSS Ratio, however, the increase was from 2% to 8%. This trend seems to be more evident in the SP10 girders. This inconsistency is most likely explained by the changing support conditions. Another

explanation could be that the pre-repair test applied a load that had never been experienced by the bridge before. Therefore, an extensive amount of AE was caused by the pre-repair tests. For the post-repair tests, the load applied was similar in magnitude to the pre-repair test. Although using ratios seems to take this fact into account, it may have had an effect on the trends that resulted between the two evaluation criteria.

No specific conclusions were made about the change in structural integrity of the bridge, but trends in the data do offer some insight into the testing procedures. The NDIS-2421 criterion needed to be adapted for this specific testing procedure. It was redeveloped to accurately describe the load effect that was being experienced by the bridge. The historic index was used to identify the onset of significant acoustic emission. A more direct approach was taken to determine the loading and unloading phases of the test. The modifications also made the approach more comprehensive by using Night 1 as the initial loading sequence and Night 2 as the reloading sequence. The results obtained from this method showed that it was a feasible way to determine the structural integrity of structural components. Although there was no conclusion made about the accuracy of the results, the method was used effectively. Future research needs to continue to develop this method for in-situ testing. The research done with laboratory testing has shown that this method can provide accurate results. However, when this method was applied to an actual structure that could not be tested to failure (as in laboratory testing), it was difficult to obtain reliable results.

The SSM Ratio indicated, like the NDIS-2421 criterion, that it can be used to determine the damage levels in prestressed concrete bridge girders. But, like the NDIS-2421 criterion, it had its limitations. The 4% damage threshold was developed for

137

laboratory-tested specimens failing primarily in flexure. Since this method was used in the field, this value may need to be different due to the characteristics of the testing. Based on the results of the post-repair test, this ratio seemed to be very low. Another limitation of this method is the definition of "heavily damaged." A clear definition of damage levels for all the evaluation criteria used in this research should be provided. Ideally, damage states should be a function of the state of the structural member; they should not depend on the procedure of AE testing or evaluation method used to assess the damage.

Finally, the Peak CSS Ratio also provided insight into the condition of the bridge girders. It was the easiest method to apply and provided similar results compared to the other two methods. Once again, however, further research should focus on developing this method for in-field testing of actual structures.

The most important conclusion made about the evaluation criteria is the idea that a single method cannot be used to evaluate the structure effectively. Multiple methods need to be used in conjunction to provide the most reliable results. Even then, however, changes in the testing procedure, support conditions, and other factors may affect the results.

In this study, acoustic emission testing has shown that it can be an effective procedure for determining the location of distress in bridge girders. Acoustic emission testing is an effective way of monitoring the bridge without having a large impact on everyday traffic, making it a very useful tool.

Acoustic emission monitoring still requires more testing to refine the evaluation criteria for in-service bridges. Standardized evaluation criteria should be established, if at

all possible, to limit the necessary data and analysis time. Other factors, such as ambient

noise, temperature changes, and other environmental effects should all be taken into

account when performing acoustic emission testing.

Chapter 6: Summary, Conclusions, and Recommendations

6.1 Summary

Nondestructive testing techniques have become much more important because of the increasing concern for the aging federal infrastructure. As of 2005, more than 25% of bridges in the United States are classified either structurally or functionally deficient (ASNT 2005). There has been a critical need to develop an effective in-place testing procedure as well as evaluation criteria to determine the damage level of in-service bridges. Acoustic emission has shown promise as a useful way of testing in-service bridges and other structures with minimal disruption of everyday operations.

This study consisted of testing an in-service bridge using acoustic emission monitoring. The elevated portion of the I-565 highway in Huntsville, Alabama was tested in May 2010 to investigate the structural behavior of four prestressed concrete bridge girders that experienced damage soon after construction. This study was a follow-up to the pre-repair testing which was conducted prior to a fiber-reinforced polymer repair. The purpose of this study was to assess the effectiveness of the repair by conducting the same test after the repair was completed. The testing was also used to determine any effect that the fiber-reinforced polymer had on acoustic emission monitoring. It was also conducted to determine how certain evaluation criteria are used and how they can be adjusted so that they offer accurate results for the type of damage experience by these girders.

6.2 Conclusions from Field Testing

The conclusions from the in-situ testing of the I-565 Bridge girders can be summarized as follows:

- AE testing of prestressed concrete girders can be readily and successfully performed in the field. Taking into account ambient noise and environmental conditions is crucial to the success of AE testing.

- Because of the effect of the bearing pads being present in the pre-repair testing and not present in the post-repair testing, a thorough investigation of the AE data collected did not reveal specific conclusions based on the comparison between the pre- and post-repair tests. However, the individual evaluation criteria from each test did yield independent results that offered some insight based upon the trends that were observed.

- All significant opening and closing deformations of cracks were associated with large increases in AE activity.

- The NDIS-2421 evaluation criterion is a feasible criterion for evaluating prestressed concrete bridge girders. The method provided results that seemed to coincide with the other evaluation criteria, but not on a consistent basis. These inconsistent results exposed some shortcomings of the method for in-situ testing.

- The signal strength moment (SSM) ratio evaluation criterion proposed by Xu (2008) was determined to be another feasible criterion to assess the condition of prestressed concrete girders. However, a flaw in this process was that the 4% critical value obtained during laboratory testing may not be suitable for in-situ testing.

- The AE 2D-LOC software provided accurate locations of visible cracks on the concrete surface. Only the active, unsealed cracks were successfully located using this software. The epoxy-sealed cracks yielded very little emission, indicating that the epoxy repair was effective in restoring integrity to individual cracks.

- The Peak CSS Ratio showed a general trend that agreed with the NDIS-2421 criterion for the post-repair test results. This method seemed to be the easiest to apply to the data and offered results with the least data processing.

- One flaw common to all of the evaluation criteria was the lack of clear definitions for damage classifications. All three evaluation criteria need to have well-defined damage classifications that are associated with damage characteristics of the actual structural component.

- Due to the changing support conditions of the I-565 girders, this study could not provide evidence of any solid relationship between the AE data and the FRP repair. However, there were some indications that the FRP did have some sort of an effect on the AE data, although that relationship was not quantifiable.

6.3 Recommendations for Future Study

In this study, acoustic emission testing showed potential viability as a nondestructive testing option for in-service bridges. Even though the results from this research did not yield a definite conclusion regarding the structural integrity of the repaired girders, the AE testing procedure was easily conducted and data was gathered efficiently. Future research needs to be conducted in the following areas:

- Research should focus on determining the most effective evaluation criteria for application to prestressed concrete girders.

- Future projects should be focused on establishing general evaluation criteria that can be used on bridge structures to determine a specific level of damage.

- Damage levels defined for new evaluation criteria should be based upon the structural state of the specimen. Levels of damage should be defined thoroughly based upon characteristics of the specimen, such as crack widths, or inelastic behavior of concrete or reinforcement.

- Future research should focus on further developing the NDIS-2421 evaluation criterion, specifically with respect defining the load ratio, or a similar parameter that is more practical for in-situ testing. Research should also be focused on developing more objective methods for identifying the onset of significant AE.

- Future study should be performed to establish a critical threshold limit for the signal strength moment (SSM) ratio evaluation criterion proposed by Xu (2008). The 4% critical threshold value may indeed be correct, but it should be tested to determine whether this value is correct for other concrete systems.

- Future research should also focus on the AE response of fiber-reinforced polymer repaired bridge girders to attempt to develop a relationship between the AE behavior and the FRP repair.

Compared with other nondestructive techniques, AE monitoring still requires refinements to current testing techniques to handle difficulties with in-situ testing prior to implementation. Acoustic emission testing should be done in conjunction with other NDT methods to ensure accurate results. Future research should focus on overcoming

the difficulties of in-situ testing to develop an easier and more standard procedure and

evaluation criterion.

References

AASHTO. 2006. *AASHTO LRFD Bridge Design* Specifications*: Customary U.S. Units*. 3rd ed. Washington D.C.: American Association of State Highway and Transportation Officials (AASHTO).

ACI 318-08. 2008. Building Code requirements for structural concrete (ACI 318-08) and commentary (318R-08). Farmington Hills, Michigan: American Concrete Institute (ACI). 430 pp.

ACI 437R-03. 2003. Strength Evaluation of existing concrete buildings (ACI437R-03). Farmington Hills, Michigan: American Concrete Institute (ACI). 28 pp.

ALDOT. 1994. Cracks in precast prestressed bulb tee girders on structure No.'s I-565-45-11.5 A. & B. on I-565 in Huntsville, Alabama. Report and attachments (A-L). Montgomery, Alabama: Alabama Department of Transportation (ALDOT).

ASNT. 1996. Nondestructive testing handbook. 2nd ed. Columbus, OH: American Society for Nondestructive Testing (ASNT). 581 pp.

ASNT. 2005. Nondestructive testing handbook. 3rd ed. Columbus, OH: American Society for Nondestructive Testing (ASNT). 446 pp.

ASTM E 1316-06. 2006. Standard terminology for nondestructive examinations. West Conshohocken, Pennsylvania: ASTM International. 30 pp.

ASTM E 2374-04, 2004. Guide for acoustic emission system performance verification. West Conshohocken, Pennsylvania: ASTM International. 5 pp.

ASTM E 2478-06, 2006. Standard practice for determining damage-based design stress for fiberglass reinforced plastic (FRP) materials using acoustic emission. West Conshohocken, Pennsylvania: ASTM International. 6 pp.

Bullock, W. 2011. Behavior of a Damaged Prestressed Concrete Bridge Repaired with Fiber-Reinforced Polymer Reinforcement. Master Thesis. Auburn, Alabama: Auburn University.

CARP. 1999. Recommended practice for acoustic emission evaluation of fiber-reinforced plastic (FRP) tanks and pressure vessels. Columbus, Ohio: Committee on Acoustic Emission for Reinforced Plastics. 11 pp.

Colombo, S., M. C. Forde, I. G. Main and M. Shigeishi. 2005. Predicting the ultimate bending capacity of concrete beams from the "'Relaxation Ratio" analysis of AE signals. *Construction and Building Materials* 19 (July): 746–754.

Fason, W. E. and R. W. Barnes. 2004. I-565 Visual inspection. Technical Report. Auburn, Alabama: Auburn University Highway Research Center. 31 pp.

Fason, W.E. 2008. Static Load Testing of a Damaged, Continuous Prestressed Concrete Bridge. Master Thesis. Auburn, Alabama: Auburn University. 318 pp.

Federal Highway Administration (FHWA). 1996. United States Department of Transportation. National Bridge Inventory 1996.

Federal Highway Administration (FHWA). 2004. United States Department of Transportation. National Bridge Inventory 2004.

Förster, F. and Scheil, E. 1936. Acoustic Study of the Formation of Martensile Needels. Zeitschrift für Metallkunde 28(9): 245-247.

Fowler, T. J., J. A. Blessing and P. J. Conlisk. 1989. New direction in testing. In *Third International Symposium on Acoustic Emission from Composite Materials AECM-3*. 16–27. Paris, France.

Fowler, T. J., Luis O. Yepez and Charles A. Barnes. 1998. "Acoustic emission monitoring of reinforced and prestressed concrete structures." Proceedings of SPIE 3400. 281 (1998).

Gao, N. 2003. Investigation of cracking in precast prestressed girders made continuous for live load. M.S. thesis. Auburn, Alabama: Auburn University. 137 pp.

Grosse, Christian U. and Masayasu Ohtsu. 2008. Acoustic Emission Testing: Basics for Research – Applications in Civil Engineering. Springer. 416 pp.

Hearn, S. W. and C. K. Shield. 1997. Acoustic emission monitoring as a nondestructive testing technique in reinforced concrete. *ACI Materials Journal* 94 (6): 510–519.

Henning, D. 1988. Josef Kaiser: His achievements in AE research. Matls. Eval. 46 (Feb 1988). pp. 193.

Huang, Miinshiou, Liang Jiang, Peter K. Liaw, Charlie R. Brooks, Rodger Seeley, and Dwaine L. Klarstrom. 1998. "Using Acoustic Emission in Fatigue and Fracture Materials Research." Vol. 50, no. 11. JOM.

Kaiser, J. 1950. A study of acoustic phenomena in tensile tests. Dr.-Ing. Dissertation, Technical University of Munich.

Kishinouye, F. 1932. An Experiment on the Progression of Fracture (A Preliminary Report). Jishin Vol. 6 (1932): pp. 25-61. Reprinted in Journal of Acoustic Emission. Vol. 9, No. 3 (July-September 1990): pp. 177-180 [English translation].

Kishinouye, F. 1937. Frequency-Distribution of the Ito Earthquake Swarm of 1930. Bulleting of the Earthquake Research Institute. Vol. 15, Part 2. Tokyo, Japan: Tokyo Imerial University (1937): pp. 785-826.

L'Hermite, R.G. 1960. Volume change of concrete. Proc. 4th Int. Symp. Chemistry of Cement, V-3, NBS Monograph 43: 659-694.

Liu, Z. and Paul H. Ziehl. 2009. Evaluation of reinforced concrete beam specimens with acoustic emission and cyclic load test methods. *ACI Structural Journal* 106-S28: 288-299.

Mason, W.P., J.H. McSkimin, and W. Shockley. 1948. Ultrasonic observations of twinning in tin. *Phys. Rev.* 73 (May 1948). pp. 1213.

Millard, D. 1950. Twinning in Single Crystals of Cadmium. Ph.D. thesis. Bristol, England: University of Bristol.

Nair, Archana. 2006. Acoustic Emission Monitoring and Quantitative Evaluation of Damage in Reinforced Concrete Members and Bridges. Master Thesis. Baton Rouge, Louisiana: Louisiana State University. 101 pp.

Niwa, Y., S. Kobayashi, and M. Ohtsu. 1977. Studies of AE in concrete structures. Proc. JSCE 261:101-112.

Obert, L. 1977. The microseismic method: Discovery and early history. Proc. 1st Conference on AE/MS. In: Hardy Jr., Leighton F.W. (Eds). Geologi Structures and Materials. Trans Tech Publication, Clausthal, Germany.

Obert, L. and W. Duvall. 1945. The microseismic method of predicting rock failure in underground mining, Part II: Laboratory Experiments. Report of Investigations 3803, U.S. Bureau of Mines, Washington D.C.

Ohtsu, M. 1989. A review of acoustic emission in civil engineering with emphasis on concrete. *Journal of Acoustic Emission* 8 (1): 93–98.

Ohtsu, M., M. Uchida, T. Okamoto and S. Yuyama. 2002. Damage assessment of reinforced concrete beams qualified by acoustic emission. *ACI Structural Journal* 99 (4): 411–417.

PCI-8 Based AE System User's Manual. 2002. Rev 0, Part #: 7030-1001. Physical Acoustics Corporation, Princeton Junction, NJ. 300 pp.

Pollock, A. A. 1995. Inspecting bridges with acoustic emission—inspection details about in-service steel bridges and monitoring weld operations: application guidelines. Prepared by: Physical Acoustics Corporation.

Rüsch, H. 1959. Physical problems in the testing of concrete. Zement Kalk-Gips 12 (1): 1-9.

Ridge, A. R. and P. H. Ziehl. 2006. Evaluation of strengthened reinforced concrete beams: cyclic load test and acoustic emission methods. ACI Structural Journal 103 (6): 832–841.

Robinson, G. S. 1965. Methods of detecting the formation and propagation of microcracks in concrete. In *Proceedings of International Conference Structure of Concrete and Its Behaviour under Load*. London, England. 131–145.

Schofield, B.H. 1961. Acoustic emission under applied stress. Report ARL-150, Lessels and Associates, Boston.

Schofield, B.H., R.A. Bareiss, and A.A. Kyrala. 1958. AE under applied stress. WADC Technical Report 58-194. Boston, MA: Lessells and Associates (April 1958).

Shield C. 1997. Comparison of acoustic emission activity in reinforced and prestressed
concrete beams under bending. *Construction and Building Materials* 11(3): 189–
194.

Swenson, K. S. 2003. Feasibility of externally bonded FRP reinforcement for repair of
cracked prestressed concrete girders. M.S. thesis. Auburn, Alabama: Auburn
University. 257 pp.

Swit, Grzegorz. 2009. Diagnostics of Prestressed Concrete Structures by Mean of
Acoustic Emission. Kielce University of Technology. Poland. IEEE.

Uomoto,T. 1987. Application of acoustic emission to the field of concrete engineering.
Journal of Acoustic Emission 6 (3): 137–144.

Vogel, Thomas, Barbara Schechinger, Stephan Fricker. 2006. Acoustic Emission
Analysis as a Monitoring Method for Prestressed Concrete Structures. Institute of
Structural Engineering, ETH. Zurich, Switzerland. ECNDT.

Xu, Jiangong. 2008. Nondestructive Evaluation of Prestressed Concrete Structures by
Means of Acoustic Emission Monitoring. Ph.D. Dissertation. Auburn, Alabama:
Auburn University. 340 pp.

Yepez, Roca, L.O. 1999. Acoustic emission examination of high strength prestressed
concrete girders. M.S. thesis. Austin, Texas: University of Texas at Austin. 97 pp.

Yuyama, S., K. Yokoyama, K. Niitani, M. Ohtsu, and T. Uomoto. 2007. Detection and
evaluation of failures in high-strength tendon of prestressed concrete bridges by
acoustic emission. *Construction and Building Materials* 21 (2007). 491-500.

Ziehl, P. and Fowler, T. 2003. "Fiber-Reinforced Polymer Vessel Design with a

    Damage Approach." *Journal of Composite Structure*. Volume 61, Issue 4, pp.

    395-411.

Ziehl, Paul H., Nestore Galati, Antonio Natti, and J. Gustavo Tumialan. 2008. In-Situ

    Evaluation of Two Concrete Slab Systems. II: Evaluation Criteria and

    Outcomes. *Journal of Performance of Constructed Facilities*. ASCE. 217-227.

Appendix A: Crack-opening Displacement Analysis Figures
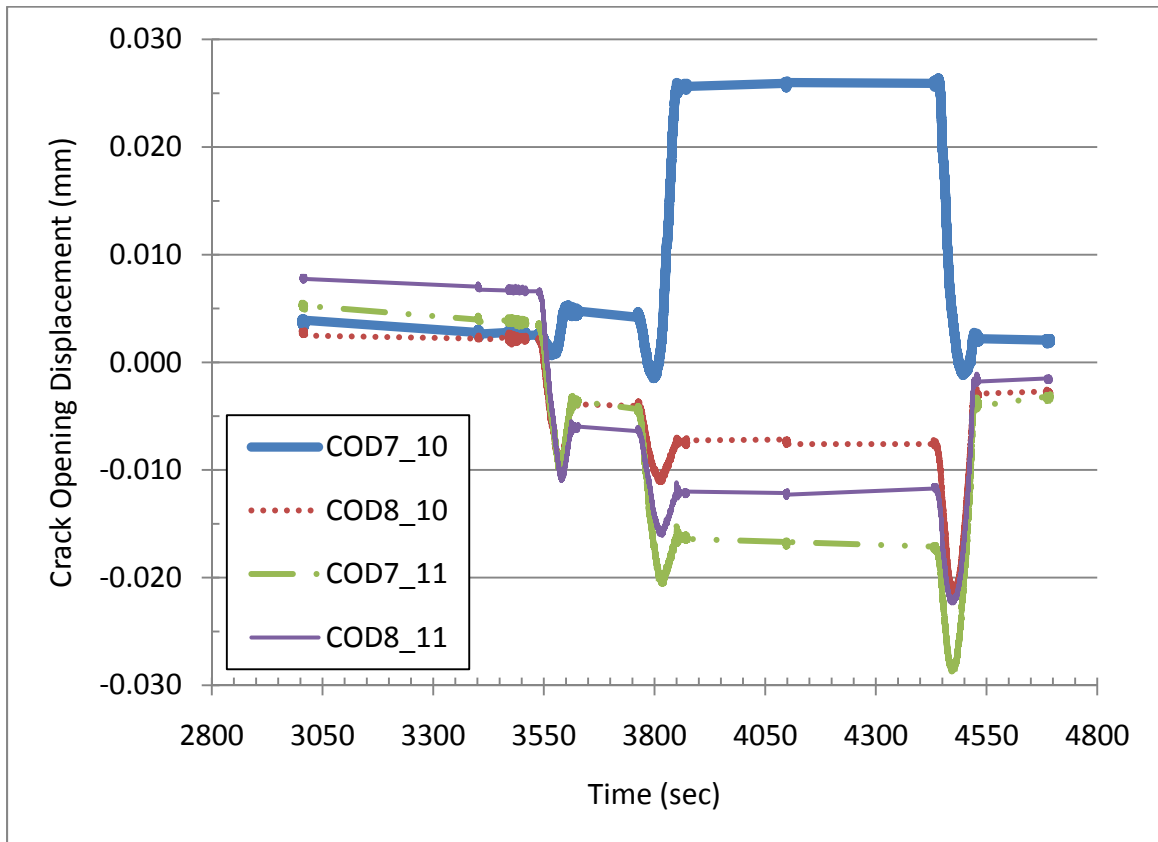
Figure A-1: Crack-opening displacement during Night 2 loading of Span 10
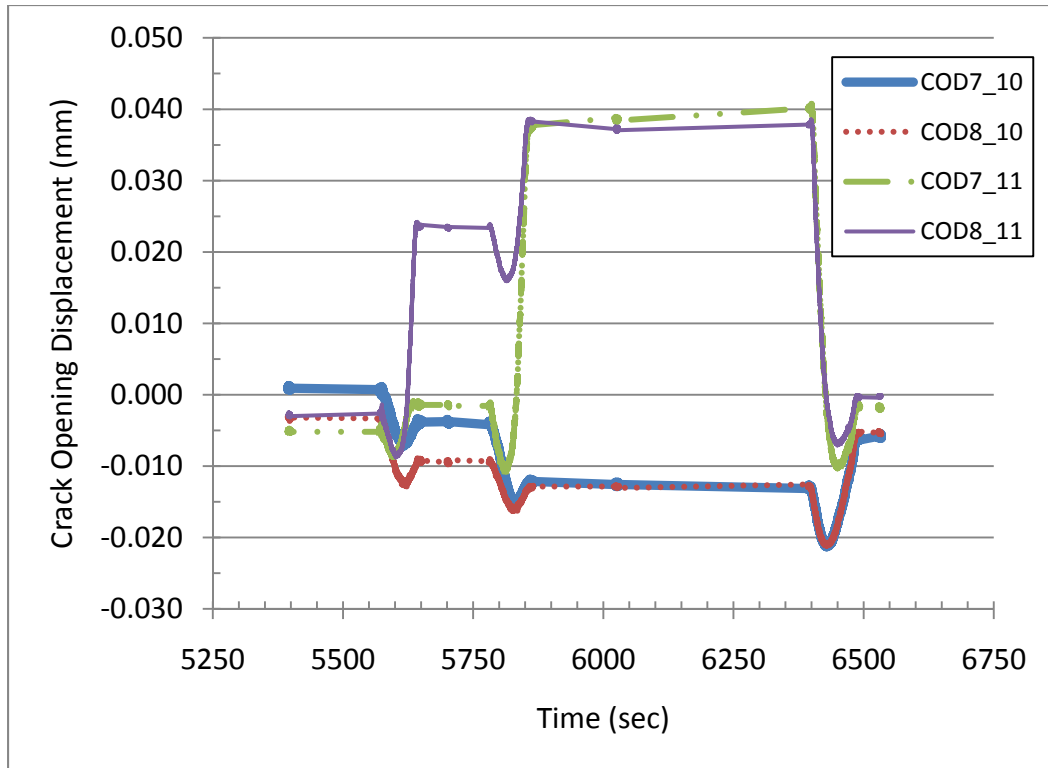
Figure A-2: Crack-opening displacement during Night 2 loading of Span 11
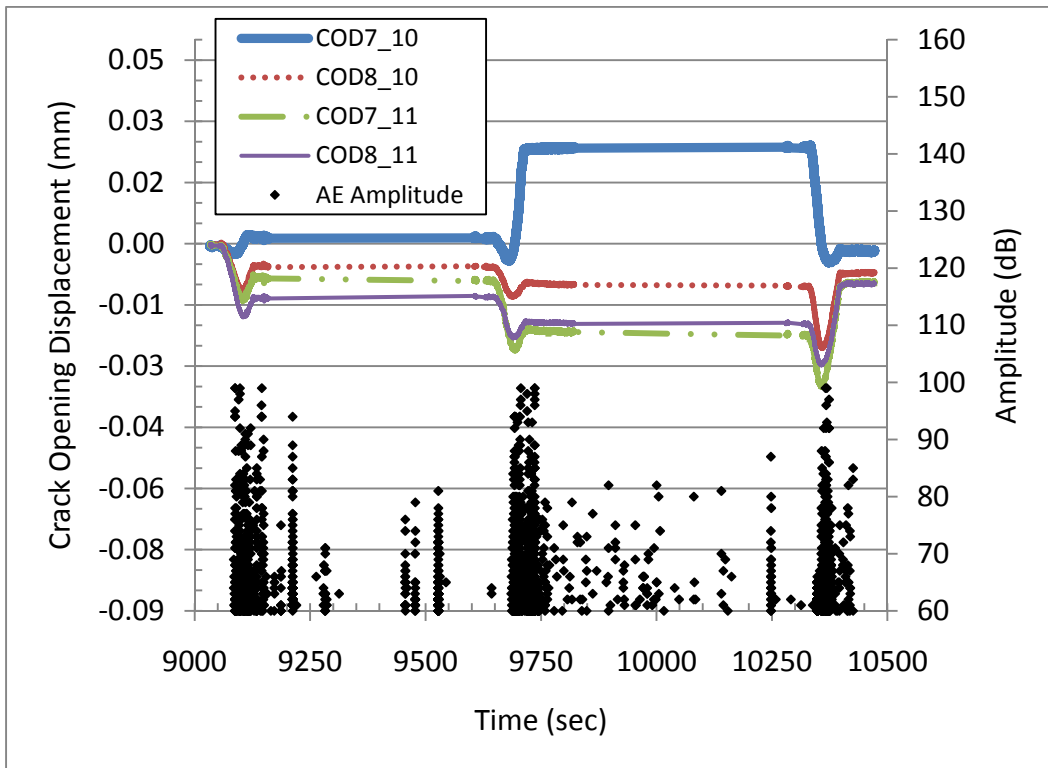
Figure A-3: AE amplitude and COD versus time of Span 10 loading on Night 1

153
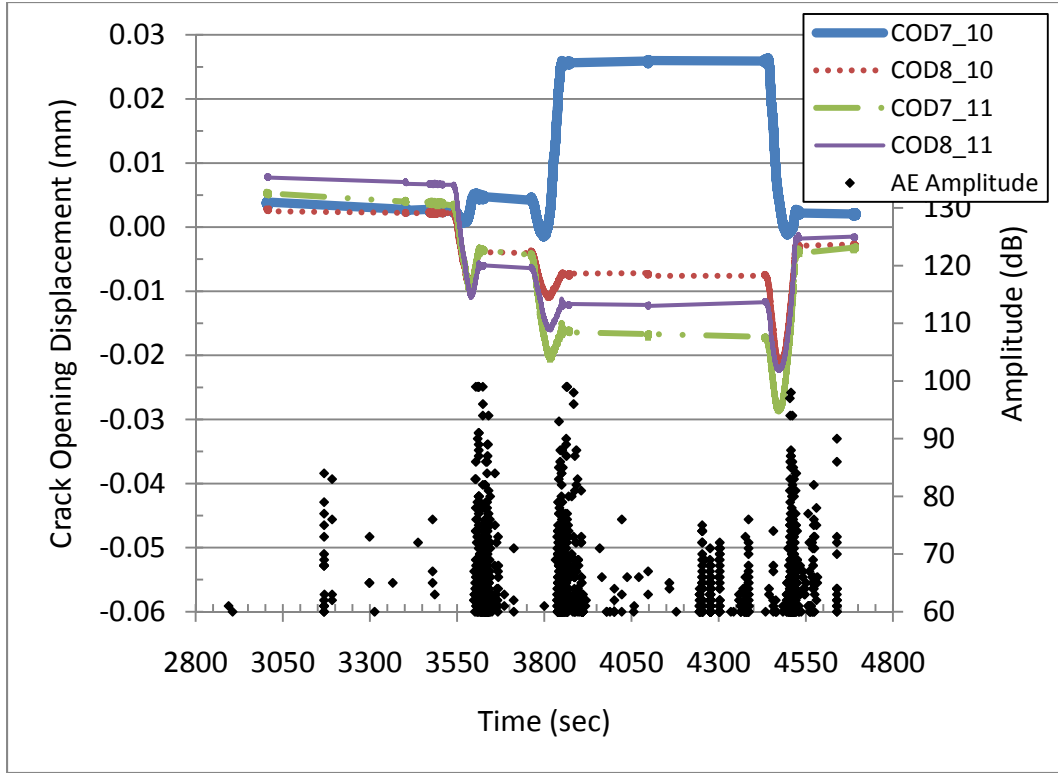
Figure A-4: AE amplitude and COD versus time of Span 10 loading on Night 2
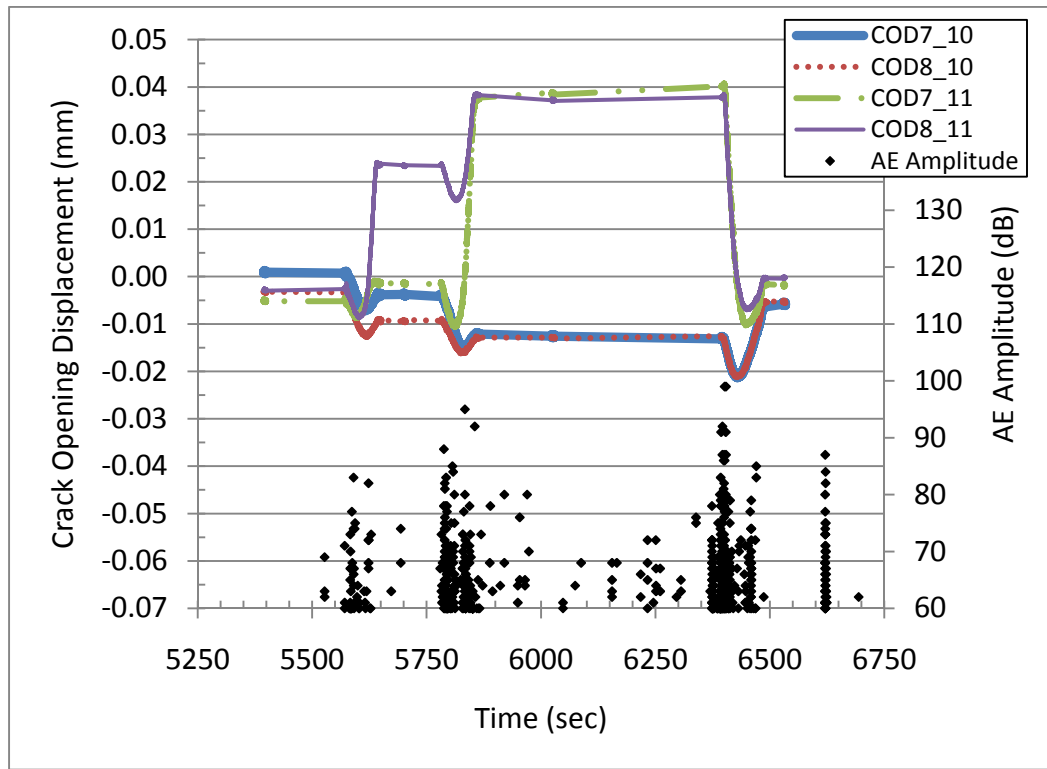
Figure A-5: AE amplitude and COD versus time of Span 11 loading on Night 2

154

Appendix B: NDIS-2421 Criterion Analysis Figures
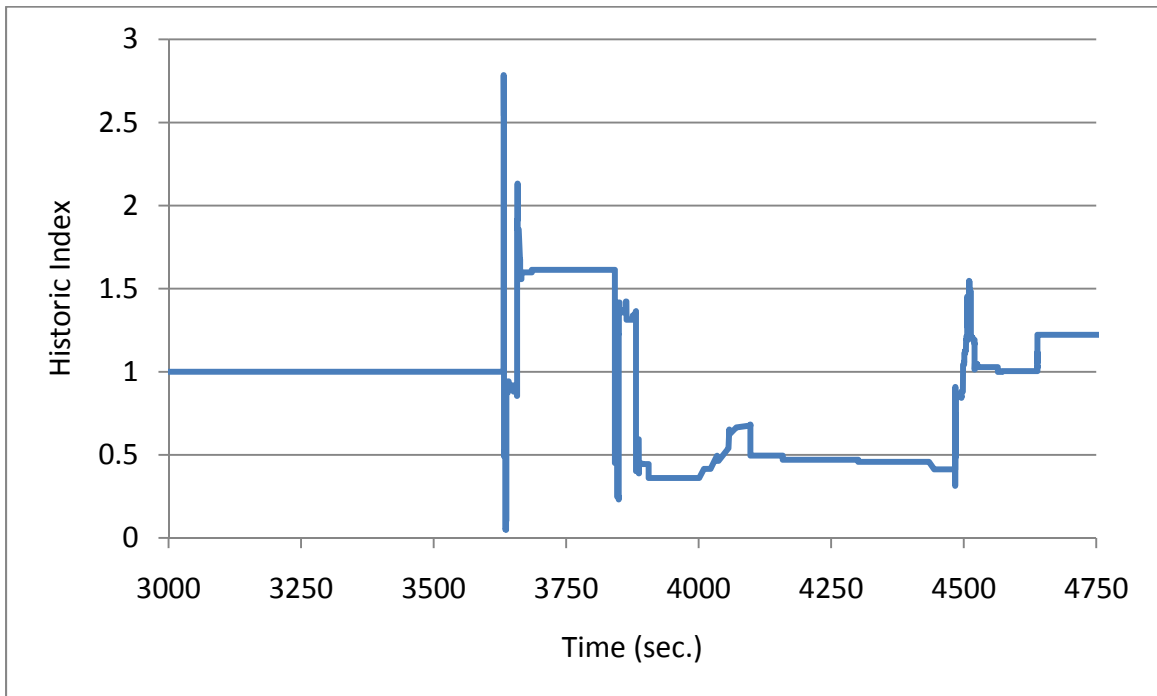
Figure B-1: Historic index plot for SP10G8 on Night 2
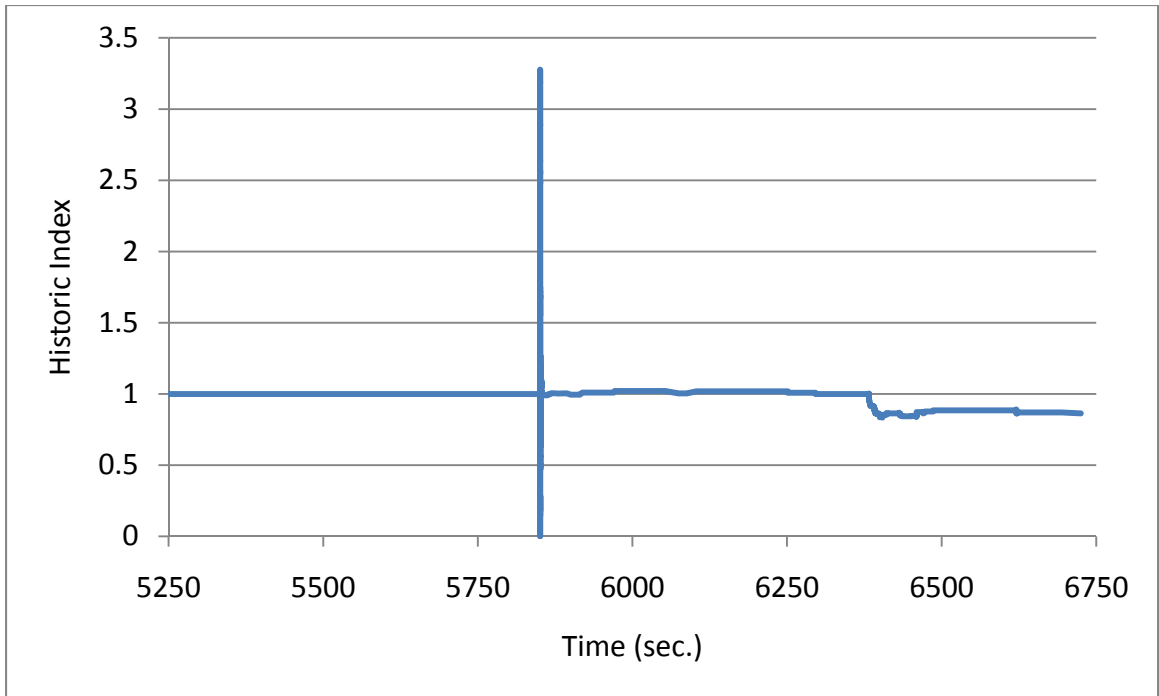
Figure B-2: Historic index plot for SP11G7 on Night 2
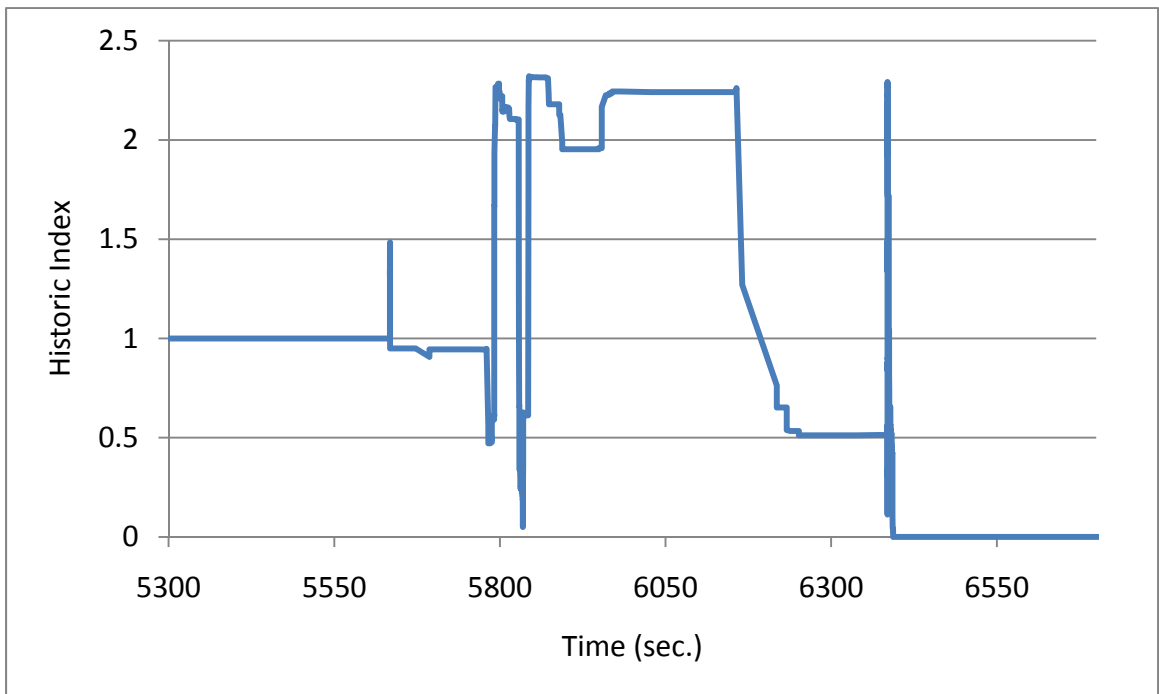
Figure B-3: Historic index plot for SP11G8 on Night 2
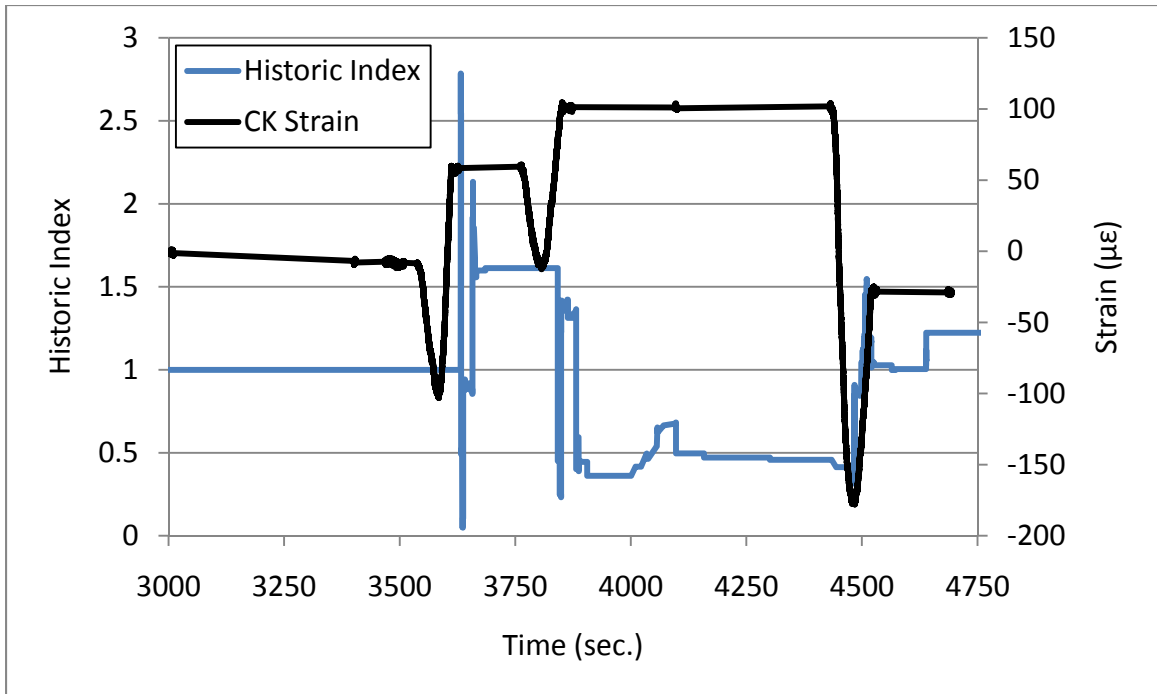
Figure B-4: Historic index versus strain for SP10G8 on Night 2
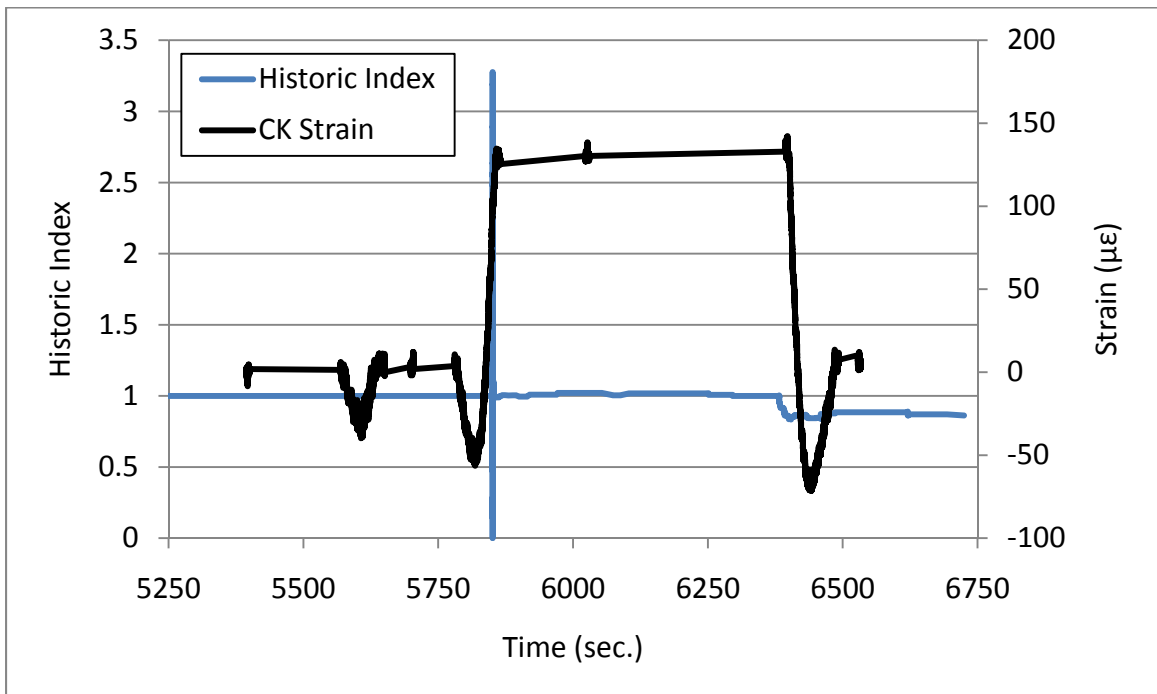
Figure B-5: Historic index versus strain for SP11G7 on Night 2
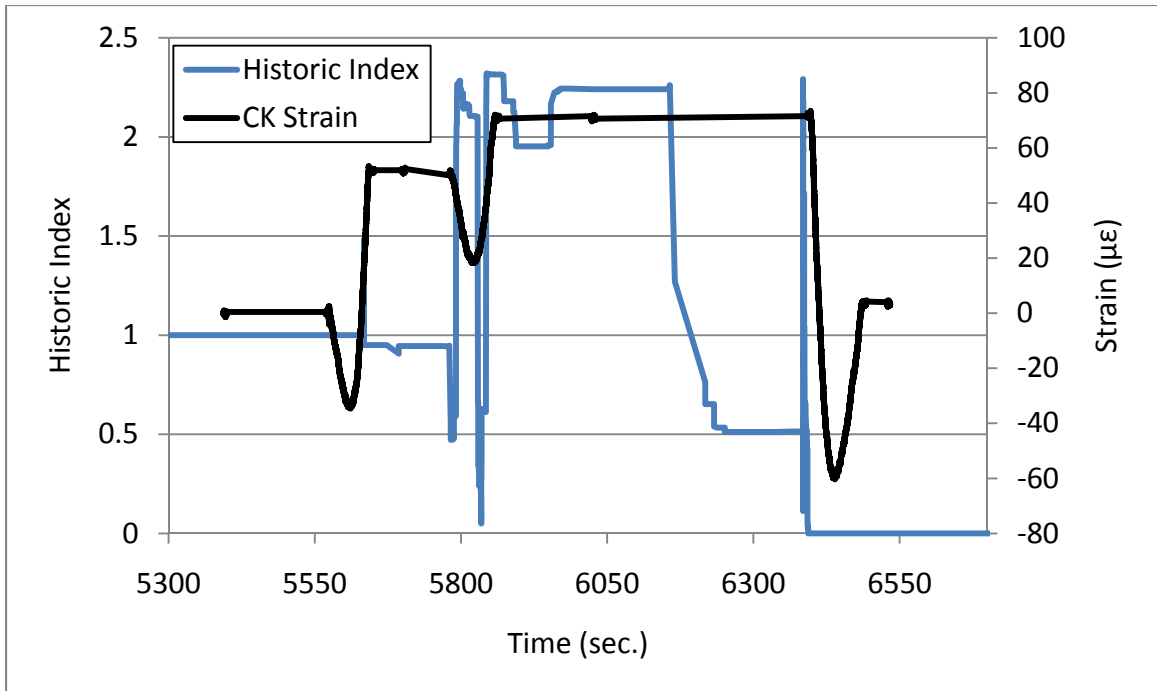
Figure B-6: Historic index versus strain for SP11G8 on Night 2
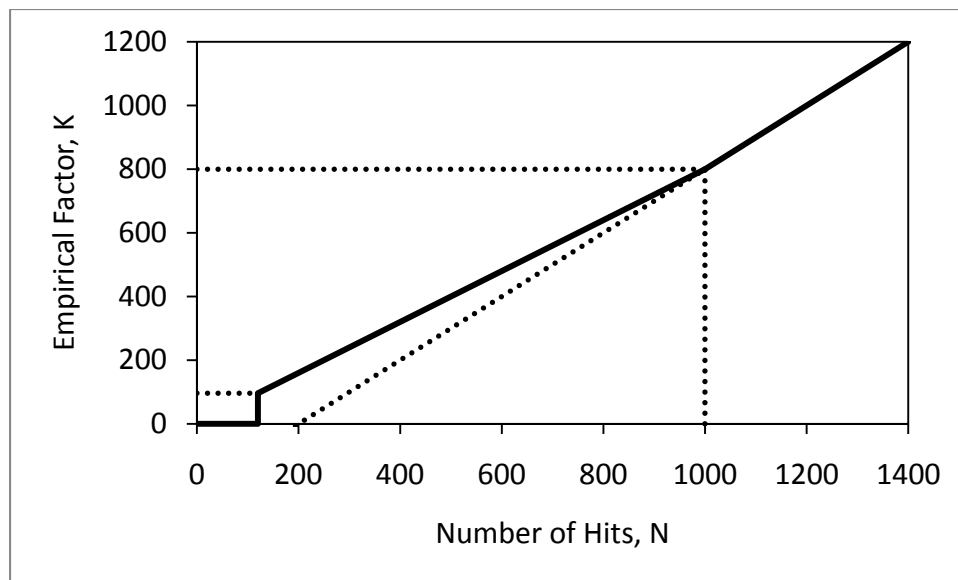
Figure B-7: Derived K-factor for SP10G8 (N=110)

158
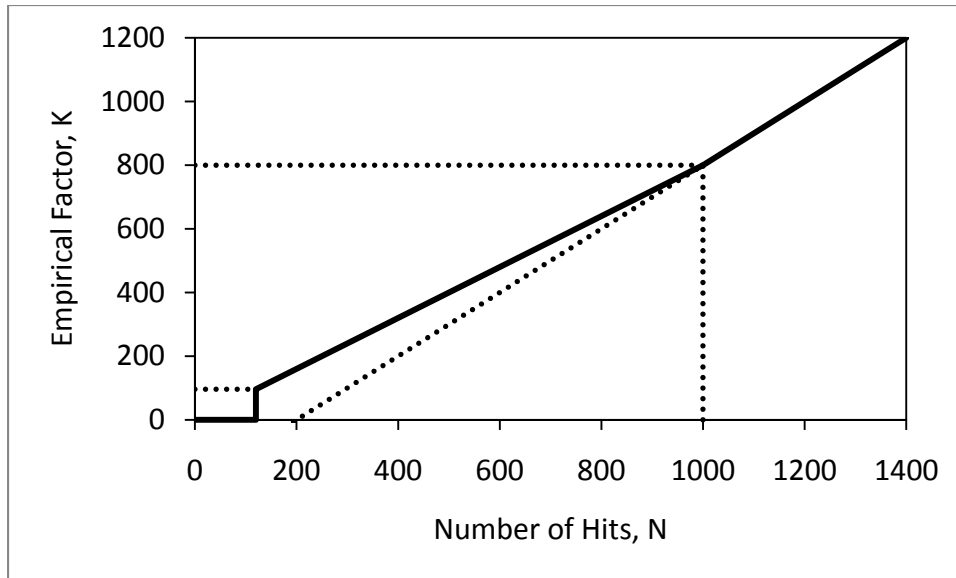
Figure B-8: Derived K-factor for SP11G7 (N=120)
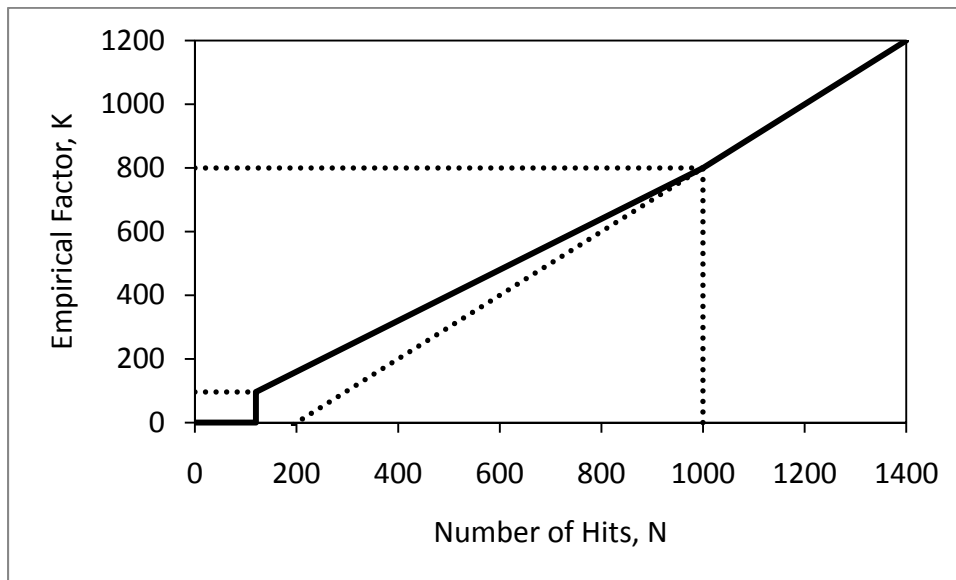
Figure B-9: Derived K-factor for SP11G8 (N=110)
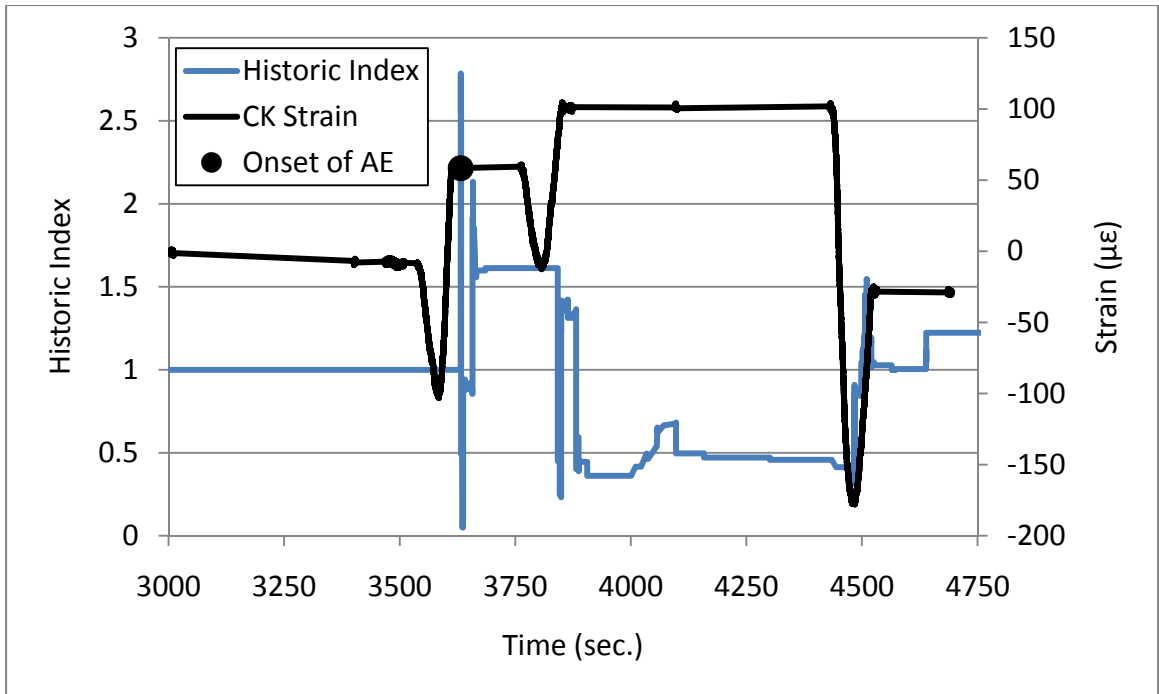
Figure B-10: Onset of AE for SP10G8 on Night 2
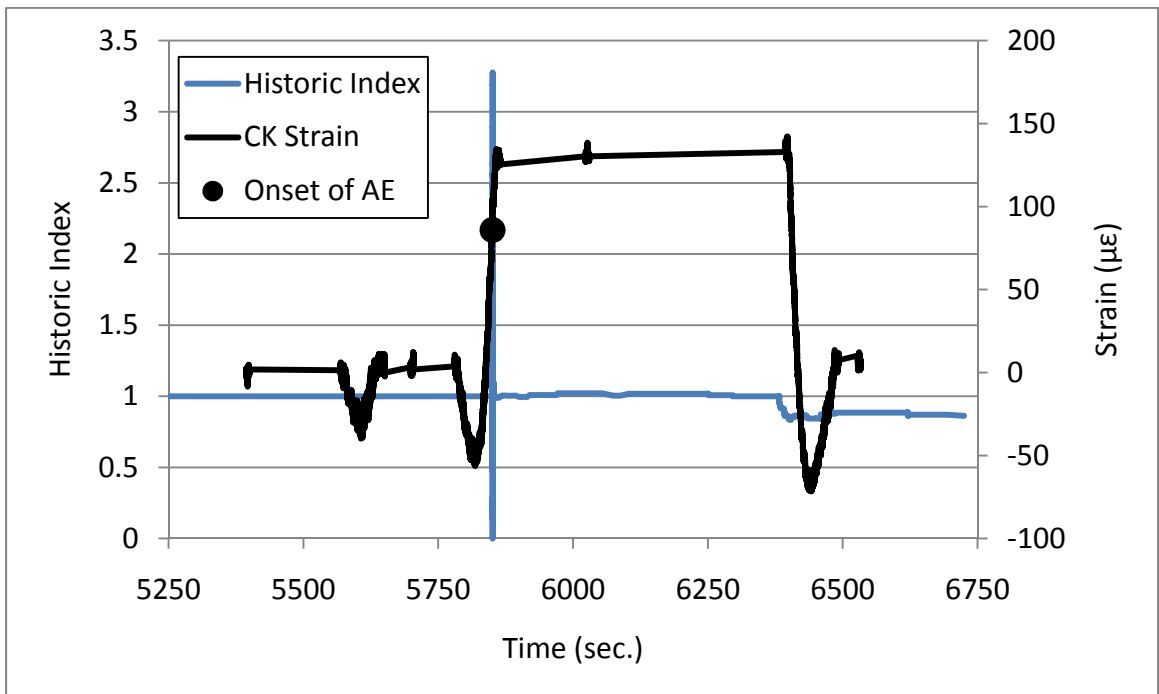
Figure B-11: Onset of AE for SP11G7 on Night 2
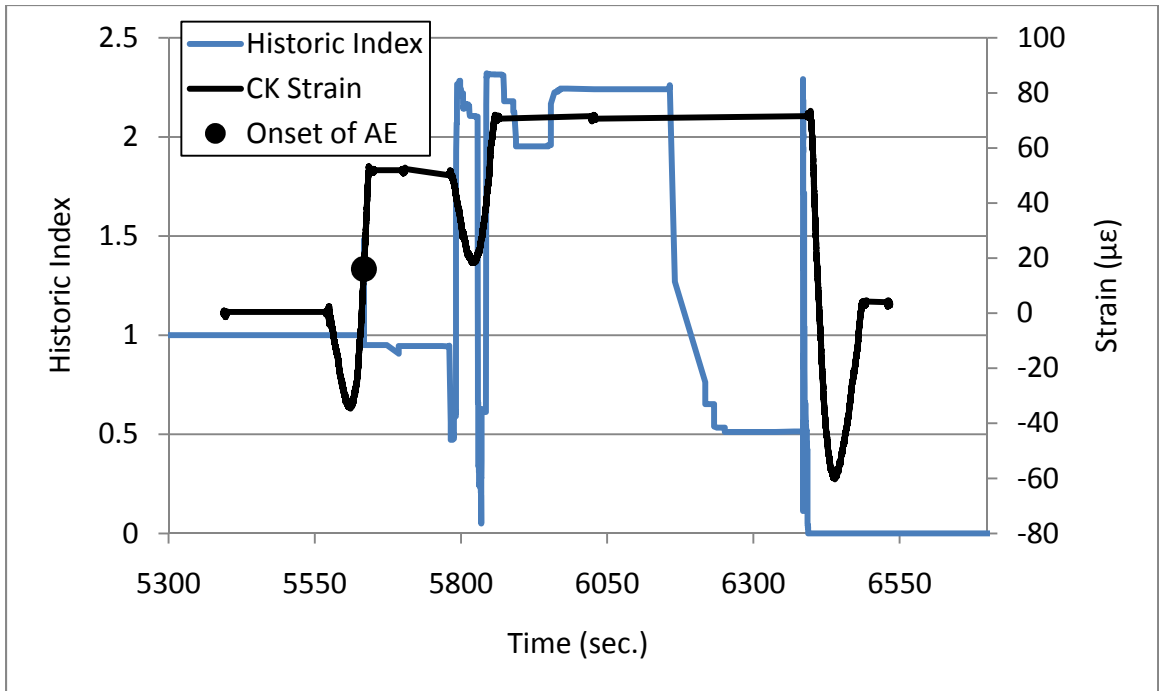
Figure B-12: Onset of AE for SP11G8 on Night 2
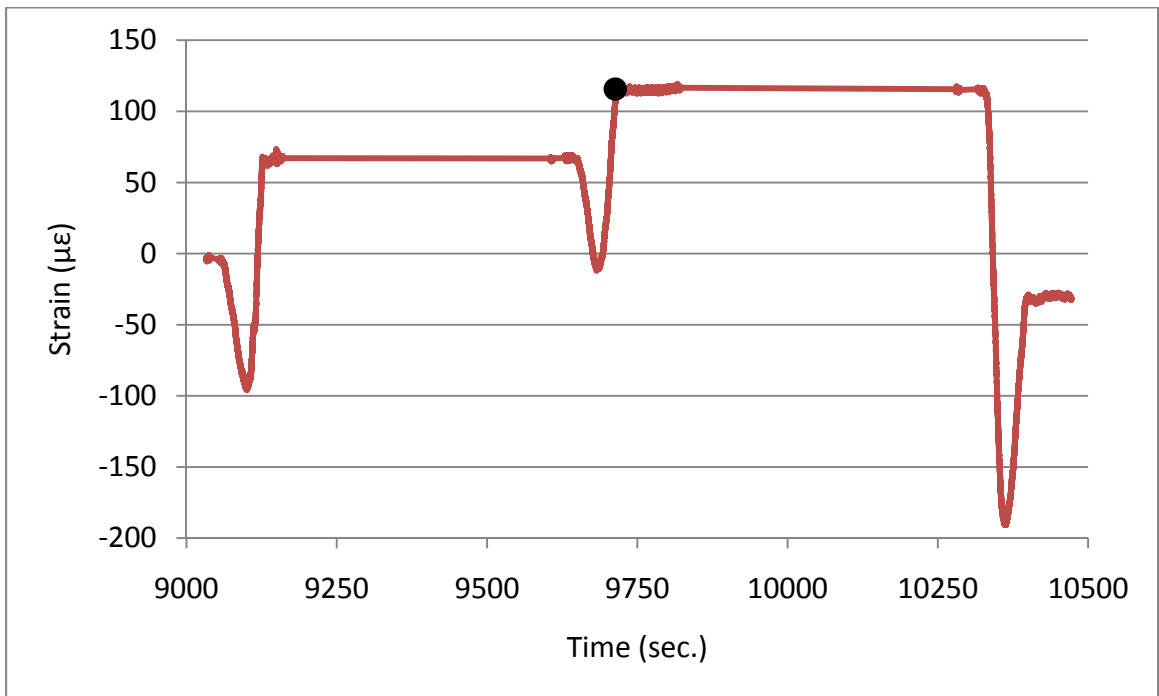
Figure B-13: Maximum strain from Night 1 for SP10G8
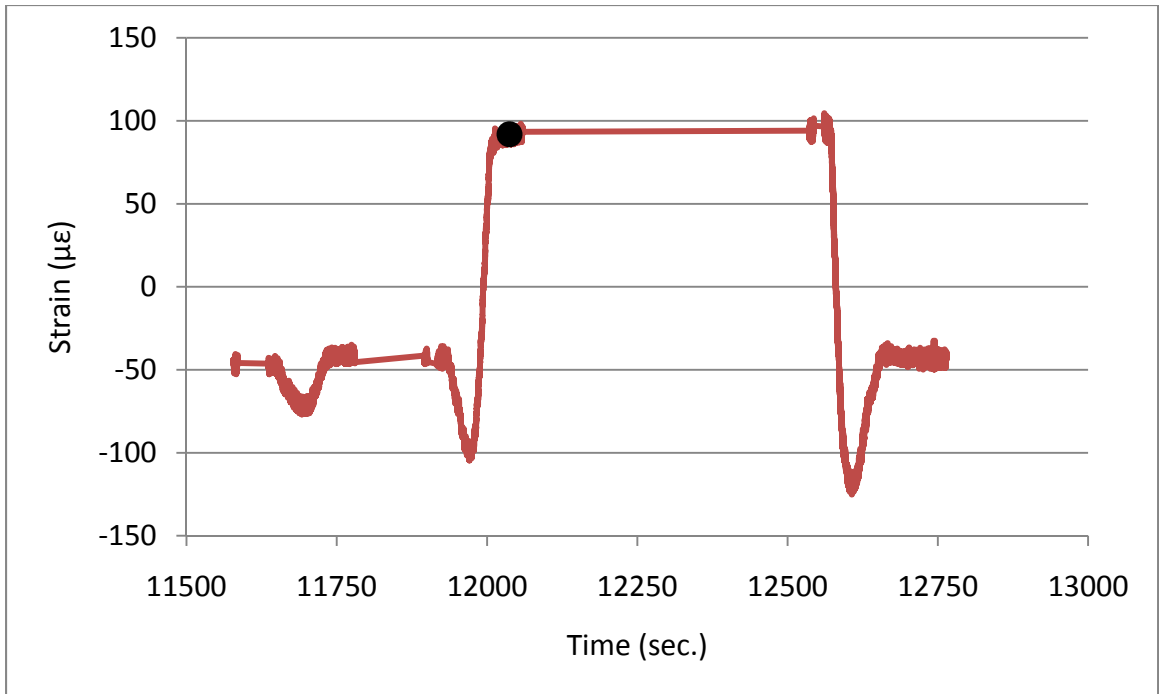
Figure B-14: Maximum strain from Night 1 for SP11G7
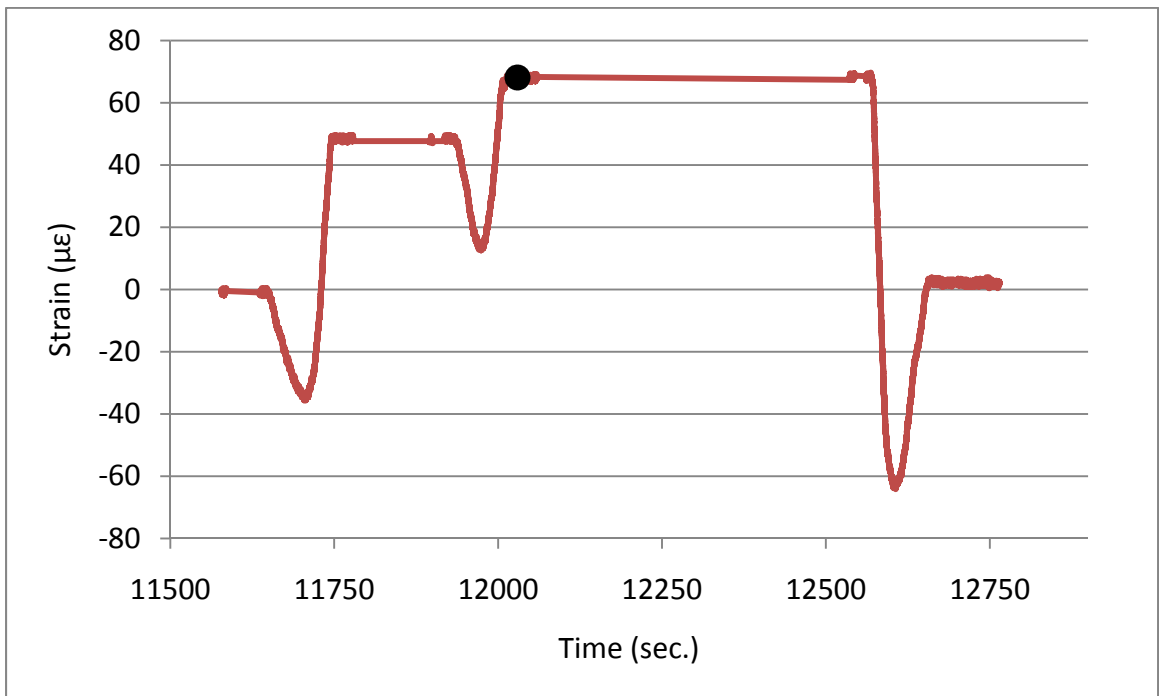
Figure B-15: Maximum strain from Night 1 for SP11G8
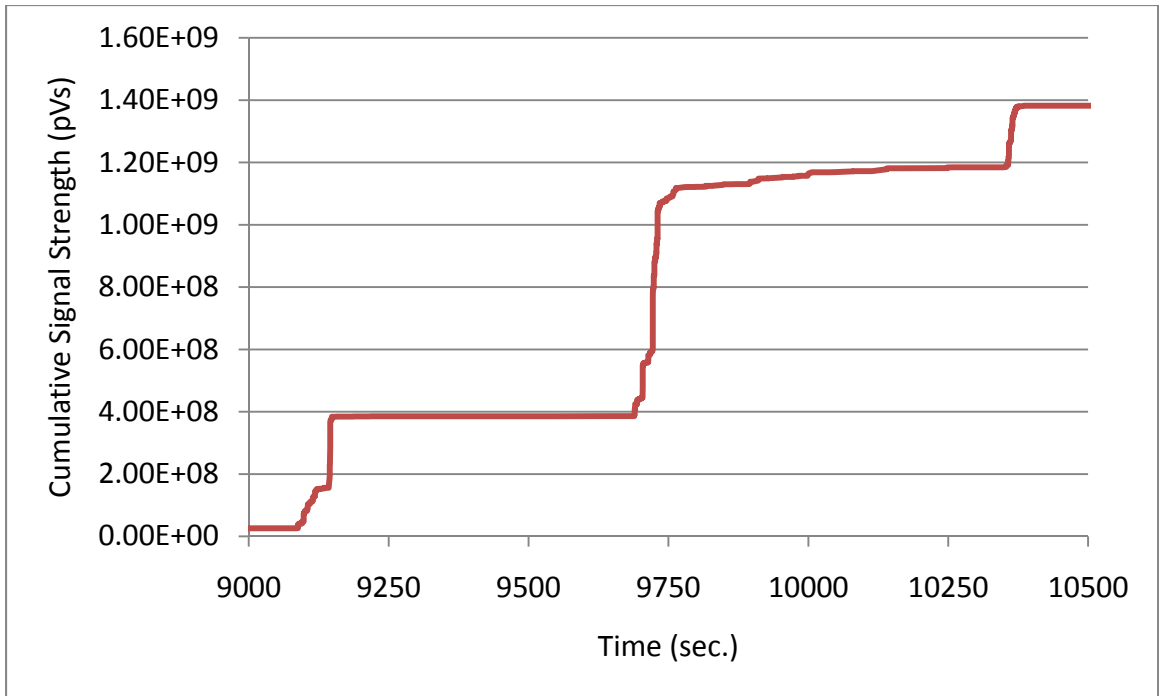
Figure B-16: CSS from SP10G8 loading on Night 1
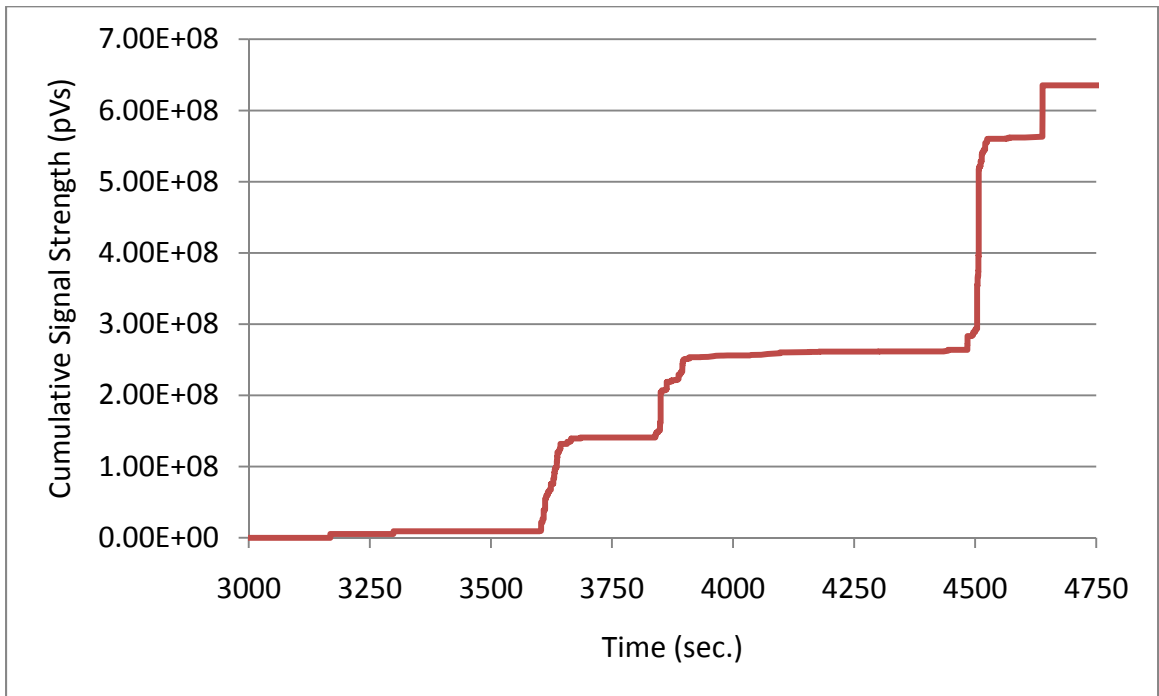
Figure B-17: CSS from SP10G8 loading on Night 2

163
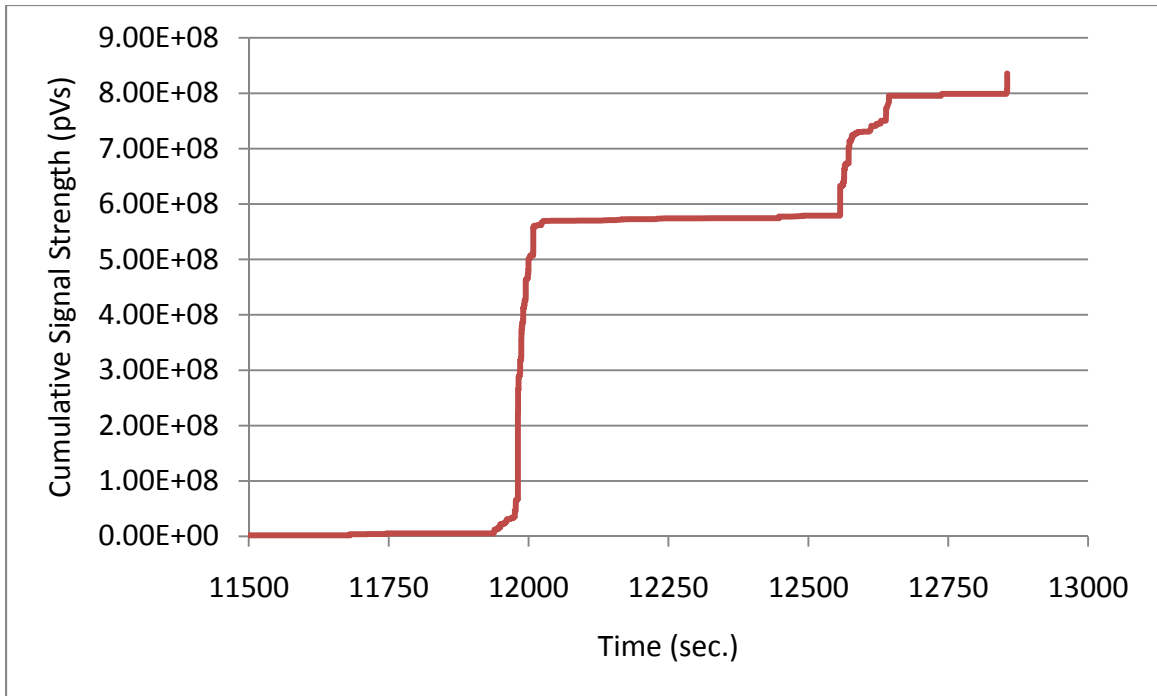
Figure B-18: CSS from SP11G7 loading from Night 1
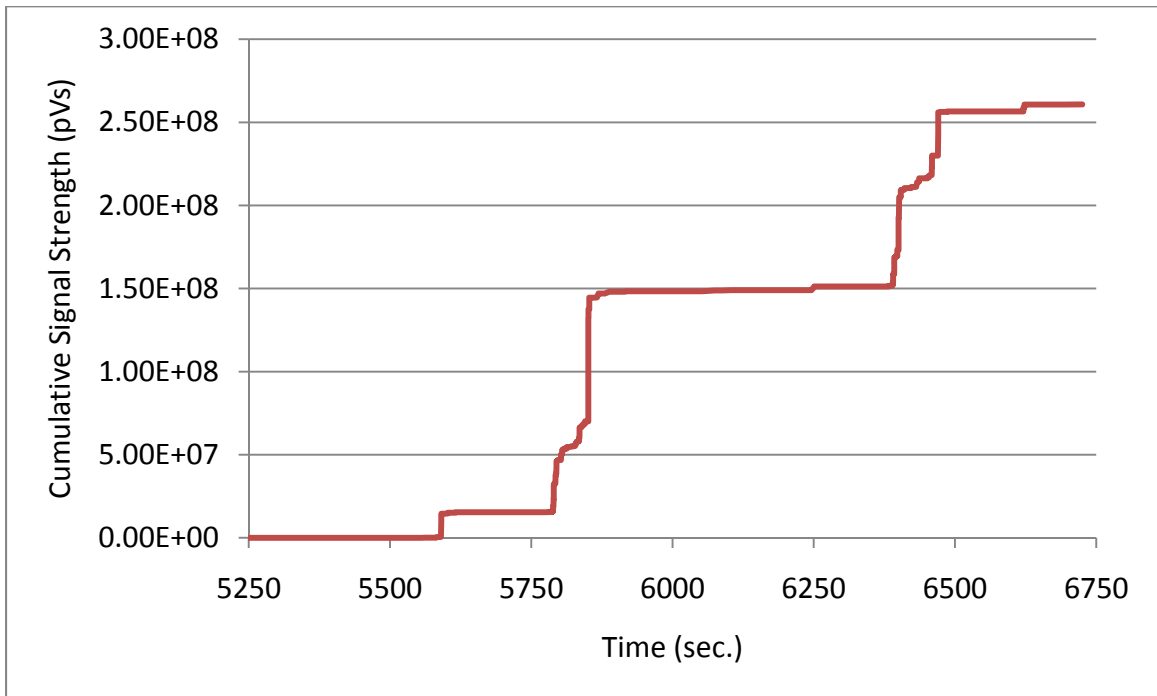
Figure B-19: CSS from SP11G7 loading from Night 2

164
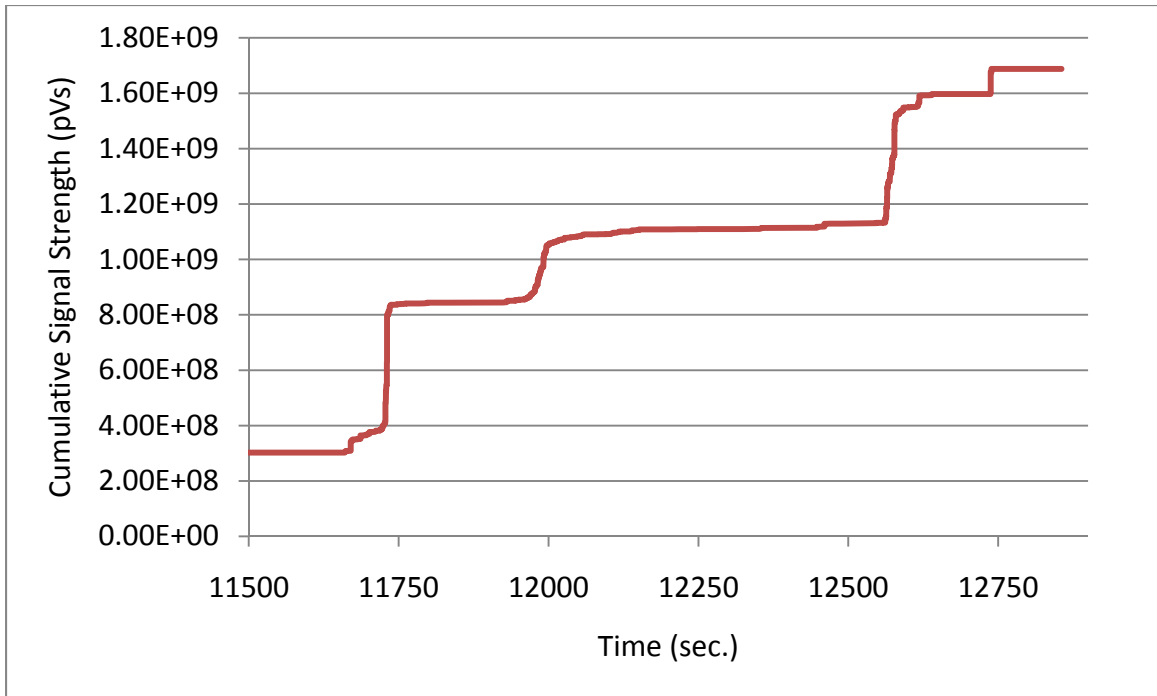
Figure B-20: CSS from SP11G8 loading from Night 1
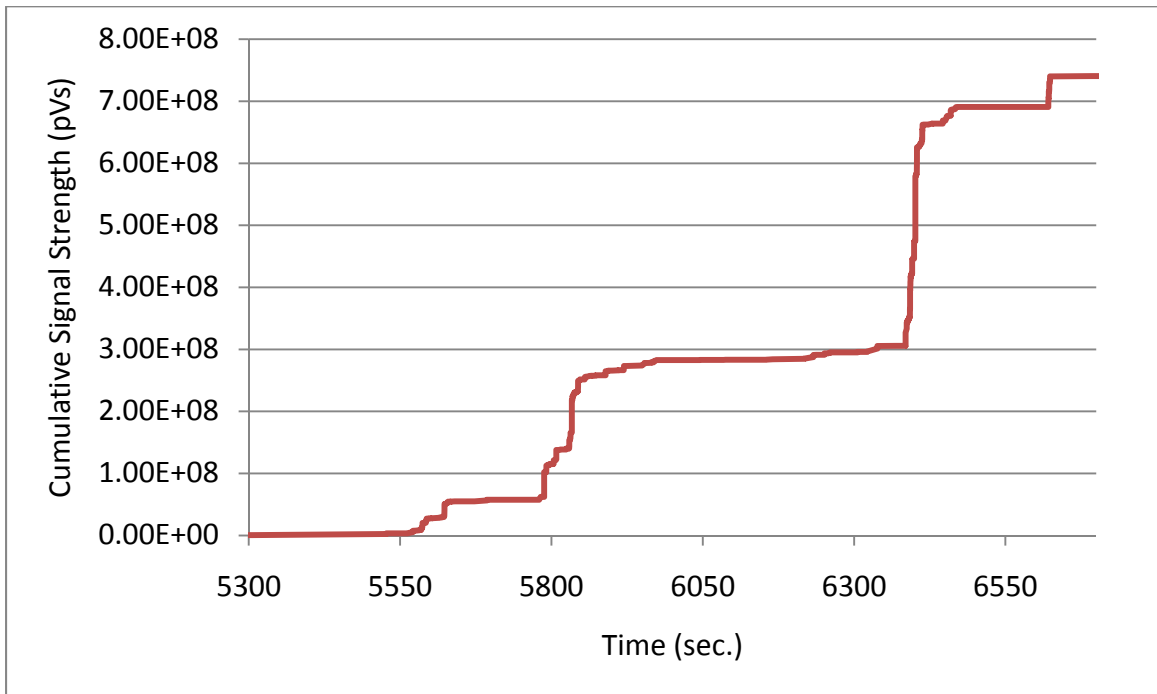
Figure B-21: CSS from SP11G8 loading from Night 2

Appendix C: SSM Ratio Analysis Figures
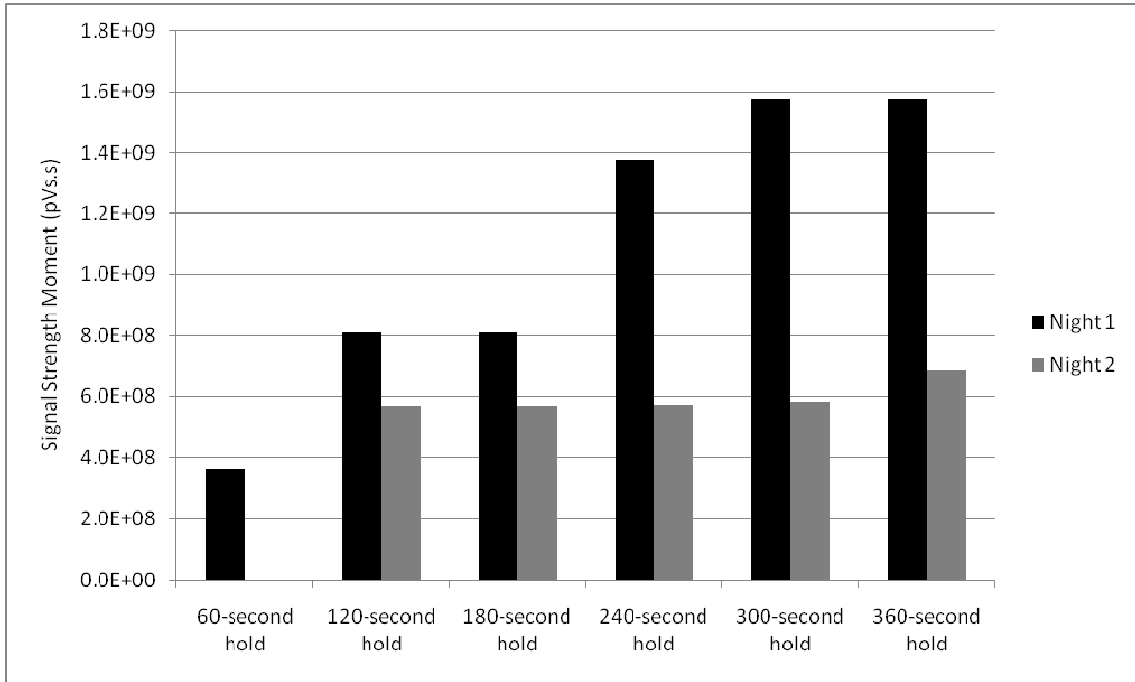
Figure C-1: SSM ratios for different data time frames for SP10G7
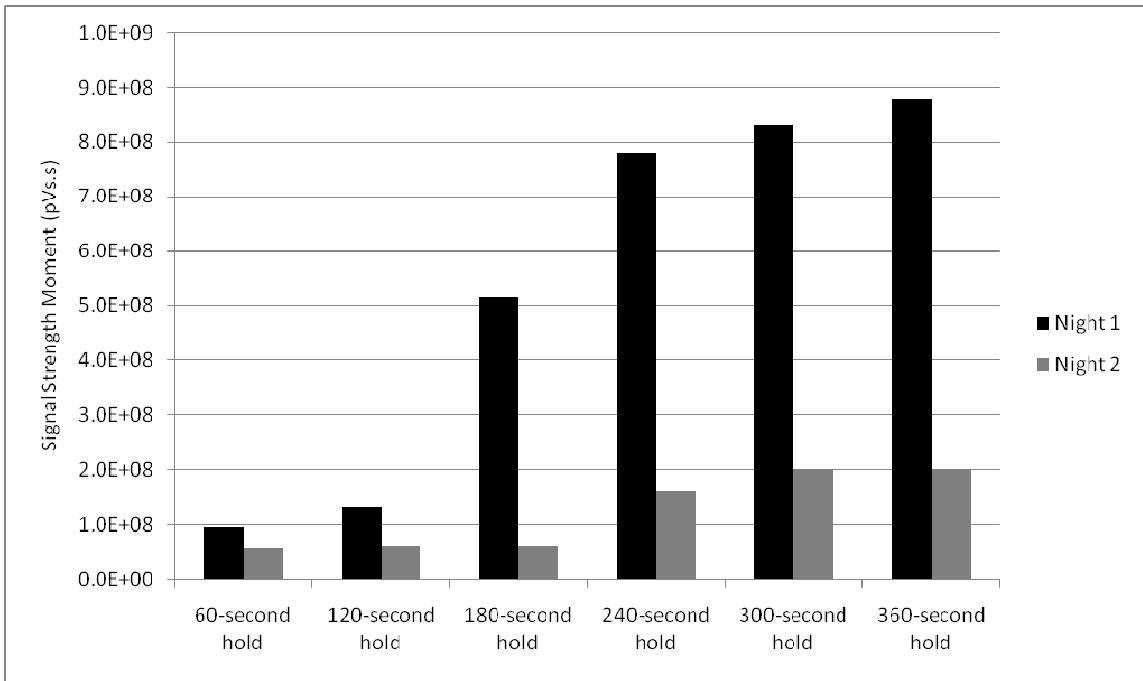
Figure C-2: SSM ratios for different data time frames for SP11G7
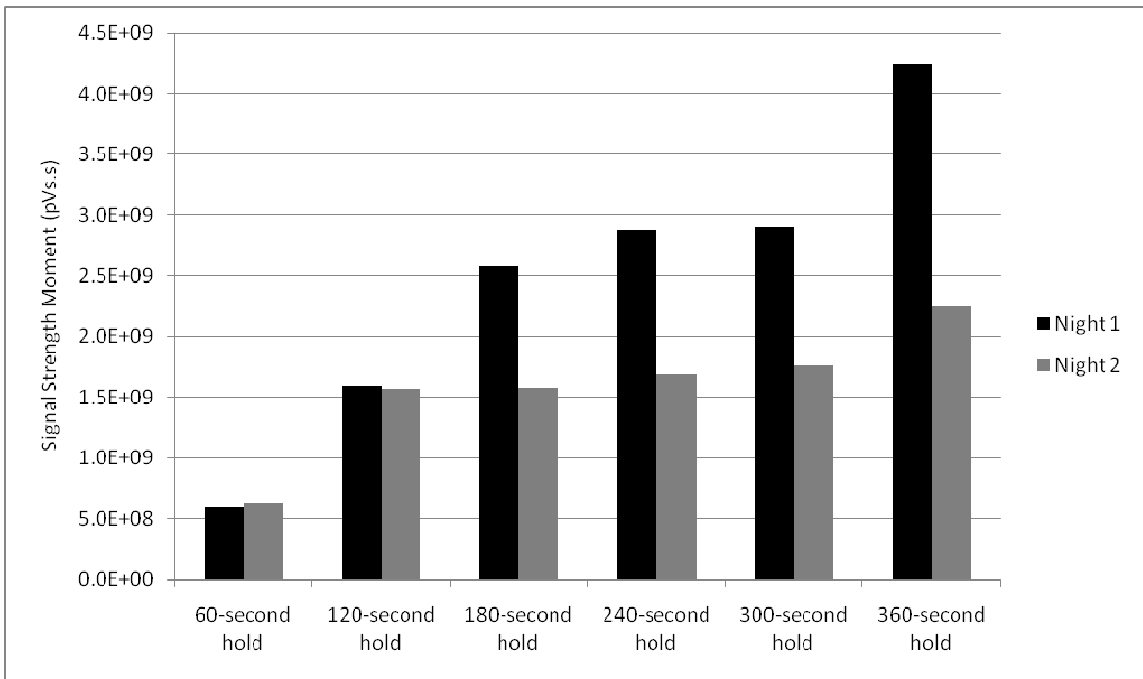
Figure C-3: SSM ratios for different data time frames for SP11G8
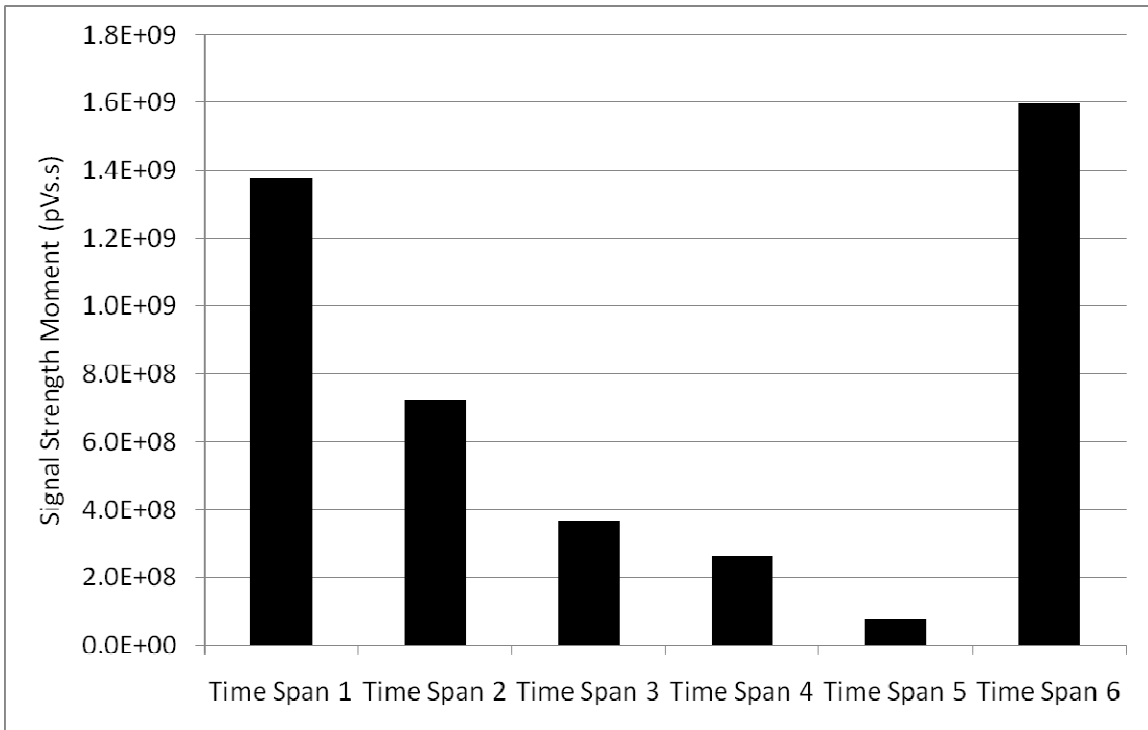
Figure C-4: SSM for different 240-second time spans for SP10G7 on Night 1
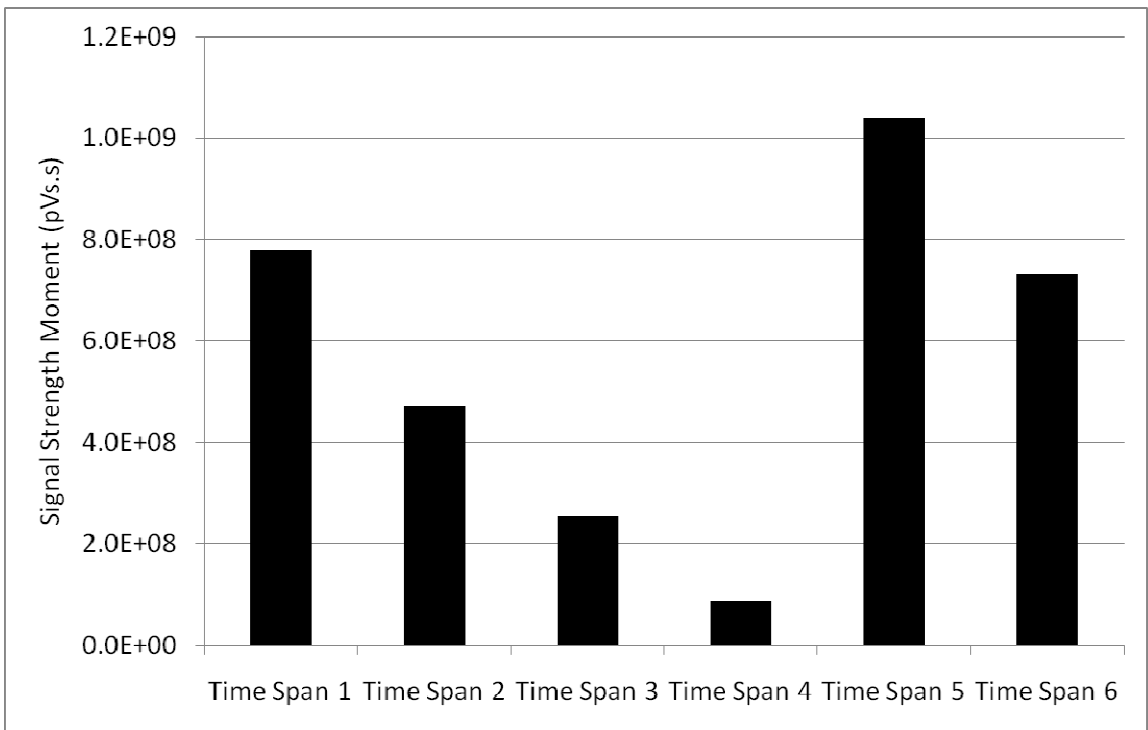
Figure C-5: SSM for different 240-second time spans for SP11G7 on Night 1
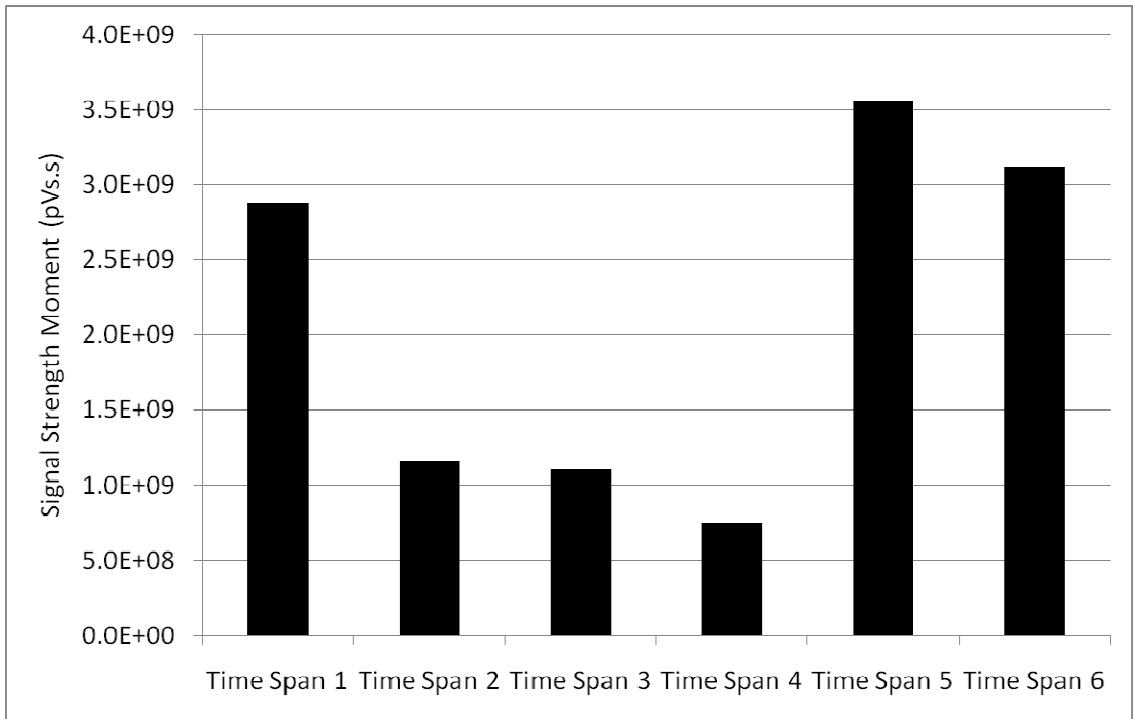
Figure C-6: SSM for different 240-second time spans for SP11G8 on Night 1
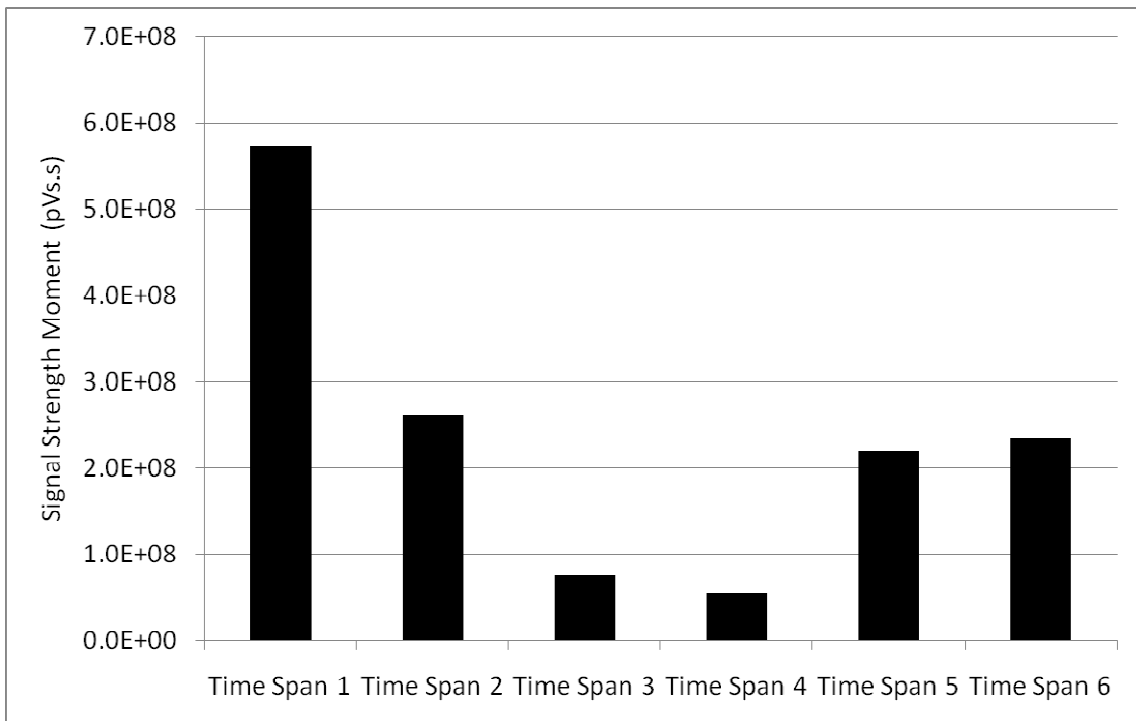
Figure C-7: SSM for different 240-second time spans for SP10G7 on Night 2
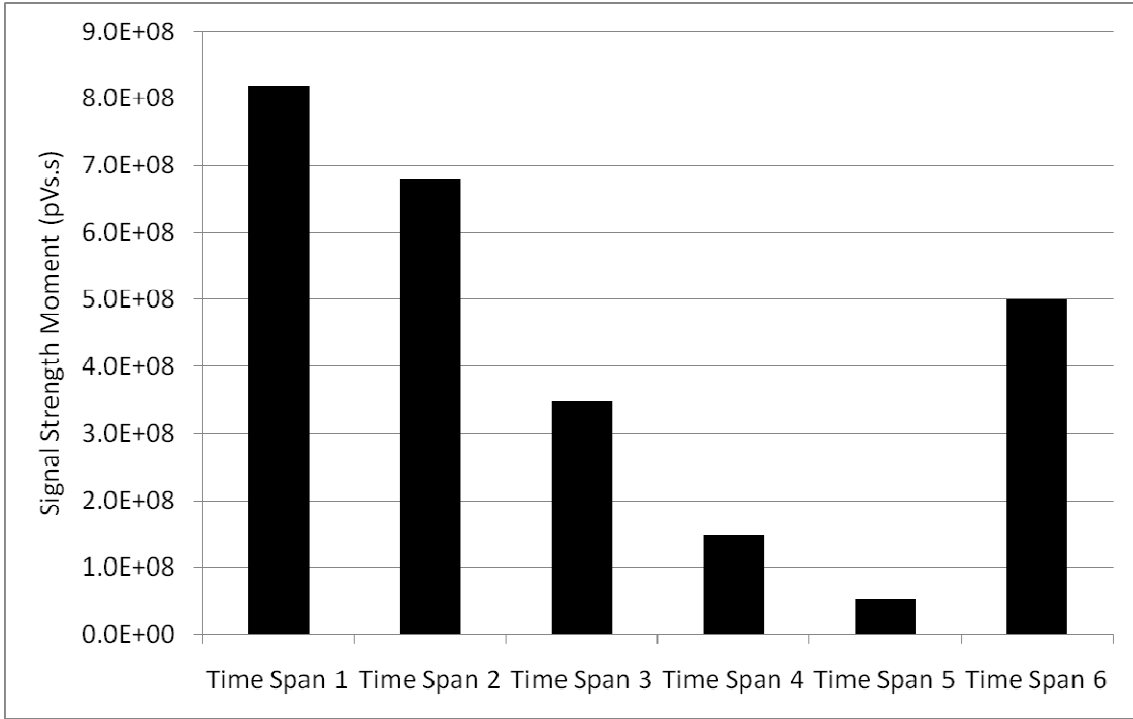
Figure C-8: SSM for different 240-second time spans for SP10G8 on Night 2
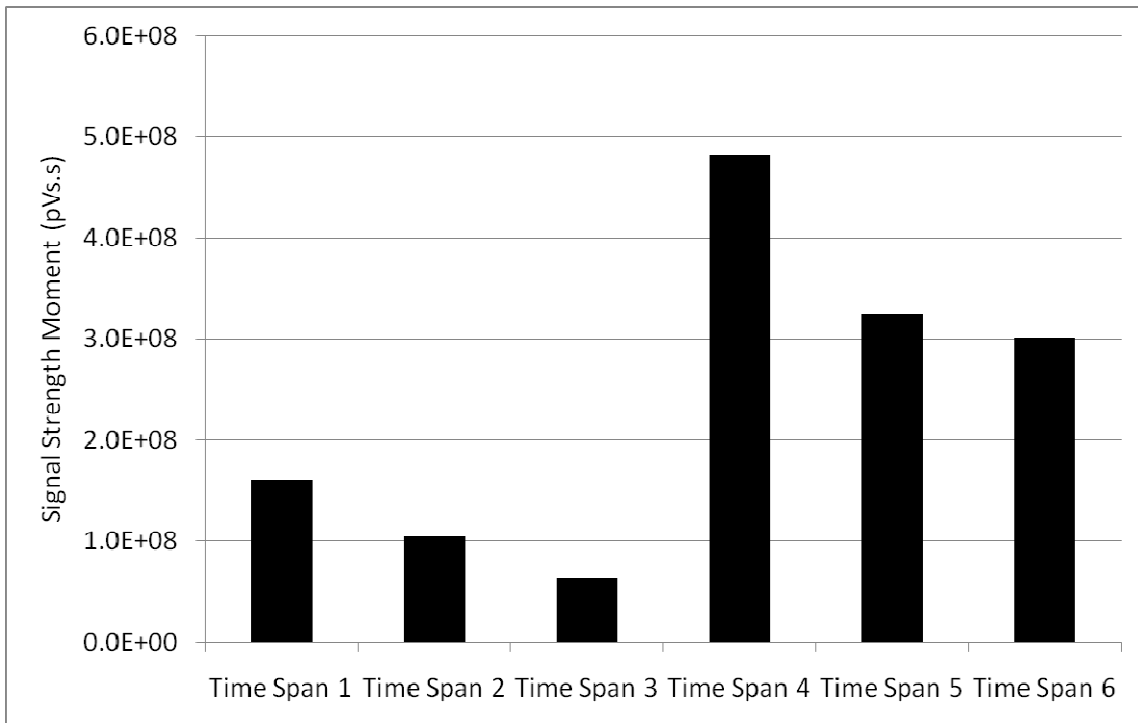
Figure C-9: SSM for different 240-second time spans for SP11G7 on Night 2
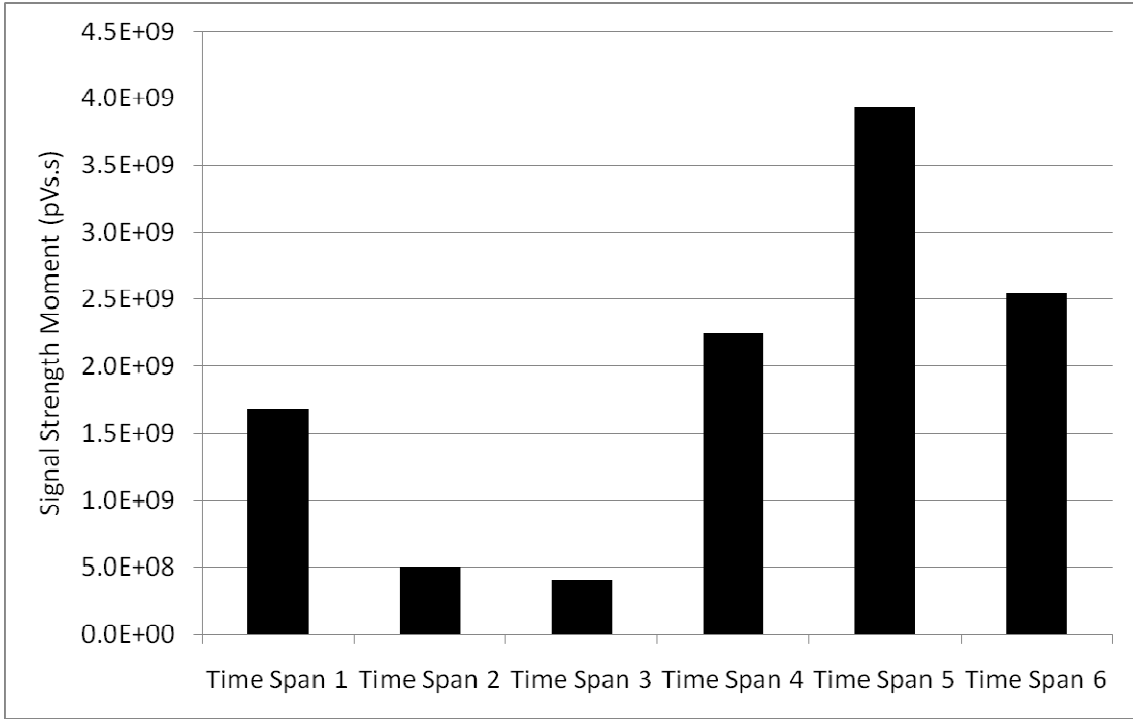
Figure C-10: SSM for different 240-second time spans for SP11G8 on Night 2
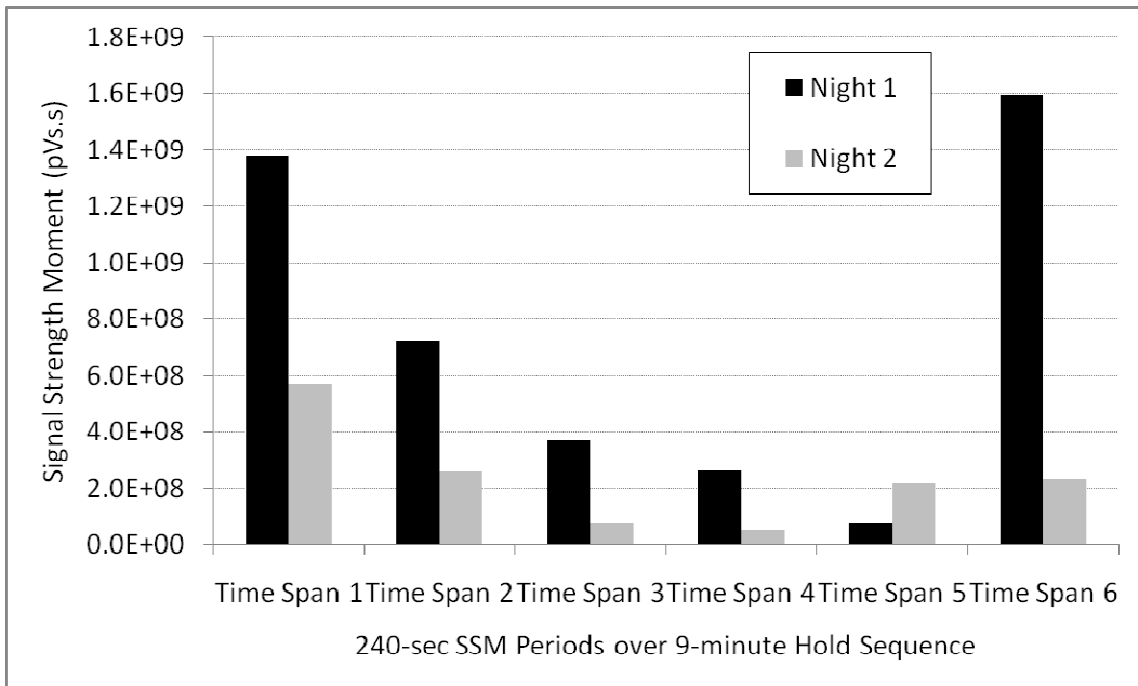
Figure C-11: SSM ratios for different 240-second time spans for SP10G7
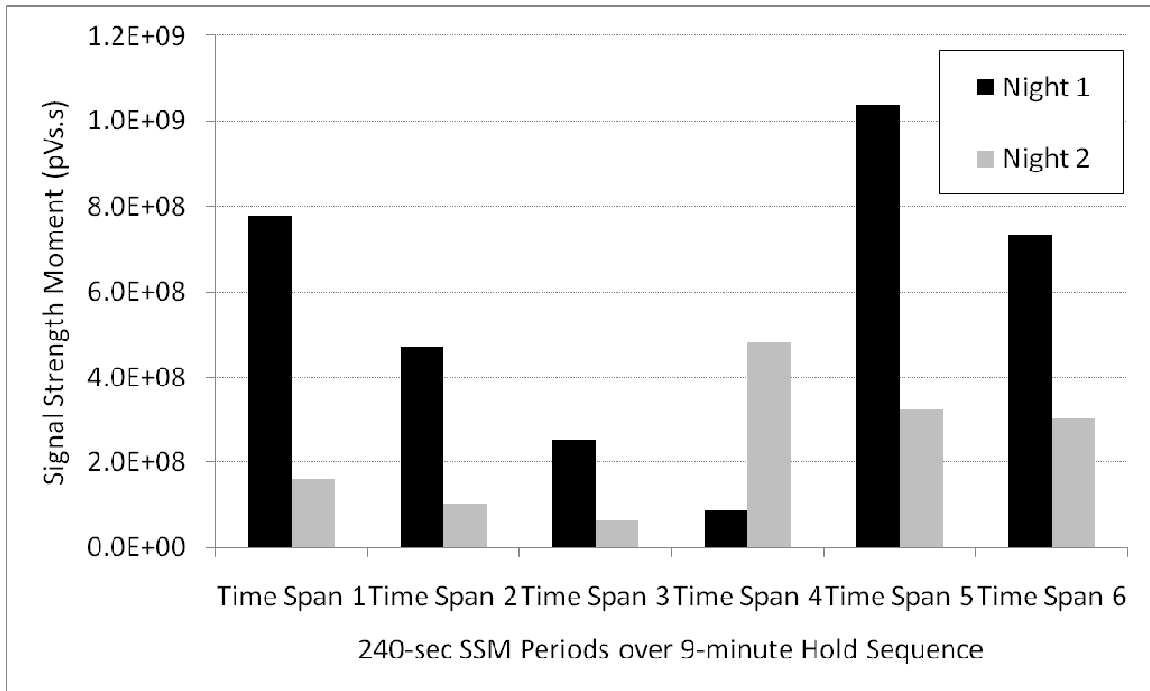
Figure C-12: SSM ratios for different 240-second time spans for SP11G7
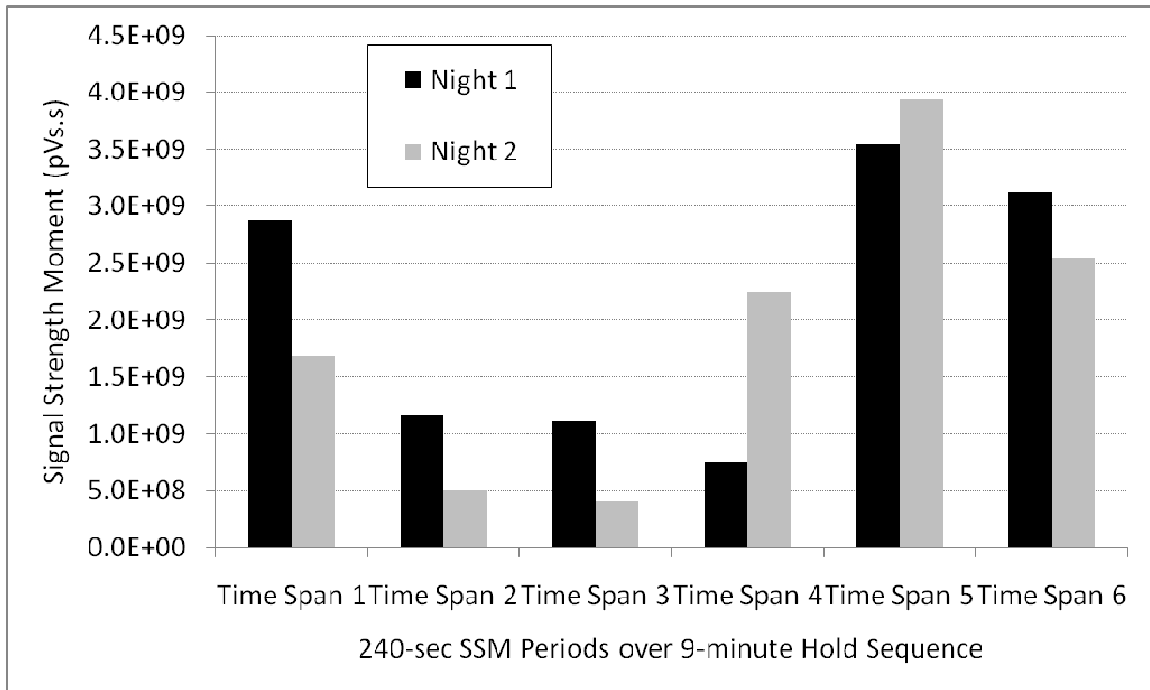
Figure C-13: SSM ratios for different 240-second time spans for SP11G8

Appendix D: AE 2D-LOC Crack Location Figure
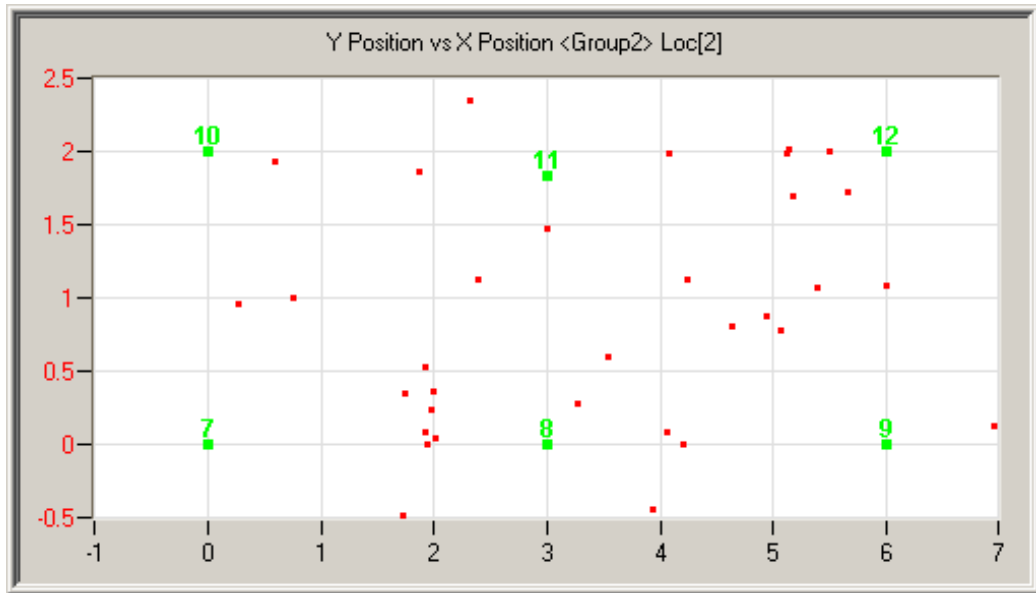
Figure D-1: AE 2D-LOC source locations for SP10G7
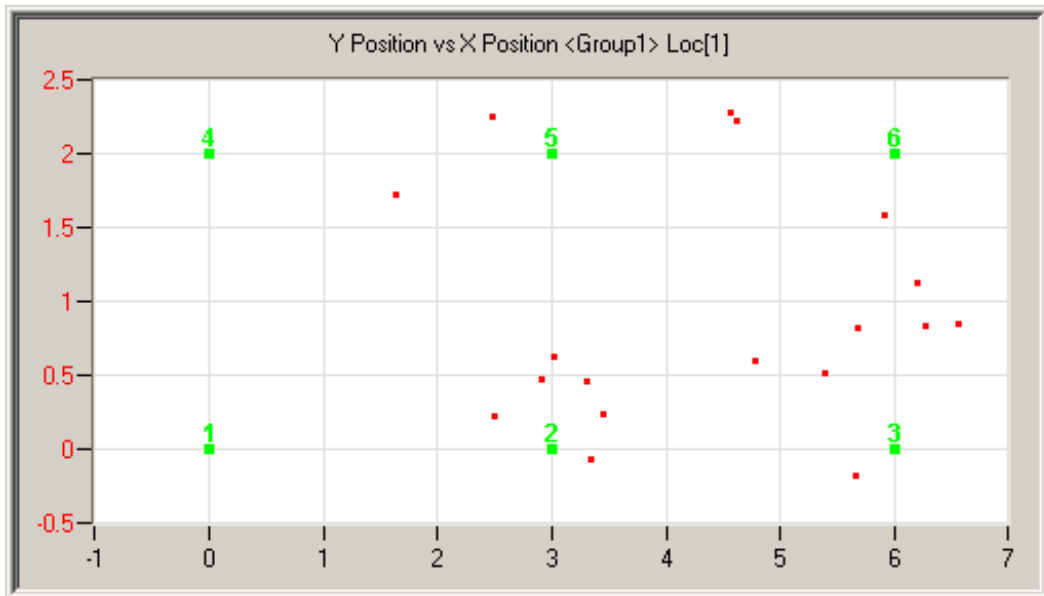
Figure D-2: AE 2D-LOC source locations for SP10G8

Figure D-3: Visible cracks on face of SP10G7

Figure D-4: Visible cracks on face of SP10G8

Appendix E: Additional Evaluation Criteria Figures
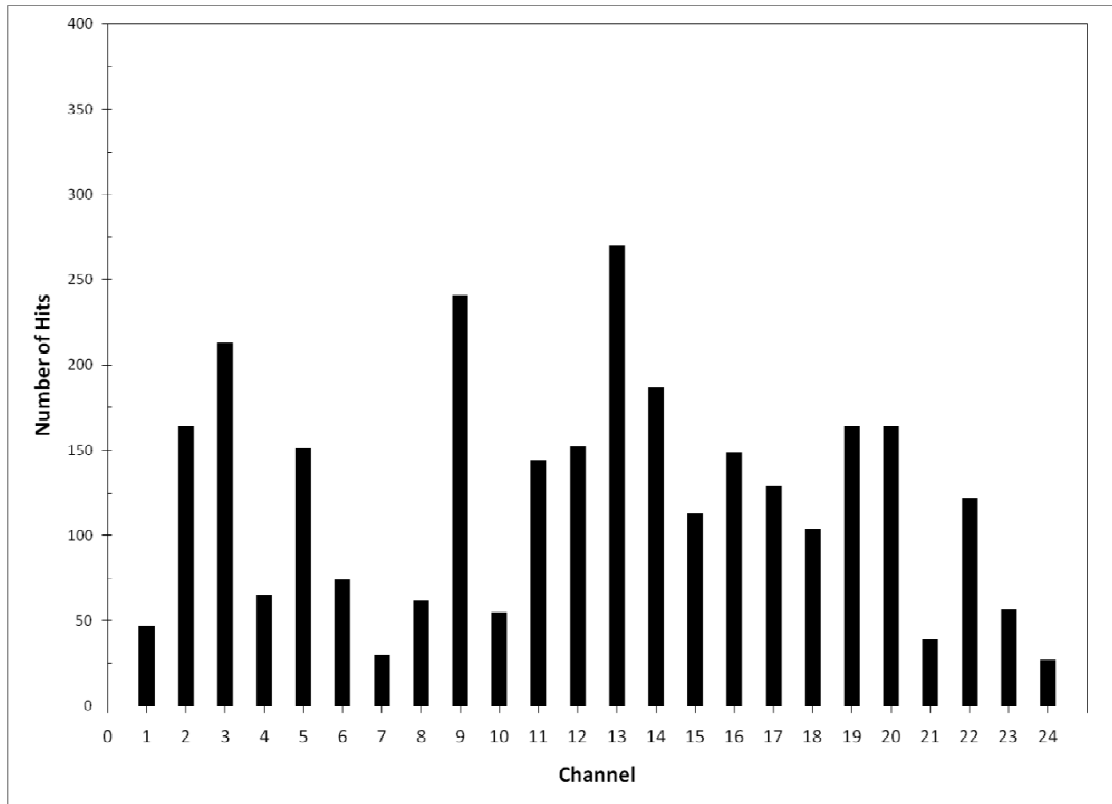
Figure E-1: Channel hit frequency for Night 1 Span 10 loading
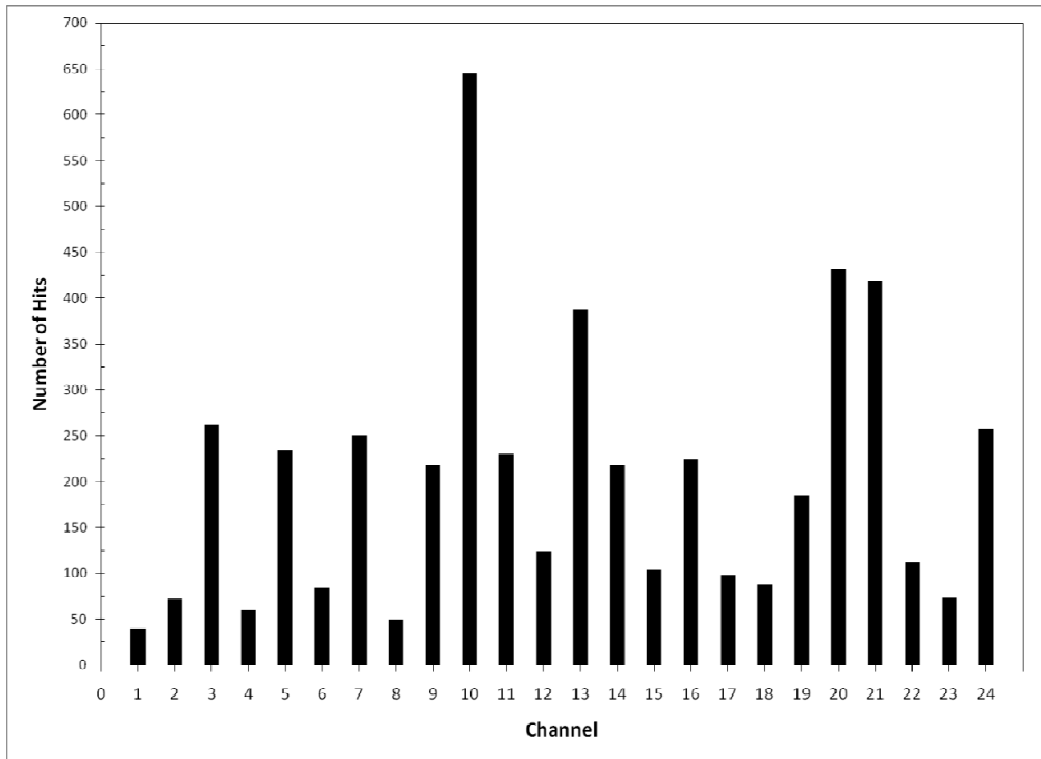
Figure E-2: Channel hit frequency for Night 2 Span 10 loading
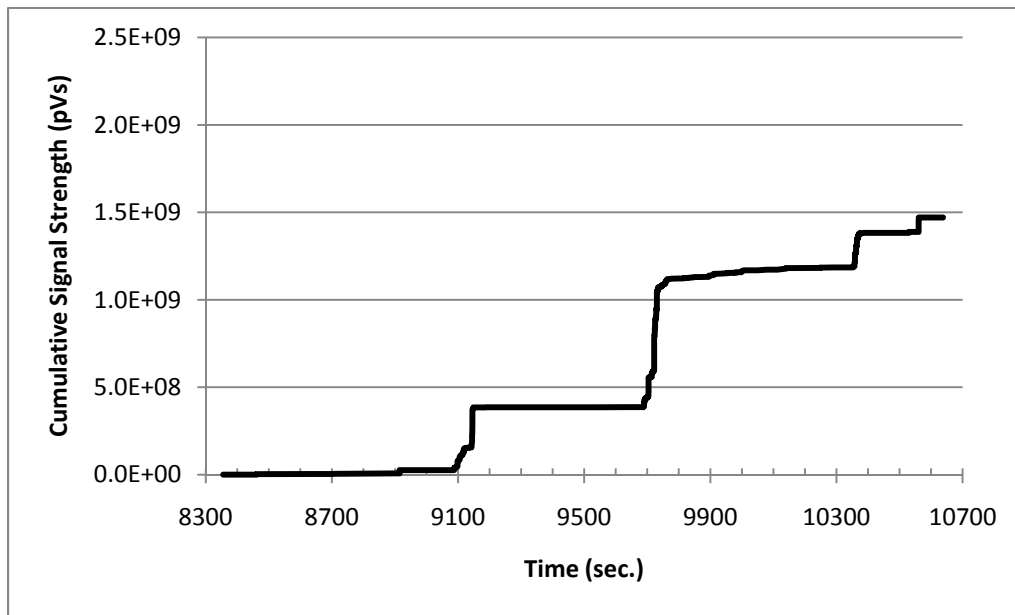
Figure E-3: CSS for Night 1 loading of SP10G8
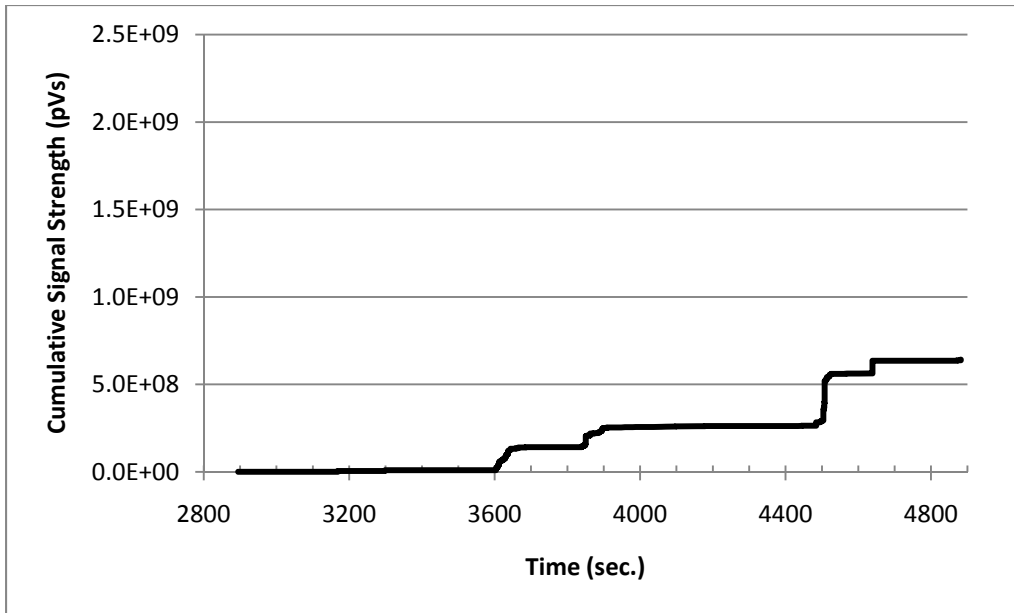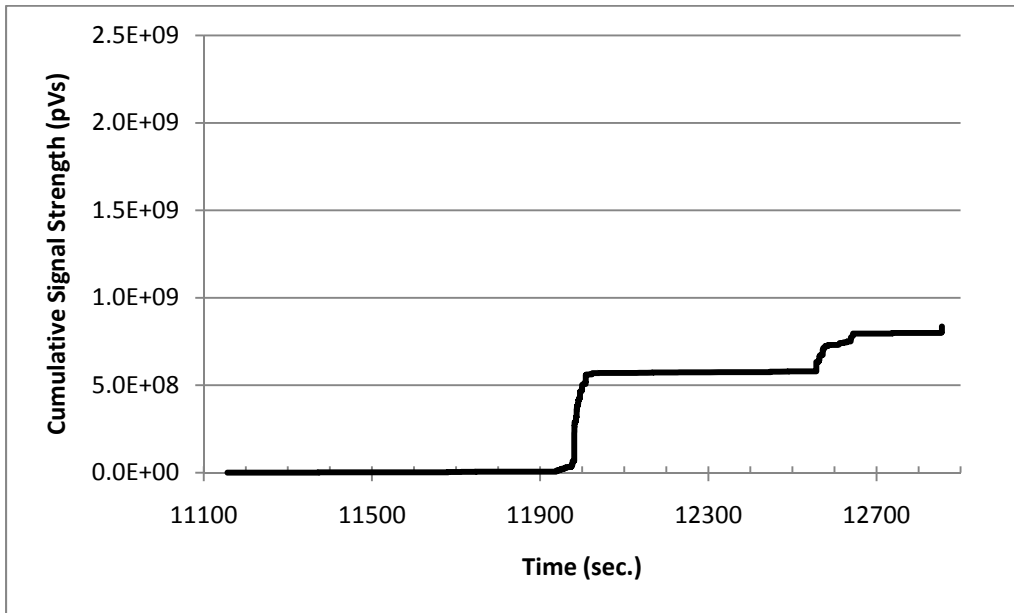
Figure E-4: CSS for Night 2 loading of SP10G8
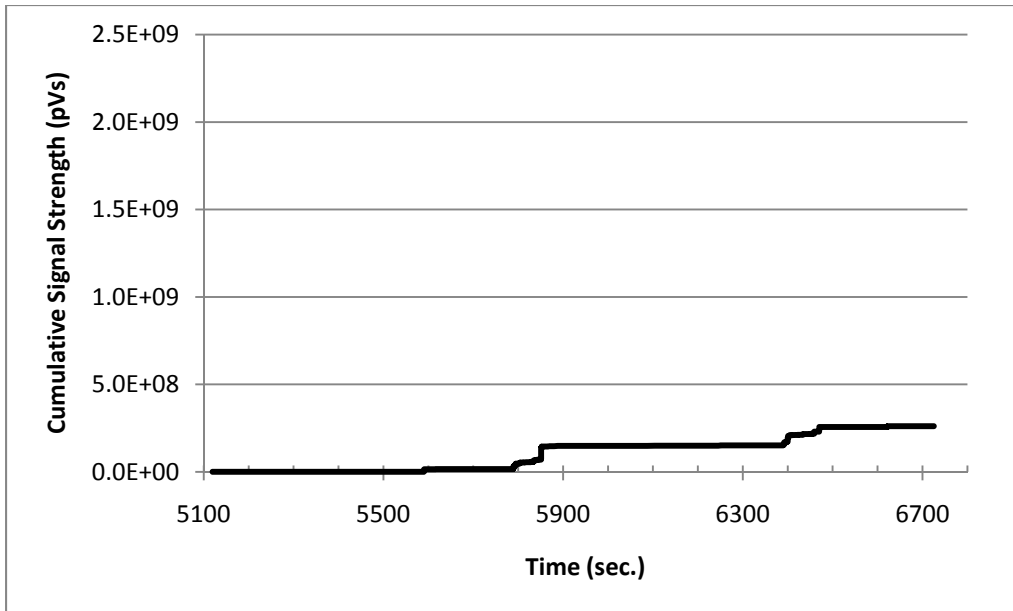

Figure E-5: CSS for Night 1 loading of SP11G7

177

Figure E-6: CSS for Night 2 loading of SP11G7
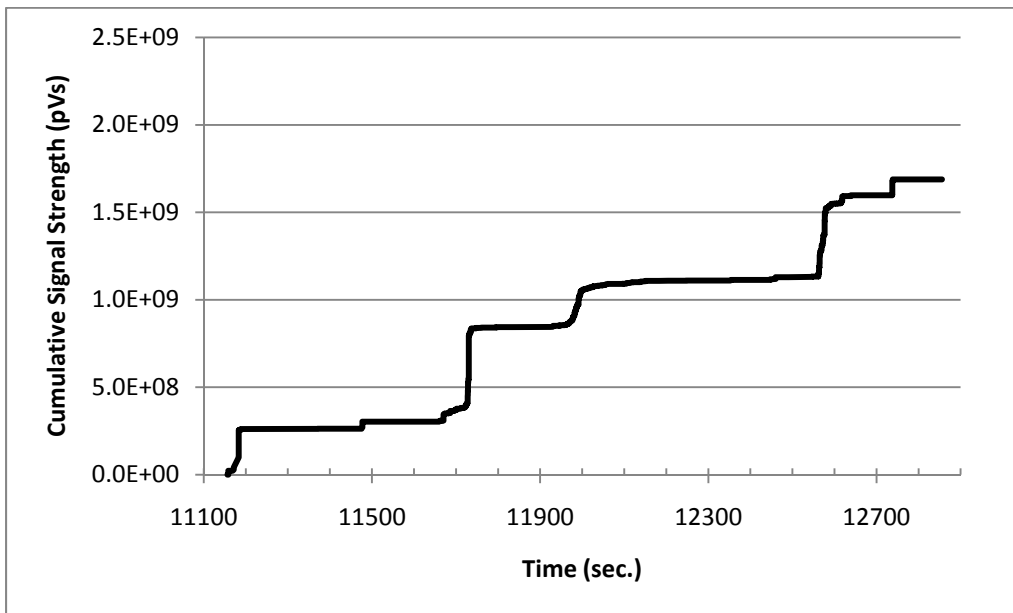

Figure E-7: CSS for Night 1 loading of SP11G8
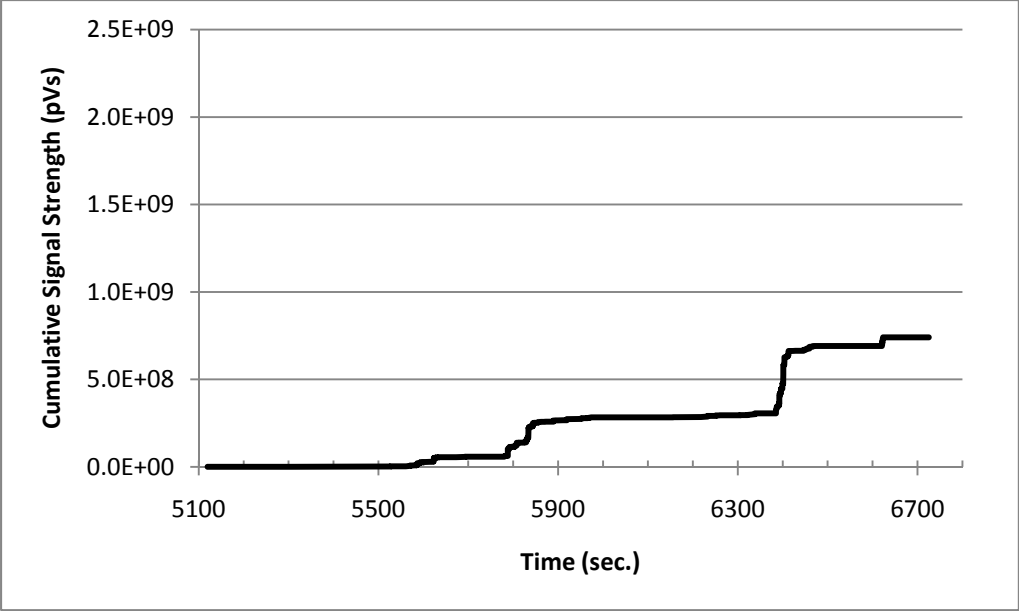
Figure E-8: CSS for Night 2 loading of SP11G8

Appendix F: On-Site Testing Pictures

Figure F-1: View of I-565 bridge structure

Figure F-2: View of false supports under Bent 11

Figure F-3: Van used for testing

Figure F-4: Testing equipment setup

Figure F-5: Cables running from bridge girders to testing van